EFFECT OF ATMOSPHERIC PRESSURE ION LENS ON AN ELECTROSPRAY ION SOURCE

by

RONG YI

B.Sc., Nankai University, 2001

A THESIS SUMBITTED IN PARTIAL FULFILLMENT OF THE REQUIREMENTS FOR THE DEGREE OF

MASTER OF SCIENCE

in

THE FACULTY OF GRADUATE STUDIES

(Chemistry)

THE UNIVERSITY OF BRITISH COLUMBIA

Aug 2005

Abstract

The effect of an atmospheric pressure ion lens on electrospray ionization mass spectrometry (ESI-MS) was investigated. In Chapter 2, the voltage combinations applied to the spray and the ion lens were systematically studied, as well as the current-voltage relationship. The ion lens showed its ability to widen the range of operational spray voltages and improve signal intensity. Through the calculations in Chapter 3, the effect of the ion lens is demonstrated to include improving the electrospray process by changing the field strength and widening the operational spray voltage range, and increasing the transmission efficiency by focusing ions through the flattened equipotential lines. The experimental results in Chapter 2 were rationalized, and the hypotheses were verified. In Chapter 4, more experiments were carried out to show solvent dependence, nebulizer optimization, and fragmentation control for the characterization of ESI-MS. Future work was proposed to combine the ion lens with a multiple-spray ion source, where the ion lens has the potential to improve the sensitivity of the ion source, and to simultaneously introduce a mass calibrant to improve the mass accuracy of mass spectrometry.

Table of Contents

List of Tables

List of Figures

List of Abbreviations

Abbreviation	Definition
BEM	Boundary element method
CE	Capillary electrophoresis
CEM	Channel electron multiplier
CI	Chemical ionization
CRM	Charged residue mechanism
DC	Direct current
E	Electric field
EHI	Electro hydrodynamic ionization
EI	Electron impact
ESI	Electrospray ionization
FDM	Finite difference method
FEM	Finite element method
HPLC	High performance liquid chromatography
IEM	Ion evaporation mechanism
MALDI	Matrix assisted laser desorption ionization
MEM	Magnetic electron multiplier
MS	Mass spectrometry
R	Radius
RF	Radio frequency
V	Potential on an Electrode

Acknowledgement

First of all, I would like to thank my supervisor Dr. David Chen, for his guidance and support during my study and research, and for the research environment he provided. I want to specially thank Wuyi Zha, Ning Fang, Irina Manisali, and Alison Holliday, for their valuable discussion, inspiration and help. Also I would like to thank all the other current and previous members in the group: David McLaren, Jingyan Zheng, Stefan Buster, Hong Zhang, Pingjia Meng. I am grateful to have met such a group of wonderful people, with whom I shared an enjoyable time.

Many thanks to Dave Tonkin for his time and patience in repairing our mass spectrometer - for so many times. I would also like to thank Dr. Damon Robb, for his help on the instrument and insightful discussion. I also appreciate Dr. Chuanfan Ding for his advice and discussion.

Finally, I would like to thank my parents for their love and unconditional support through all these years. At last I want to thank my husband, for his invaluable love, support, and encouragement.

Chapter 1

Background of Electrospray Ionization

1 Background of Electrospray Ionization

It is an inevitable but awkward starting point for this thesis to introduce the phenomenon of Electrospray Ionization (ESI), for there are a great many publications concerning different aspects of this topic. Although this thesis does not focus on ESI itself, all the previous work we have done is for the purpose of making ESI more effective. A brief introduction to ESI is therefore necessary. Electrospray (ES) is an ionization method that generates gaseous ions directly from solution by spraying the sample solution under high electric potential at atmospheric pressure. Twenty years after its invention by Fenn in 1984[1], electrospray ionization mass spectrometry (ESI-MS) has been widely used for detection of large, non-volatile biomolecules including proteins, peptides, polysaccharides, nucleotides, and other compounds which are too large to be vaporized or too fragile to remain intact when other ionization methods are used. Since the ions are generated directly from the liquid phase, ESI can be coupled to separation techniques like high performance liquid chromatography (HPLC)[2-6] and capillary electrophoresis (CE)[7-9]. The mass spectrometers used for analysis and detection are normally continuous mass analyzers, such as quadrupoles, but pulsed mass analyzers, such as time-of-flight, and ion traps are also suitable for coupling with electrospray.

This chapter gives a brief introduction to the development, mechanism, and some ongoing improvements of ESI-MS, with great appreciation to all those who made this technology as widely used as it is today.

1.1 Ionization Methods for Mass Spectrometry

A mass spectrometer works by mass analyzing charged particles in a vacuum. All samples should be converted into gaseous ions before being mass analyzed in vacuum, no matter what neutral or charged forms they existed in before. If samples are not in the gas-phase, they have to be vaporized as well. Some types of ion sources act directly on a gaseous sample, such as electron impact (EI) and chemical ionization (CI); these are generally restricted to small compounds with molecular weight less than 1000 Dalton and boiling point less than 500°C. Samples are vaporized at a high temperature and ionized by bombarding the molecular vapour with a beam of energetic electrons (EI) or reagent gas (CI). For macromolecules, the difficulty lies not in ionization but in vaporization. Due to their extremely low vapour pressure, vaporization of macromolecules has never been an easy task. Upon heating to high temperature, macromolecules are likely to degrade or decompose before vaporization.

Other types of ion source are based on desorption ionization, where gaseous ions are generated directly from solution or from a solid matrix, such as in matrix-assisted desorption ionization (MALDI) and electrospray ionization (ESI). In MALDI, the analyte molecules are dispersed on a surface in a thin layer of matrix, usually an organic compound. The energy of an incident pulse of photons is absorbed mostly by the matrix to assist the evaporation of analytes as ions by mechanisms that are still not well understood. ESI, which will be discussed in detail in this thesis, generates gaseous ions directly from solution by spraying out liquid droplets under high electric field.

Ion sources are also categorized by "hard" and "soft" ionization. EI is often referred to as "hard" ionization sources because the high energy encounter of analytes with electron or reagent gas usually results in extensive fragmentation. Quite different from those violent ionization methods, MALDI and ESI are two major "soft" ionization methods that can generate intact macromolecular ions without much fragmentation at the ion source. To obtain further functional information, controlled fragmentation is possible if tandem mass spectrometry with a collision cell in between two mass analyzers is used.

1.2 History of the Development of Electrospray Ionization

In 1968, Malcolm Dole published an article about molecular beams of macroions[10], showing the production of negative macroions by electrospray of a dilute solution into an evaporation chamber. It might be the first time ever that intact gas-phase macromolecular ions were obtained, but at that time few people knew this would become such an important ionization technique.

All of the ionization methods at that time relied on gas phase energetic collisions between a neutral molecule and an electron, photon, or light-weight reagent gas. The high temperature required for vaporization and high energy for bombardment inevitably cause decomposition and fragmentation of macromolecules. Electrospray of charged droplets under a high electric field had been widely applied in automobile painting and other applications, but it was hard to imagine that the droplets would be so small that single ions could be generated. In this sense, it is a remarkable contribution that Dole realized that the charged droplets of non-volatile analyte solutions generated by electrospray could eventually produce intact

macromolecule ions. Getting precise molecular weight for large biomolecules was claimed possible for the first time. Yet another and perhaps more noteworthy contribution that Dole made is the recognition of the importance of dispersing the droplets into gas at near atmospheric pressure. The collision of droplets with ambient gas provides a supply of energy, which is necessary for the evaporation of solvent. Without the additional supply of energy, as in the case of the so-called "electro hydrodynamic ionization" (EHI) in which droplets are dispersed into vacuum[11], most solvent behaves as in "freeze drying", leading to extreme difficulty in isolation of solute ions. Moreover, any ions produced by EHI in vacuum have such high kinetic energies that magnetic sector instruments are generally required for their mass analysis. In Dole's work, sample solution was injected through a needle into a flow of dry-bath gas (nitrogen) through a cylindrical glass chamber. When dispersing droplets at near atmospheric pressure, the collisions limit the ion motion to a constant mobility. The macroion flux was mass analyzed by a retarding potential method, wherein unwanted ions are repelled from the ion beam by negative voltages on a repelling grid, and detected by a Faraday cage. Accurate *m/z* of the macroions was obtained from the scanning repelling voltages.

However, Dole's work did not solve some of the major problems concerning the connection of ESI to MS. Mass spectrometers available at that time were unable to mass resolve singly charged ions with masses higher than ten thousand Daltons. In later work, he resorted to ion mobility measurements to identify macroions instead of using mass spectrometers.

When Fenn first read Dole's paper in 1968, he was working on supersonic free jets. This ESI idea intrigued him very much, since it was a possible application of free jets. Then he discovered some important flaws in Dole's design. First, the concurrent flow of bath gas and droplets resulted in the presence of solvent vapour in the mixture of gas and ions. When the mixture entered the skimmer, it was highly likely that adiabatic cooling during free jet-expansion condensed the solvent molecules to the solute ions. Familiar with the properties of free jets, Fenn and Labowsky realized that desolvation would be much more effective if the bath gas was flowing counter-current to the flux of ions and droplets. Thus, the solvent vapour evaporated from the droplets was carried away from the entrance to the orifice. This counter-current curtain gas successfully solved the problem of resolvation or condensation of solvent during the free jet expansion and greatly improved reproducibility. However, the retarding-potential mass analyzer still did not respond well to the incoming ions.

When Yamashita joined Fenn's group in the early 1980s, he connected a simple quadrupole to the ESI. Even though the mass range of the quadrupole was only 450 Dalton, ions from single molecules were present in the resulting spectra[1]. It was probably the first real ESI-MS in the world, created about 15 years after Dole's first innovative attempt of ESI.

With the rising demand for an interface between mass spectrometry and liquid chromatography, they started to investigate possible ways of connecting ESI between LC and MS. In the 1980s, most LC-MS interfaces used thermospray ionization (TSI). However, Fenn and colleagues managed to prove that ESI is a better method. The high voltage required by ESI imposed difficulty on this application. To avoid maintaining the LC system at high voltage,

they used a glass capillary, which was plated with metal at both ends to provide electric contact while floating the ion source from the rest of the apparatus, which was grounded. This design turned out to be quite successful[2] and gradually replaced most of the TSI interfaces.

The mass range of mass spectrometers restricted the use of ESI for the study of macromolecues until multiply charged ions were discovered to dominate the spectrum. When Fenn's group carried out ESI for poly (ethylene glycol) (PEG) oligomers, they found multiply charged ions with different numbers of Na^+ adducts, varying from 1 to 100 positive charges[12]. The spectrum became very complex when a mixture was sprayed, because each of the polymer molecules formed a cluster of multiple-charged peaks. However, with the increased power of personal computers, analysis of complicated spectra of mixtures has become feasible. In addition, analyzing more than a single peak gave more accurate results with regard to the molecular weight.

From then on, the research and application of ESI has seen a rapid development. The number of publications about ESI increased from a few papers per year in 1980s to over 1500 per year in 2001, and the number is still growing[13, 14]. ESI-MS has become one of the major analytical techniques for macromolecules.

1.3 Electrospray Ionization Mechanism

Electrospray ionization refers to the process of dispersing a liquid sample in an electric field to produce gas phase ions. During typical electrospray ionization, a voltage of 2 to 5 kV is applied to the tip of the capillary. The sample is dissolved in a polar, volatile solvent and pumped through a narrow, stainless steel or silica capillary (50 to 150 μm i.d.) at a flow rate of

between 0.5 μL/min and 1 mL/min. For flow rates of 1 μL/min or higher, the electrospray process is often aided by a co-axial nebulizer gas. The nebulizer gas, which is either nitrogen or air, helps to evaporate neutral solvent and to break up large liquid droplets, as well as to push the gaseous ions and charged droplets towards the mass spectrometer. The charged droplets diminish in size by solvent evaporation. Eventually, desolvated solute ions are released from the droplets by one of two possible mechanisms: charged residue mechanism (CRM) and ion evaporation mechanism (IEM). Then the ions pass through the orifice into an intermediate vacuum region, while most neutral solvent molecules are dissipated by a skimmer. Finally, the ions pass through the mass analyzer and hit an electron multiplier detector under high vacuum, and the ion counts are recorded by a computer.

The overall process of electrospray ionization is expected to be two relatively independent processes: (1) Dispersion of electrolytic sample solution into a bath gas to produce charged droplets, and (2) evaporation of the charged droplets resulting in the formation of gas phase ions. The first process can be interpreted literally as *electrospray*, and the second as *ionization*.

1.3.1 Electrospray

Forming the Taylor Cone

Under a positive electric field, positive ions will be in excess and will accumulate at the tip of the needle. The mutual repulsion among the positive ions at the liquid surface leads to the protrusion of the liquid towards the counter electrode, and it is the surface tension of the solvent

that holds the liquid still. With more charges gathering on the surface, the coulomb repulsion overcomes the surface tension. The liquid then begins to expand, allowing liquid to move downfield, and forming a so called "Taylor cone"[15, 16]. The Taylor cone was originally named to describe a static non-conducting liquid cone formed when the surface tension is balanced with the pressure induced by an electrostatic force. Taylor found that this balance resulted in a static liquid cone with straight sides and a half cone angle of 49.3°. In electrospray, where the emerging liquid is both conductive and dynamic, and with the presence of a flow of charge, the term "Taylor cone" is therefore somewhat inappropriate. However, the name is still used to describe the cone shaped liquid tip in most ESI studies.

Emission of Charged Droplets

When the Taylor cone forms, both the electric field intensity and the concentration of excess charge are highest at the cone tip, so that a static sharp Taylor cone tip only exists in calculation. As a result, a thin surface layer at the cone tip moves toward the counter electrode, like it is being pulled off from the cone, to form a liquid filament, which some refer to as a liquid "jet". The instability of this jet due to the interaction of viscosity and surface tension of the liquid gives birth to the "varicose waves" characterized by Rayleigh[14]. The liquid jet is truncated by the waves into a series of uniform droplets (Figure 1-1). The droplets are all positively charged (if ESI is run under the positive ion mode) due to the excess of positive charges at the surface of the cone. The Coulombic repulsion causes the divergence of the droplet trajectories to form a conical "electrospray" of charged droplets.

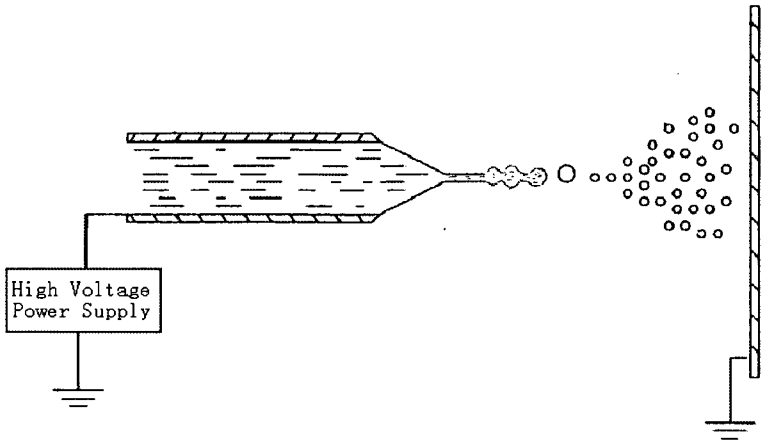

Figure 1-1 Emission of charged droplets from a Taylor cone. A liquid filament is pulled off from a Taylor cone and truncated to generate small uniformly charged droplets.

This is the process of "electrospray" as the first step of ESI, namely the dispersion of sample solution to form charged droplets.

1.3.2 Ionization

Charged Droplets Fission

After the charged droplets are dispersed, they shrink in size by solvent evaporation, while the charges they bear remain constant. The droplets become smaller until electrostatic repulsion of the surface charges becomes equal to the force due to surface tension; this is defined as the "Rayleigh limit". Rayleigh proposed that the limit between the charge, q, and the radius of droplets, R, can be described by:[14, 17]

$$q_R = 8\pi(\varepsilon_0 \gamma R^3)^{1/2}$$

where q is the charge on the droplet, ε_0 the vacuum permittivity, and γ the surface tension. Equation 1 describes the limit at which the coulomb force surpass the surface tension, and

charged droplets become unstable. Beyond the Rayleigh limit, the droplets undergo fragmentation, or "coulombic fission" to produce smaller offspring droplets[18]. This fission does not result in uniform offspring droplets. Since the droplets are often distorted into oblate and prolate shapes[19, 20], this fission often happens with a fine jet thrown from the droplet, as was observed and photographed by Gomez and Tang[20]. Taflin[18] predicted that the offspring droplets carry off only about 1-2.3% of the mass and 10-18% of the charges of the parent droplets, and this behaviour is often referred to as "uneven fission". Figure 1-2 shows the fission of a charged droplet that creates a miniature Taylor cone and emits a series of offspring droplets.

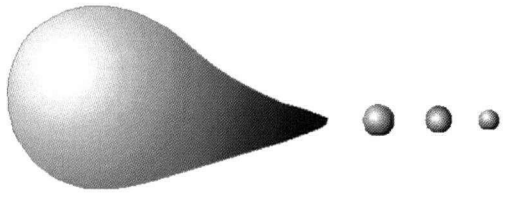

Figure 1-2 Schematic description of a fission process for charged droplet. The droplet is distorted, creating a miniature Taylor cone, and a string of offspring droplets are ejected.

Formation of Gas Phase Ions by the Charged Residue Mechanism and the Ion Evaporation Mechanism

The mechanism by which the small highly charged droplets become gas phase ions is still under debate. The shrinkage and fission of the droplets have been accepted widely, but even after a series of successive fissions, the offspring droplets are still much larger than a single molecule because they are still highly solvated. Dole proposed a mechanism that, when the solution is dilute enough, successive coulomb fission will produce droplets so small that

each one would contain only one solute molecule[10, 21]. With continuing evaporation of solvent, single gas phase ions could be eventually set free, bearing one or more excess charges. Dole did the work for the purpose of measuring the molecular weight of large molecules. However, it was doubted by some people that completely desolvated ions could be obtained. Nevertheless, the charged residue mechanism (CRM) has survived, and has displayed some validity for large biomolecules.

The low concentration condition is not always met, and the evaporation of solvent at the beginning normally happens much faster than coulombic fission, so that the residue that is formed contains more than one solute molecule. Furthermore, the singly charged ions that Dole observed could not be explained by CRM, because it is almost impossible for each of the ultimate offspring droplets to contain only one charge if the fission happens slower than the evaporation.

Iribarne and Thomson[22, 23], meteorologists at the University of Toronto, suggested another mechanism for the formation of gas phase ions. Inspired by the possibility that charged droplets of seawater could be the origin of some of the ions present in the atmosphere, they carried out experiments to show that after the radii of the droplets decrease to a certain limit by solvent evaporation, direct ion emission from the droplets becomes possible. Their explanation is that, with a critical size still large than the Rayleigh limit, the charge density on the droplet surface is high enough to emit a charged analyte molecule from the surface of the droplet, and this reduces the coulombic repulsion. This was the so-called ion evaporation mechanism (IEM), which is complementary to the charged residue mechanism (CRM). Iribarne and Thomson

derived an equation to predict the rate of ion emission from the charged droplets in detail, with a radius limit suggested to be R $\leq$10 nm[23].

The basic difference between CRM and IEM is the manner by which the analyte ions are detached from other components in the solution. In CRM, the analyte molecules and excess charges are left over as residues by the successive fission and continuous solvent evaporation. Thus desorption of the analyte molecules is a passive process, and so is the analyte charging process. In IEM, the analyte ions are emitted from the droplets by means of an active process. Both CRM and IEM have their supporters and are more applicable in some situations[24]. However, CRM is believed to be the mechanism by which ionic forms of very large molecules, including multiply charged ones, are formed in ESI[25, 26].

Atmospheric Pressure Condition

ESI is normally operated at atmospheric pressure. The formation of gas phase ions from the charged droplets requires a source of enthalpy to evaporate the solvent. The most convenient source of enthalpy is the thermal energy of ambient air, which, by colliding with the charged droplets, increases the thermal energy of the solvent molecules and assists in the desolvation of the charged droplets. Even if the solvent has extremely high vapour pressure which would allow evaporation in vacuum without much enthalpy, or if the droplets are evaporated by heating, the kinetic energy that ions obtain in vacuum would be so high that no mass analyzer could accommodate the ions. By collision with surrounding gas molecules, the ion kinetic energy is limited. Furthermore, electric discharge is greatly suppressed by the ambient air, especially when ESI is performed in negative mode. The discharge would increase

the capillary current and degrade the ESI performance. In the presence of air, especially oxygen, which has a positive electron affinity, free electrons are captured by the ambient gas, reducing the possibility of discharge[27-29].

1.3.3 Electrochemical Processes in ESI

The electrochemical processes in ESI have not been completely understood. In half of the experiments carried out in this thesis (see Chapter 2 for details), a non-conducting fused silica capillary is used as the ESI tip. The silica capillary, although concentrically surrounded by a stainless steel tube, totally isolates the sample solution from any high voltage applied by the electrode. Although we were trying to maintain a liquid contact with the metal tube at the tip of the capillary during the experiment, that was not always the case. Figure 1-3 shows the configuration of the sprayer. When ESI was in process, the out-coming liquid only formed a cone based on the capillary, without showing any evidence of touching the metal tube. However, the spray still continued for several hours.

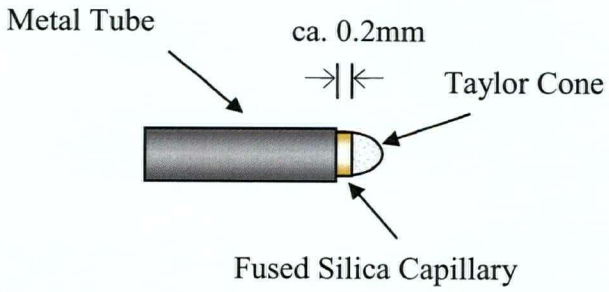

Figure 1-3 Configuration of the spray tip with the liquid sample coming out from a silica capillary and not contacting the metal tube.

Although without complete agreement, some consensus has formed that, in the long term, electrochemical reactions are necessary for maintaining the excess charges that are

separated from the liquid[30]. If the charged droplets bear excess positive charges, there must be extra positive charges produced or negative charges consumed in the bulk solution, which can only happen at contacting surfaces between the liquid and metal electrode by way of electrochemical reactions[31, 32]. One possible electrolytic reaction involves the metal atoms from the needle giving their electrons to the power supply and becoming cations to compensate for the loss of positive charge due to electrospray (case 1). Another possibility is that one or several of the solvent components lose electrons to the power supply electrolytically to become cations in the solution. The electrochemical reactions could be the discharge of anions (case 2) or the oxidation of neutral solvent (case 3), with the examples as following:

Case 1, anodic corrosion of the needle:

$$Fe(s) = Fe^{2+} + 2e^{-} \text{ (Electrons to the electrode)}$$

Case 2, discharge of anions:

$$2Cl^{-} = Cl_2 + 2e^{-} \text{ (Electrons to the electrode)}$$

Case 3, solvent oxidation:

$$H_2O = 2H^{+} + \frac{1}{2}O_2 + 2e^{-} \text{ (Electrons to the electrode)}$$

No matter the form of the electrochemical reactions, the final result is the loss of electrons to the power supply. When the needle is made of metal, the electrochemical reactions should happen at the needle tip and cannot take place any further upstream inside the needle[33, 34]. When the needle is a non-conducting extension of the stainless steel tube, the electrolytic reactions happen where the extension is connected to the metal tube. As for the case that the

needle is made of silica, any loss of positive charges still has to be equalized somewhere in the solution path, usually back to wherever the solution is in contact with an electron-accepting surface which ultimately has a connection to the power supply. We suspect that in the experiment we have done, where the silica capillary is the only solution path, the connection could be at the metal needle of a sample infusing syringe, which is the only contact between the solution and a conductor.

It is worthwhile to mention that electrochemical reactions are not a necessity for the production of charged droplets[30]. As mentioned above, when Iribarne and Thomson were studying ion evaporation from charged seawater droplets, they produced charged droplets by induction which involved no electrochemical reactions. By ion evaporation, the charged droplets generate gas phase ions the same as those produced by electrospray.

In electrospray, when all the charges separated from the liquid have the same sign, the electrochemical reactions are clearly the electron acceptor, compensating for the loss of cations and maintaining the electrospray. However, in most cases, ions that are not present in the solution but produced by the reactions do not have a significant effect on the sample being analyzed, nor do the ions show on the spectra obtained by MS because of their very low abundance. Furthermore, the ions produced electrolytically are usually low in molecular weight compared to the sample molecules. Therefore, under most common operating conditions, the electrochemical processes rarely have an obvious effect on the identity and relative abundances of the ions in an ESI mass spectrum.

1.4 Improving the performance of ESI

When ESI became an ion source for mass spectrometry, the transmission of ions into the mass spectrometer had to be taken into account. There are thus three main processes whose efficiency accounts for the overall efficiency of the performance of ESI as an ion source. The first two processes are electrospray and ionization. The third process is the "transmission" of ions from atmospheric pressure into the vacuum driven by electric forces.

To improve the efficiency of the overall process, a great many variables are inevitably involved and interacting with each other. Optimizing the overall process requires the understanding of the parameters involved in each of the steps, as well as the combined effect. However, the mechanism of ESI introduced above could provide the basis of an improvement.

1.4.1 Improving Electrospray Efficiency

The most important factors affecting electrospray are the chemical and physical properties of the sample solution, as well as the sample flow rate and peripheral pneumatic conditions. The solution properties include surface tension, viscosity, conductivity, permittivity, and polarizability, as well as the chemical composition of the sample[35]. The sample flow rate has a significant influence on the ESI efficiency. It was shown by Wilm *et al.*[36] that the size of charged droplets produced from the Taylor cone emission was proportional to the two-thirds power of the flow rate. Small droplets have high surface-to-volume ratio, which makes available a large proportion of analyte molecules for evaporation from the droplets[37] if the ion evaporation mechanism (IEM) is followed. At the same time, if the charged residue

mechanism (CRM) is dominant, the evaporation of solvent also happens faster when the initial droplet size is smaller. With the evaporation of solvent, the salt in the sample accumulates in the droplets, resulting in a salt concentration increase. Producing smaller droplets reduces the amount of salt in the original droplets and prevent crystallization of salt in the residue[38]. Furthermore, considering the charge separated from the ion source remains constant, smaller droplets bear a higher charge density compared to larger ones[37].

The configuration of the needle on which the liquid cone is based has been shown to be irrelevant to the electrospray process[35]. However, a smaller needle diameter is preferred for low flow rates. Although not immediately dominating the efficiency of electrospray, the smaller diameter of the needle tip is believed to stabilize the liquid cone when the sample flow rate is small, as in the case of nanospray[36]. The tip for nanospray is typically a few micrometers in diameter.

The electric field that induces the electrospray is sometimes overlooked by researchers in this area. Some suggested that there is a threshold for the potential on the sprayer, and once the potential reached the threshold, the onset voltage as we call it in later chapters, the current emitted from the electrospray becomes constant[25, 35]. However, it has been found that there are different spray pulsation modes associated with the applied voltage on the sprayer[39, 40]. At lower voltages, the electrospray takes the form of a pulsation spray instead of forming a continuous spray. The increase of voltage on the sprayer changes the pulsation from low frequency to high frequency, and, eventually, continuous emission. In the continuous emission mode, further increases to the potential have little impact on the current[40]. However, it was

suggested by Wilm and Mann that, higher spray voltage would reduce the size of charged droplets emitted from the Taylor Cone[36], and thus improve the ionization process. Therefore, even at the continuous electrospray stage, ion signal can still increase, until the voltage gets so high that a discharge appears. In most ESI studies, adjusting the voltage attracts little interest compared to other parameters, because the improvement in signal is difficult to characterize. Despite this, the high voltage is the first necessity of ESI.

1.4.2 Improving Ionization Efficiency

The term "ionization" here refers to the process by which gas phase ions are produced from the charged droplets. This process is a series of actions including droplet shrinkage, Coulomb fission, and the formation of gaseous ions from the droplets through one of the two mechanisms: CRM and IEM. This process is almost completely dependent on the properties of the droplet itself. One important property is the surface activity of the analyte in the droplet. It is generally believed that the surface active analytes that have high affinity for the surface of the droplets have higher ESI-MS response[26, 41, 42]. For most ESI operations where water is the solvent, nonpolar ions would prefer to move to the droplets surface and tend to evaporate from the droplet first. The effect of surface activity on the response of ESI was shown by Cech and Enke[43] in their study of peptides. Peptides that had more nonpolar (hydrophobic) side-chains appeared with higher intensity on the mass spectrum than those with less nonpolar side-chains.

The environmental conditions, such as ambient gas property, pneumatic nebulization and even temperature, have a great impact on the "ionization" process. However, the external

electric field seems to have little effect. Once dispersed from the Taylor cone, a droplet is floating in the air, and the electric field only provides kinetic energy to the droplet.

1.4.3 Improving Ion Transmission

The third process, i.e. the transmission, always has a low efficiency due to the spreading of gaseous ions caused by columbic repulsion among ions and collisions with ambient air.

Operating electrospray at a low flow rate (reduced flow rate (80 nL/min - 1μL/min) or nanospray (<80 nL/min)) allows the capillary tip to be located only 0.5 to 2 mm from the orifice of the MS, so that almost the entire spray is drawn into the vacuum region[37, 44]. Nanospray generates smaller droplets and improves the ionization efficiency. As a result, the transmission efficiency is greatly improved compared to higher flow rate ESI sources. In nanospray applications, the capillary tips have to be drawn out by a mechanical or laser puller to make the orifice 1 to 10 μm in diameter. This imposes a technical difficulty and leads to the possibility of clogging of the capillary. No syringe or sample infusing device is needed for nanospray, as the sample is dispersed only by the electric field at a flow rate of about 20-50 nL/min. Since there is no other connection to the capillary, the tip of the capillary has to be coated with a thin layer of metal, e.g. gold, or a thin metal wire has to be inserted into the capillary for the electric contact. Because of its closeness to the counter plate, nanospray only requires a voltage of 500-1000 volts.

However, many ESI applications are used to interface HPLC and MS, where the sample flow rates are between 1 to 100 μL/min or higher. In normal high flow rate (1 - 20 μL/min) ESI, to avoid neutrals from entering MS, the tip of capillary is placed 1 to 3 cm away from the

curtain plate aperture, while the aperture in the orifice is only 0.25 mm in diameter. Furthermore, the repulsion among the ions results in ion dispersion. The geometry, as well as coulombic repulsion, determines that low ion transmission efficiency is inevitable. The ion loss due to the transmission process can be greater than 99.99%. This prediction might be conservative, but it is generally accepted that the transmission efficiency limits the overall sensitivity of ESI-MS[45, 46].

Research to improve the transmission efficiency has been carried out by many scientists, and the most practical way is some kind of focusing that can be realized by either gas flow focusing or electric field focusing.

Covey *et al.* developed an ion spray with an intersecting flow of heated gas[47]. Sample coming out from LC or another sample source, assisted by a high velocity coaxial gas jet, is sprayed through a capillary towards the entrance aperture of the MS. A flow of heated gas intersects with the first flow at a region upstream of an orifice, providing a focusing effect and helping to evaporate the droplets. Alternatively, the two flows can be located directly opposite to each other and both at right angles to the axis through the orifice. A third gas flow can be used to draw the droplets toward the orifice. The heated intersecting gas flow provides a 10 to 100 times increase in sensitivity and also allows controlled desolvation of ions.

Zhou *et al.*[48] and Hawkridge *et al.*[49] described an industrial air amplifier assembled on the ESI source. Based on the venturi effect, at the inside of a rapid gas flow, the gas pressure decreases dramatically resulting in a pressure difference between the gas flow and the surrounding air environment. Therefore the air outside of the air amplifier is drawn towards the

inside. In their modified ion source, a flow of high-velocity nitrogen is supplied concentrically into an air amplifier which drags aerosols produced by ESI together with it and greatly improves the efficiency. The rapidly moving gas tends to flow along the surface it attaches to, known as the Coanda effect, which helps to direct the gas flow to the aperture, therefore providing a focusing effect. This converging gas flow around the electrospray tip also assists in desolvating the charged droplets. When a voltage was applied to the air amplifier to further assist in ion focusing, an 18-fold increase in ion intensity was observed.

Franzen invented a device for the introduction of ions into the gas stream of an aperture to a mass spectrometer[50]. The device provided ion guidance by using a ring electrode that is located outside of the mass spectrometer. Ions passing through the ring electrode are guided into a funnel-shaped isolating inlet path through which they enter the mass spectrometer. The ring electrode has an ion-drawing potential and generates an electrostatic field between the spray cloud and the inlet aperture which has field lines that are primarily concentrated on the ring-shaped electrode. This ion-attracting ring electrode is different from most other electrical lens devices that are ion-repelling. However, all of them are designed for the purpose of focusing.

Gulcicek *et al.* described an ion focusing system at the interface region between the mass spectrometer and atmospheric ion source[51]. Proper positioning of the electrostatic lens within a transition flow pressure region allows for collimation of the ion beam, enhancing the transmission efficiency of ions to the mass spectrometer. The configuration allows the increase

in ion transmission efficiency to be independent of the adjustment of the desired degree of collision induced dissociation and declustering processes.

The work of Smith *et al.* on improving the transmission efficiency includes the use of a ring electrode[52-54], an ion funnel[46, 55-59], and multi-capillary inlet[56, 58].

The ring electrode[52, 53] is located downstream from the ESI sprayer and in front of the orifice. Although the function of the ring electrode was not described, the purpose of this lens system should be some kind of electric guidance.

The ion funnel, reported by Shaffer *et al.*[46, 55-57, 59] consists of a series of cylindrical ring electrodes of progressively smaller internal diameters to which RF and DC potentials are co-applied for the purpose of collisional focusing under pressures of 1-10 torr. A heated multi-capillary inlet, described by Kim *et al.*, was assembled between the ion spray source and the ion funnel to produce more uniform droplet evaporation conditions. The combination of the ion funnel and multi-capillary inlet resulted in a 23 times improvement of ion transmission.

Thompson reported the use of a hemispherical-shaped ion lens at atmospheric pressure positioned at the back of a nanospray source[60]. With a novel profiling devise, the three dimensional current density of the spray plum was obtained. It was found that the current density was increased by three times with the ion lens. The ion flux current measurement suggests that the ion transmission to the mass spectrometer was doubled.

Our previous work demonstrated that an atmospheric pressure ion lens improved the performance of the electrospray ion source at flow rates from 0.2 μL to 5 μL/min[61, 62]. An at

least 2-fold increase in the ion signal with 2-fold reduction in signal variation, and a much broader range of applicable sprayer positions, were achieved with the help of the ion lens. These improvements were obtained partly due to the change in the shape of the equipotential lines near the tip of the sprayer. The electric field at the capillary tip was less defocusing, thus improving the trajectories of gaseous ions, and allowing more ions enter into the MS.

1.5 Scope of This Study

This study further investigates the effect of the atmospheric ion lens, and focuses on the electric field and possible influence on the performance of ESI as a mass spectrometry ion source. A systematic study of lens and spray voltages is carried out both experimentally and theoretically. In Chapter 2, the ion lens experimental results are shown with respect to the relationship of the spray and lens voltages and their effects on ion signal, as well as the current-voltage relationship. The results show that the ion lens has two effects: changing the operational spray voltage range and ion focusing. Chapter 3 demonstrates theoretical calculation of the potential distribution and the electric field in the space, and provides a possible explanation of the experimental results. The electric field calculation is carried out directly as well as by numerical methods. The exact value of the field is obtained by a finite element method using a program named FEMLAB®. The results suggest that adjusting the ion lens voltage can change the electric field significantly, even when the spray voltage remains constant. In Chapter 4, more experimental results concerning other aspects of ESI are explained. A new ion source and its configuration are described, followed by the suggestion of combining

the new source with an additional spray source, with ion lenses on both of them. Chapter 5 is the conclusion and future prospects of this research.

1.6 References

1. Yamashita, M. and Fenn, J.B., *Electrospray ion-source - another variation on the free-jet theme.* Journal of Physical Chemistry, 1984. **88**(20): p. 4451-4459.

2. Whitehouse, C.M., Dreyer, R.N., Yamashita, M. and Fenn, J.B., *Electrospray interface for liquid chromatographs and mass spectrometers.* Analytical Chemistry, 1985. **57**(3): p. 675-679.

3. Schlichtherle-Cerny, H., Affolter, M. and Cerny, C., *Hydrophilic interaction liquid chromatography coupled to electrospray mass spectrometry of small polar compounds in food analysis.* Analytical Chemistry, 2003. **75**(10): p. 2349-2354.

4. Mauri, P., Migliazza, B. and Pietta, P., *Liquid chromatography/electrospray mass spectrometry of bioactive terpenoids in ginkgo biloba l.* Journal of Mass Spectrometry, 1999. **34**(12): p. 1361-1367.

5. Pergantis, S.A., Winnik, W. and Betowski, D., *Determination of ten organoarsenic compounds using microbore high-performance liquid chromatography coupled with electrospray mass spectrometry mass spectrometry.* Journal of Analytical Atomic Spectrometry, 1997. **12**(5): p. 531-536.

6. Gelpi, E., *Biomedical and biochemical applications of liquid-chromatography mass-spectrometry.* Journal of Chromatography A, 1995. **703**(1-2): p. 59-80.

7. Bateman, K.P., *Electrochemical properties of capillary electrophoresis-nanoelectrospray mass spectrometry.* Journal of the American Society for Mass Spectrometry, 1999. **10**(4): p. 309-317.

8. Mazereeuw, M., Hofte, A.J.P., Tjaden, U.R. and vanderGreef, J., *A novel sheathless and electrodeless microelectrospray interface for the on-line coupling of capillary zone electrophoresis to mass spectrometry.* Rapid Communications in Mass Spectrometry, 1997. **11**(9): p. 981-986.

9. Bednar, P., Lemr, K., Bartak, P., Sevcik, J., Hlavac, J., Styskala, J., Wiedermannova, I. and Stransky, Z., *Capillary electrophoresis/mass spectrometry: A promising tool for the control of some physiologically hazardous compounds. I - derivatives of 3-quinuclidinol.* Journal of Mass Spectrometry, 2002. **37**(12): p. 1213-1218.

10. Dole, M., Mack, L.L. and Hines, R.L., *Molecular beams of macroions.* Journal of Chemical Physics, 1968. **49**(5): p. 2240-2249.

11. Cook, K.D., *Electrohydrodynamic mass-spectrometry.* Mass Spectrometry Reviews, 1986. **5**(4): p. 467-519.

12. Fenn, J.B., Mann, M., Meng, C.K. and Whitehouse, C.M., *Electrospray ionization for mass spectrometry of large biomolecules.* Science, 1989. **246**: p. 64-71.

13. Fenn, J.B., *Electrospray wings for molecular elephants (nobel lecture).* Angewandte Chemie-International Edition, 2003. **42**(33): p. 3871-3894.

14. Fenn, J.B., *Electrospray ionization mass spectrometry: How it all began.* Journal of Biomolecular Techniques, 2002. **13**: p. 101-118.

15. Taylor, G., *Electrically driven jets.* Proceedings of the Royal Society of London Series a-Mathematical and Physical Sciences, 1969. **313**(1515): p. 453-475.

16. Taylor, G., *Disintegration of water drops in an electric field.* Proceedings of the Royal Society of London Series a-Mathematical and Physical Sciences, 1964. **280**: p. 383-397.

17. Cole, R.B., *Electrospray ionization mass spectrometry.* 1997, New York: John Wiley & Sons, Inc.

18. Taflin, D.C., Ward, T.L. and Davis, E.J., *Electrified droplet fission and the rayleigh limit.* Langmuir, 1989. **5**(2): p. 376-384.

19. Kebarle, P. and Tang, L., *From ions in solution to ions in the gas phase: The mechanism of electrospray mass spectrometry.* Analytical Chemistry, 1993. **15**: p. 973A-986A.

20. Gomez, A. and Tang, K.Q., *Charge and fission of droplets in electrostatic sprays.* Physics of Fluids, 1994. **6**(1): p. 404-414.

21. Mack, L.L., Kralik, P., Rheude, A. and Dole, M., *Molecular beams of macroions.Ii.* Journal of Chemical Physics, 1970. **52**(10): p. 4977-4986.

22. Thomson, B.A. and Iribarne, J.V., *Field-induced ion evaporation from liquid surfaces at atmospheric-pressure.* Journal of Chemical Physics, 1979. **71**(11): p. 4451-4463.

23. Iribarne, J.V. and Thomson, B.A., *Evaporation of small ions from charged droplets.* Journal of Chemical Physics, 1976. **64**(6): p. 2287-2294.

24. Kebarle, P., *A brief overview of the present status of the mechanisms involved in electrospray mass spectrometry.* Journal of Mass Spectrometry, 2000. **35**(7): p. 804-817.

25. Cole, R.B., *Some tenets pertaining to electrospray ionization mass spectrometry.* Journal of Mass Spectrometry, 2000. **35**: p. 763-772.

26. Fenn, J.B., *Ion formation from charged droplets - roles of geometry, energy, and time.* Journal of the American Society for Mass Spectrometry, 1993. **4**(7): p. 524-535.

27. Smith, D.P.H., *The electrohydrodynamic atomization of liquids.* IEEE Transactions on Industry Applications, 1986. **22**(3): p. 527-535.

28. Ikonomou, M.G., Blades, A.T. and Kebarle, P., *Electrospray mass-spectrometry of methanol and water solutions suppression of electric-discharge with sf6 gas.* Journal of the American Society for Mass Spectrometry, 1991. **2**(6): p. 497-505.

29. Wampler, F.M., III, Blades, A.T. and Kebarle, P., *Negative ion electrospray mass spectrometry of nucleotides: Ionization from water solution with sf6 discharge suppression.* Journal of the American Society for Mass Spectrometry, 1993. **4**: p. 289-295.

30. de la Mora, J.F., Van Berkel, G.J., Enke, C.G., Cole, R.B., Martinez-Sanchez, M. and Fenn, J.B., *Electrochemical processes in electrospray ionization mass spectrometry - discussion.* Journal of Mass Spectrometry, 2000. **35**(8): p. 939-952.

31. Van Berkel, G.J. and Zhou, F.M., *Electrospray as a controlled current electrolytic cell - electrochemical ionization of neutral analytes for detection by electrospray mass-spectrometry.* Analytical Chemistry, 1995. **67**(21): p. 3958-3964.

32. Van Berkel, G.J. and Zhou, F.M., *Characterization of an electrospray ion-source as a controlled-current electrolytic cell.* Analytical Chemistry, 1995. **67**(17): p. 2916-2923.

33. Van Berkel, G.J., Zhou, F.M. and Aronson, J.T., *Changes in bulk solution ph caused by the inherent controlled-current electrolytic process of an electrospray ion source.* International Journal of Mass Spectrometry and Ion Processes, 1997. **162**(1-3): p. 55-67.

34. VanBerkel, G.J. and Zhou, F.M., *Observation of gas-phase molecular dications formed from neutral organics in solution via the controlled-current electrolytic process inherent to electrospray.* Journal of the American Society for Mass Spectrometry, 1996. **7**(2): p. 157-162.

35. Fernandez De La Mora, J. and I.G., L., *The current emitted by highly conducting taylor cones.* Journal of Fluid Mechanics, 1994. **260**: p. 155-184.

36. Wilm, M.S. and Mann, M., *Electrospray and taylor-cone theory, doles beam of macromolecules at last.* International Journal of Mass Spectrometry and Ion Processes, 1994. **136**(2-3): p. 167-180.

37. Wilm, M. and Mann, M., *Analytical properties of the nanoelectrospray ion source.* Analytical Chemistry, 1996. **68**: p. 1-8.

38. Juraschek, R., Dulcks, T. and Karas, M., *Nanoelectrospray-more than just a minimized-flow electrospray ionization source.* Journal of the American Society for Mass Spectrometry, 1999. **10**: p. 300-308.

39. Loeb, L.B., Kip, A.F. and Hudson, G.G., *Pulses in negative point-to-plane corona.* Physical Review, 1941. **60**: p. 714-722.

40. Juraschek, R. and Rollgen, F.W., *Pulsation phenomenon during electrospray ionization.* International Journal of Mass Spectrometry, 1998. **177**: p. 1-15.

41. Iribarne, J.V., Dziedzic, P.J. and Thomson, B.A., *Atmospheric-pressure ion evaporation mass-spectrometry.* International Journal of Mass Spectrometry and Ion Processes, 1983. **50**(3): p. 331-347.

42. Cech, N.B. and Enke, C.G., *Effect of affinity for droplet surfaces on the fraction of analyte molecules charged during electrospray droplet fission.* Analytical Chemistry, 2001. **73**: p. 4632-4639.

43. Cech, N.B. and Enke, C.G., *Relating electrospray ionization response to nonpolar character of small peptides.* Analytical Chemistry, 2000. **72**: p. 2717-2723.

44. Karas, M., Bahr, U. and Dulcks, T., *Nano-electrospray ionization mass spectrometry: Addressing analytical problems beyond routine.* Fresenius' Journal of Analytical Chemistry, 2000. **366**: p. 669-676.

45. Cech, N.B. and Enke, C.G., *Practical implications of some recent studies in electrospray ionization fundamentals.* Mass Spectrometry Reviews, 2001. **20**: p. 362-387.

46. Shaffer, S.A., Tolmachev, A., Prior, D.C., Anderson, G.A., Udseth, H.R. and Smith, R.D., *Characterization of an improved electrodynamic ion funnel interface for electrospray ionization mass spectrometry.* Analytical Chemistry, 1999. **71**: p. 2957-2964.

47. Covey, T.R. and Anacleto, J.F., *Ion spray with intersecting flow, US Patent 5,412,208.* 1995.

48. Zhou, L., Yue, B.F., Dearden, D.V., Lee, E.D., Rockwood, A.L. and Lee, M.L., *Incorporation of a venturi device in electrospray ionization.* Analytical Chemistry, 2003. **75**(21): p. 5978-5983.

49. Hawkridge, A.M., Zhou, L., Lee, M.L. and Muddiman, D.C., *Analytical performance of a venturi device integrated into an electrospray ionization fourier transform ion*

cyclotron resonance mass spectrometer for analysis of nucleic acids. Analytical Chemistry, 2004. **76**(14): p. 4118-4122.

50. Franzen, J., *Method and device for the introduction of ions into the gas stream of an aperture to a mass spectrometer, US Patent 5,747,799.* 1998.

51. Gulcicek, E.E. and Whitehouse, C.M., *Ion focusing lensing system for a mass spectrometer interfaced to an atmospheric pressure ion source, US Patent 5,432,343.* 1995.

52. Olivares, J.A., Nguyen, N.T., Yonker, C.R. and Smith, R.D., *Online mass-spectrometric detection for capillary zone electrophoresis.* Analytical Chemistry, 1987. **59**(8): p. 1230-1232.

53. Smith, R.D., Barinaga, C.J. and Udseth, H.R., *Improved electrospray ionization interface for capillary zone electrophoresis - mass-spectrometry.* Analytical Chemistry, 1988. **60**(18): p. 1948-1952.

54. Smith, R.D., Olivares, J.A., Nguyen, N.T. and Udseth, H.R., *Capillary zone electrophoresis mass-spectrometry using an electrospray ionization interface.* Analytical Chemistry, 1988. **60**(5): p. 436-441.

55. Shaffer, S.A., Tang, K., Anderson, G.A., Prior, D.C., Udseth, H.R. and Smith, R.D., *A novel ion funnel for focusing ions at elevated pressure using electrospray ionization mass spectrometry.* Rapid Communications In Mass Spectrometry, 1997. **11**: p. 1813-1817.

56. Kim, T., Udseth, H.R. and Smith, R.D., *Improved ion transmission from atmospheric pressure to high vacuum using a multicapillary inlet and electrodynamic ion funnel interface.* Analytical Chemistry, 2000. **72**: p. 5014-5019.

57. Shaffer, S.A., Prior, D.C., Anderson, G.A., Udseth, H.R. and Smith, R.D., *An ion funnel interface for improved ion focusing and sensitivity using electrospray ionization mass spectrometry.* Analytical Chemistry, 1998. **70**: p. 4111-4119.

58. Kim, T., Tang, K., Udseth, H.R. and Smith, R.D., *A multicapillary inlet jet disruption electrodynamic ion funnel interface for improved senstivity using atmospheric pressure ion sources.* Analytical Chemistry, 2001. **73**: p. 4162-4170.

59. Tang, K., Tolmachev, A.V., Nikolaev, E., Zhang, R., Belov, M.E., Udseth, H.R. and Smith, R.D., *Independent control of ion transmission in a jet disrupter dual-channel ion funnel electrospray ionization ms interface.* Analytical Chemistry, 2002. **74**: p. 5431-5437.

60. Thompson, J.W., Eschelbach, J.W., Wilburn, R.T. and Jorgenson, J.W., *Investigation of electrospray ionization and electrostatic focusing devices using a three-dimensional electrospray current density profiler.* Journal of the American Society for Mass Spectrometry, 2005. **16**(3): p. 312-323.

61. Schneider, B.B., Douglas, D.J. and Chen, D.D.Y., *An atmospheric pressure ion lens to improve electrospray ionization at low solution flow-rates.* Rapid Communications In Mass Spectrometry, 2001. **15**: p. 2168-2175.

62. Schneider, B.B., Douglas, D.J. and Chen, D.D.Y., *An atmospheric pressure ion lens that improves nebulizer assisted electrospray ion soursces.* Journal of the American Society for Mass Spectrometry, 2002. **13**: p. 906-913.

Chapter 2

Effect of the Ion Lens Voltage on ESI Performance

2 Effect of the Ion Lens Voltages on ESI Performance

2.1 Introduction

The operation of the electrospray ion source includes three processes: the generation of charged droplets from the liquid surface ("electrospray"), the break-down of the droplets and the generation of gaseous ions ("ionization"), and the transmission of the ions from atmospheric pressure into the mass spectrometer ("transmission"). The overall efficiency of these three processes is generally believed to be less than 0.1%[1, 2]. Research into improving the efficiency is complicated by a number of variables, which have been described in Chapter 1. Furthermore, those factors are not independent, and it is likely that a change in one variable has an influence on the effectiveness of other variables. For example, when the flow rate is reduced, the applied voltage, the diameter of the sprayer tip and the flow of nebulizer gas might all need to be readjusted to optimize the ion source efficiency.

Among all of the variables related to these three processes, the electric field is always a factor that needs to be considered. It is the origin of the electrospray and the driving and focusing forces to transmit ions into the mass spectrometer. Therefore, in this chapter, we will focus on the study of applied voltages on the sprayer and ion lens, since the electric field required by the ESI process is determined by the potential differences on the electrodes (sprayer, lens, and the curtain plate).

In most of our experiments, we tried to fix all the other variables but one. However, because of charging of the orifice and skimmer, other variables had to be optimized in longer

period of times, therefore we only compared results within a short experiment period (normally no longer than a few hours).

2.2 Experimental Methods

2.2.1 Mass Spectrometer

Most of the work in this thesis was done on a prototype single quadrupole ion spray mass spectrometer from SCIEX (Toronto, ON, Canada). Figure 2-1 is a schematic diagram of the prototype mass spectrometer. The external electrospray ion source is situated in the atmospheric pressure area in front of the curtain plate. The MS system can be divided into three vacuum sections. The first section is the interface region between the orifice and skimmer. This region was pumped by a rotary vane mechanical pump to a pressure of approximately 5 torr. Following this is an RF-only quadrupole ion guide (Q0 region), which is pumped to a pressure of approximately 7 mtorr. The short RF-only rods help focus the ions into the quadrupole rods (Q1 region), which comprise the mass analyzer. The Q1 region is pumped to about 4.5×10^{-5} torr. The Q0 and Q1 regions are pumped by two turbo pumps and are backed by a second rotary vane pump. Ions are detected with a Channeltron electron multiplier operated in ion counting mode, which converts the count of ions to an electrical signal that can be processed by the computer.

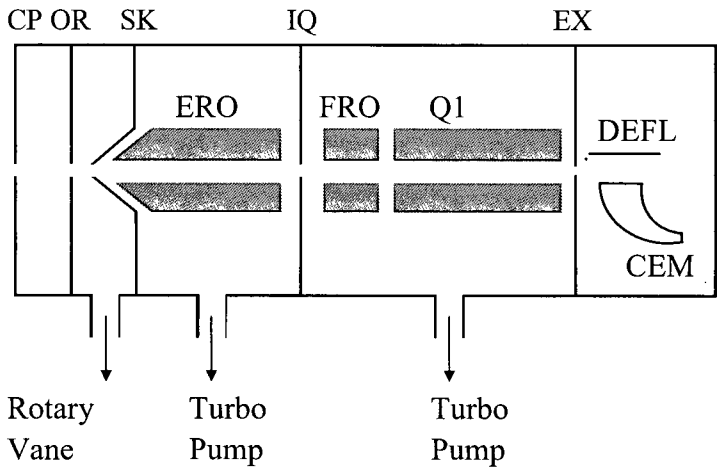

Figure 2-1 Schematic diagram of the single quadrupole mass spectrometer. CP: curtain plate; OR: orifice; SK: skimmer; IQ: interquad lens; EX: exit lens; ERO: entry rods; FRO: focus rods; Q1: quadrupole; DEFL: deflector; CEM: channel electron multiplier.

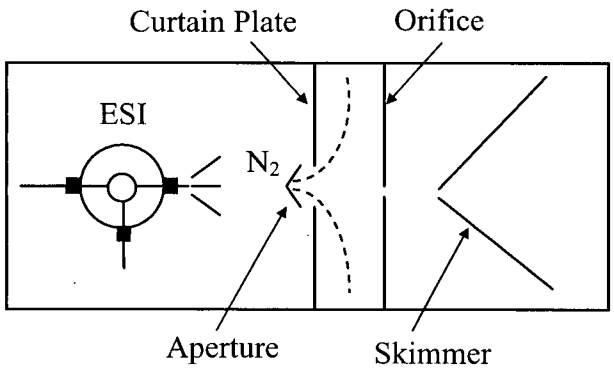

Figure 2-2 Schematic diagram of the electrospray ion source and the curtain gas N_2.

A curtain gas flows through the interface region between the curtain plate and the orifice, pushing outwards through the aperture in the curtain plate (Figure 2-2). Air and ions enter from atmospheric pressure into the interface region through a 0.25 mm aperture in the orifice plate. A skimmer with a 0.75 mm diameter aperture is placed behind the orifice. A potential drop is applied between the orifice and skimmer to accelerate the ions and facilitate the desolvation of ions. Furthermore, by adjusting the orifice-skimmer potential difference and curtain gas flow rate,

the degree of collision induced dissociation (CID) can be partially controlled[3-5]. Ultra high-purity nitrogen from Praxair (Mississauga, ON, Canada, manufacturer's stated purity 99.9995%) was used as the curtain gas for the single quadrupole system.

2.2.2 Ionspray Source and Ion Lens

A home-built ionspray source (Figure 2-3) is used in the experiment. Figure 2-4 shows the schematic geometry of the ion source and the ion lens. Sample was introduced to the sprayer through a fused silica capillary (Polymicro Technologies, Phoenix, AZ) with a 150 μm o.d. and a 50 μm i.d. The capillary was inserted into the two concentric stainless steel tubes (Small Parts Inc., Miami Lakes, FL) with standard wall thickness of 19 gauge and 27 gauge, respectively. The inner tube was to hold the silica capillary, and the space between the inner and outer tubes was used for the flow of the sheath gas (nebulizer). A stainless steel tee (Valco Instruments, Houston, TX) was used to hold the sprayer in place and to connect the nebulizer gas. The electrospray potential was applied through the mounting bracket to the stainless steel tee.

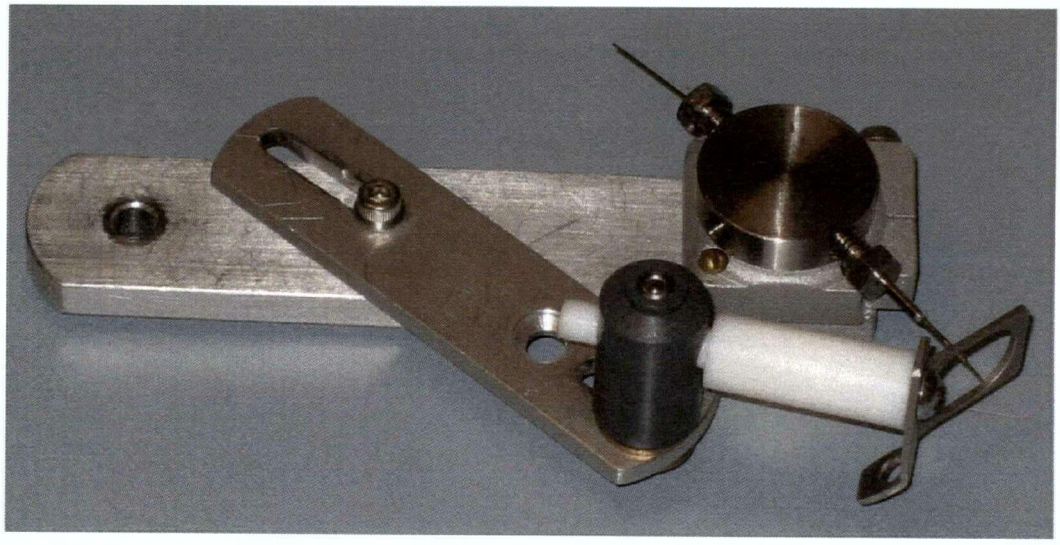

Figure 2-3 Homemade ionspray source.

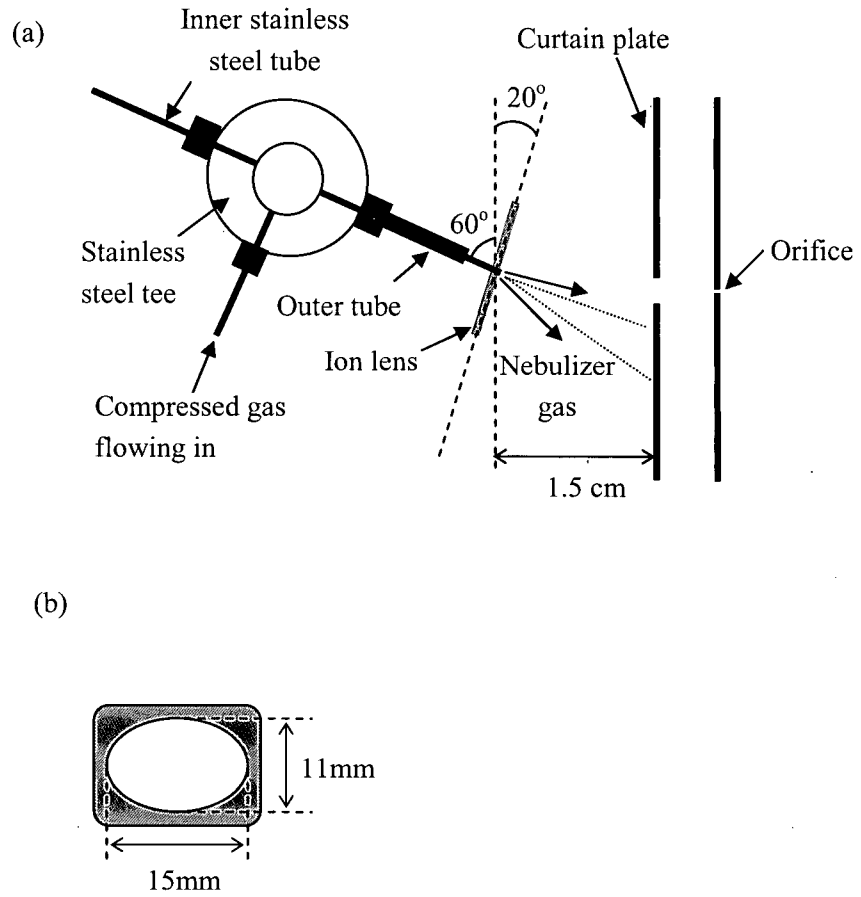

Figure 2-4 Schematic diagram of an electrospray ion source with an atmospheric pressure ion lens. (a) The configuration of the electrospray ion source and the ion lens. (b) Dimension of the ion lens.

The orientation of the sprayer capillary was about 60 degrees with respect to the curtain plate (also called the interface plate), as shown in Figure 2-4a. The ion lens was made from an oblong-shaped stainless steel ring with 1 mm thickness (Figure 2-4b). The vertical and horizontal distances of the ring were 11 mm and 15 mm, respectively. An arm on the mounting bracket was used to adjust the position of the ion lens with respect to the sprayer. The lens was set just behind the tip of the sprayer with about 80 degrees to the axis of the stainless steel sprayer. A Spellman (Hauppauge, NY) CZE 1000R power supply was used to provide high voltage to the lens.

The relative positions of the capillary tip, the inner stainless steel tube, and the outer stainless steel tube are illustrated in Figure 2-5. The capillary tip should not extend out of the metal tube too much, nor should it hide inside the metal tube. The sprayer tip is located off-axis to the aperture to prevent the neutral solvent from entering the mass spectrometer and to reduce contamination of the interface region. The sprayer is oriented at 60 degrees towards the curtain plate, in order to allow smaller peripheral ions to enter into the mass spectrometer.

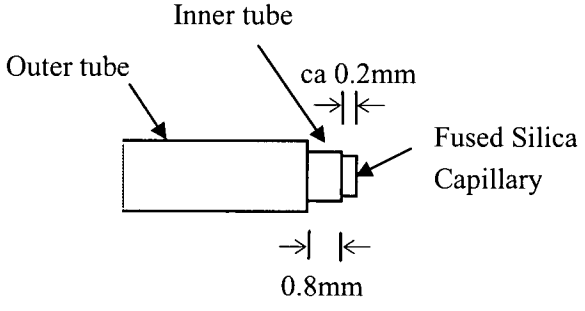

Figure 2-5 The relative position of the outer and inner stainless steel tube and the fused silica capillary. The inner tube is 0.8 mm longer than the outer tube, and the tip of capillary is placed out of the inner tube at a distance that just can be seen (ca. 0.2 mm).

The nebulizer gas is flushed concentrically with the sample flow to assist the breakdown and desolvation[6] of charged droplets sprayed out of the capillary end. In this work, the nebulizer gas used was compressed air (Praxair, Mississauga, ON, Canada, medical grade).

The solution flow was controlled by a syringe infusion pump (Model 22, Harvard Apparatus, South Natick, MA). A flow rate of 1-2 μL/min is most frequently used in this work.

2.2.3 Samples and Solutions

α- and β-Cyclodextrins (CDs) were purchased from Sigma (St. Louis, MO), and γ-CD was from Aldrich (Milwaukee, WI). The solutions were prepared by dissolving the powders in 10

mM certified ACS grade ammonium acetate (BDH Chemicals, Toronto, ON, Canada) to a concentration of about 1×10^{-4} M. Bradykinin, purchased from Sigma (St. Louis, MO) as acetate salt of 99% purity, was also prepared by dissolving the solid in 10 mM ammonium acetate to a concentration of 1×10^{-4} M.

α-, β- and γ-CDs have a ring shaped structure composed of 6, 7, and 8 monosaccharide units of 162 amu each. It is possible to dissociate the CD molecules when colliding them with other gas molecules, and, in the case of β-CD, shown in Figure 2-6, fragments of 1 to 6 monosaccharides are usually seen in MS spectra.

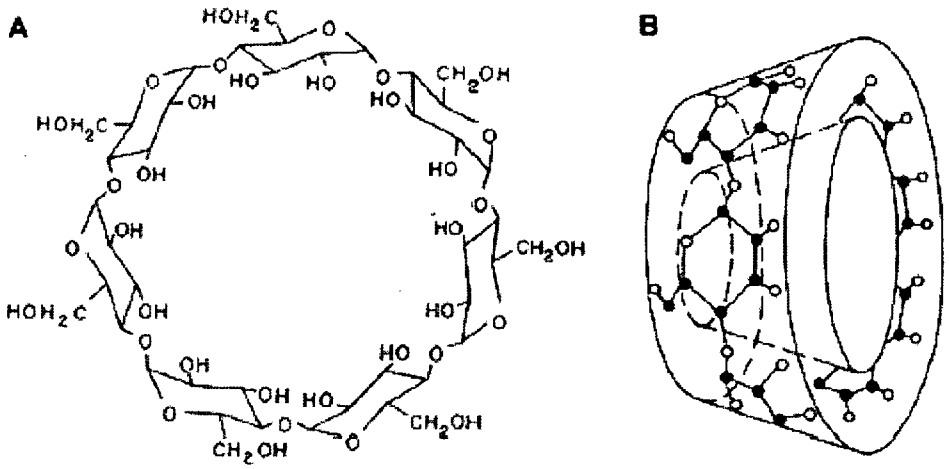

Figure 2-6 The chemical structure (A) and the toroidal shape (B) of theβ-Cyclodextrin molecule.

2.3 Results and Discussion

It has been reported that, when an appropriate voltage is applied, the ion lens flattens the shape of equipotential lines near the tip of the sprayer[4, 7] and helps to focus the ion trajectories more towards the center. Given the three processes mentioned in 2.1, this changing of equipotential lines and focusing effect is beneficial to the "transmission" process.

The "electrospray" process may also be improved by the use of the ion lens, since it also has a close dependence on the electric field. The electric field was predicted to be linearly proportional to the applied voltage based on a model with a capillary and a large, planar counter electrode[8-10]. However, the application of the ion lens will inevitably complicate this simple relationship and make the prediction of electric field and current a lot more difficult. The goal of our experiment is to study the possible variations in electric field, ion current, and ion signal caused by the atmospheric pressure ion lens.

2.3.1 Signal Intensity vs. Sprayer and Lens Voltages

Since the electric field is a determining factor that is created by the voltage difference on the three electrodes (sprayer, lens and the curtain plate), the primary study should be on the relationship of the ion lens voltage and the sprayer voltage with the signal intensity. The relationship between the ion lens voltage and the sprayer voltage and their impact on the ion signal were studied using α-, β-, and γ-CDs as analytes. In one experiment, 1.7×10^{-4} M γ-CD in 10 mM ammonium acetate was introduced with a sample flow rate of 2 μL/min, and the single ion mode was used to obtain the ion intensity at mass to charge ratio (m/z) 1298 for the molecular ion of γ-CD ($[M+H]^+$). As shown in Figure 2-7, each trace is plotted for the signal intensities under a fixed ion lens voltage. For each ion lens voltage, signals were measured under a series of different electrospray voltages, as indicated by the points in each of the traces. When the ion lens was set at 0 V, the maximum signal of 1.04×10^5 cps was observed at the electrospray voltage of about 3750 V. With increasing ion lens voltage, the maximum signal intensity increased accordingly. The electrospray voltage with which the maximum signal intensity was obtained

shifted from 3800 V to higher than 6000 V. At the ion lens voltage of 3500 V and the electrospray voltage of 6000 V, the signal intensity was observed to be 5.47×10^5 cps, which is more than 5 times of the maximum ion signal with ion lens at 0 V. This trend continues when the spray and ion lens voltages are raised even higher, but the power supply coming with the instrument does not allow the spray voltage to go higher than 6500 V, which is a reasonable limit for conventional ES operations.

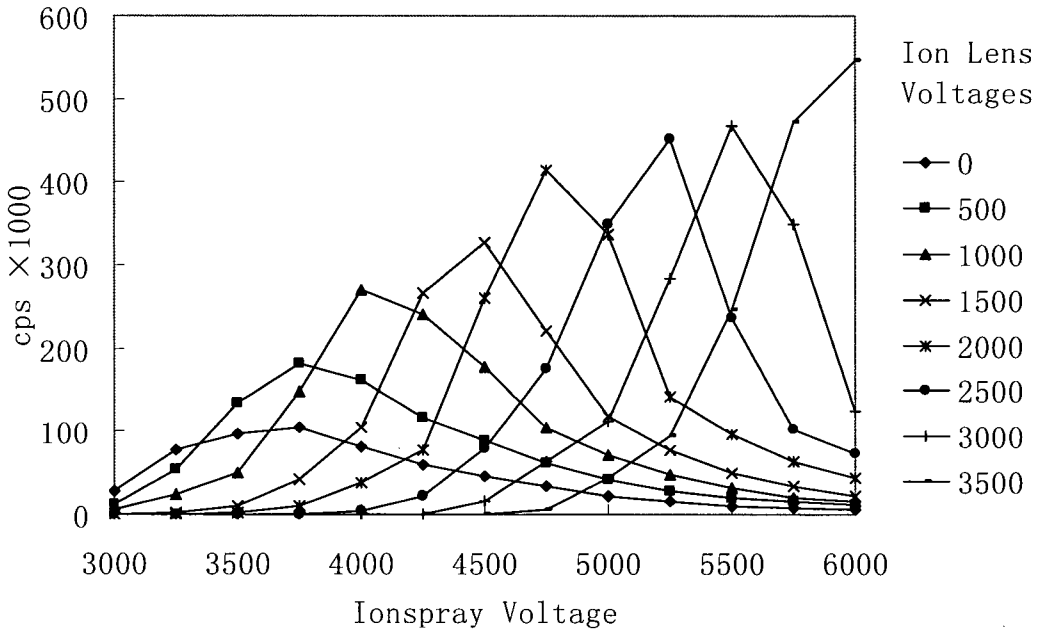

Figure 2-7 Signal intensity of γ-CD vs. sprayer voltage at different ion lens voltages. The ion lens voltages used are from 0 to 3500 V.

Similar trends were observed for α- and β-CDs, as shown in Figure 2-8 and Figure 2-9, and also singly charged ions of bradykinin, as shown in Figure 2-10. The multi-ion scans were set at m/z 974 and 1136 for α- and β-CDs, respectively. For bradykinin, singly, doubly and triply charged ions were observed in the spectra, but only the intensity of singly charged ions, m/z 1061, was plotted to show the trend. A 4-fold overall increase was observed for the singly charged

bradykinin. It should be noted that the ratio of singly, doubly, and triply charged ion intensity varied at different electrospray and ion lens voltages, but the general trends of signal variations with the voltage changes are similar.

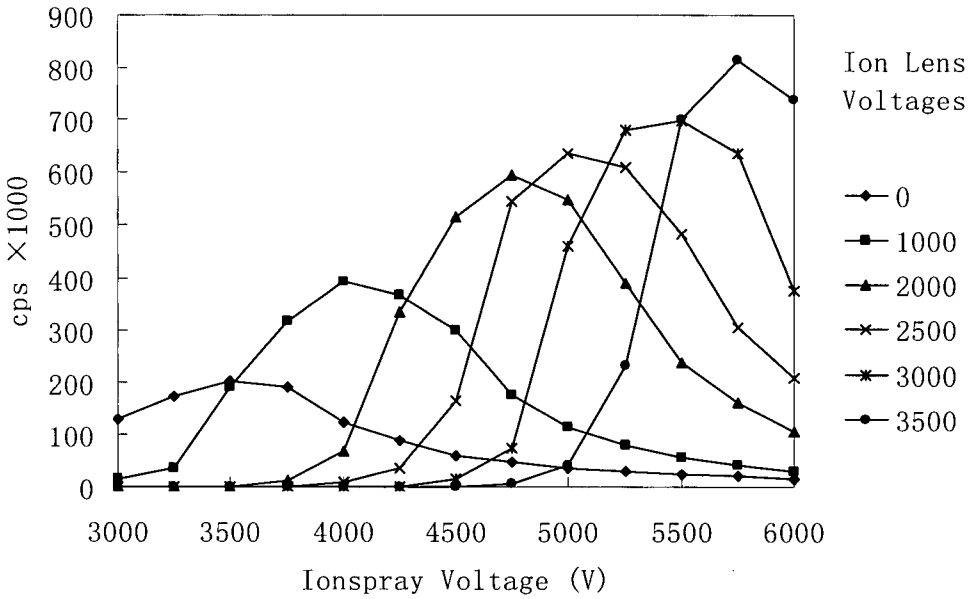

Figure 2-8 Signal intensity of α-CD vs. sprayer voltage at different ion lens voltages. The ion lens voltages used are from 0 to 3500 V.

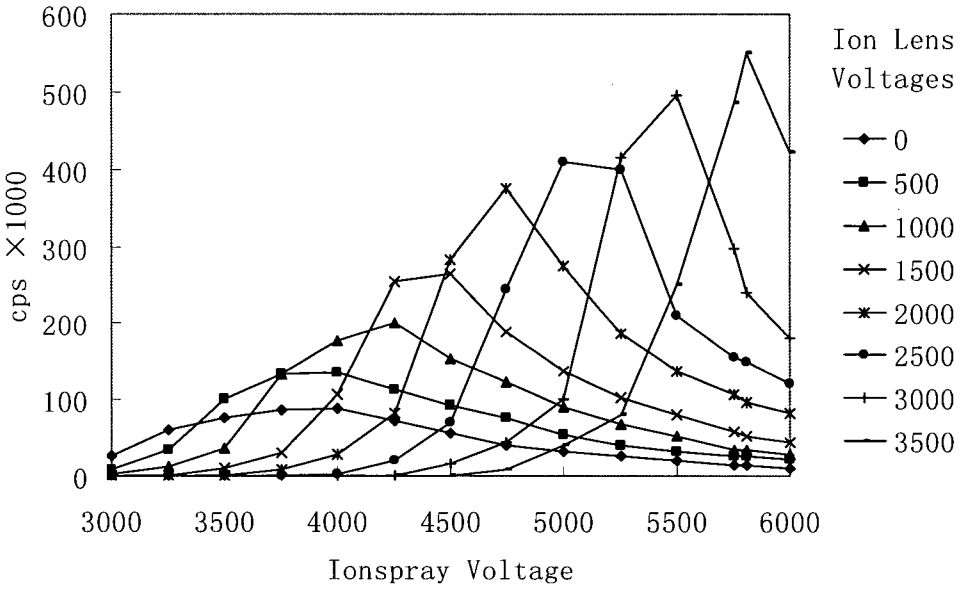

Figure 2-9 Signal intensity of β-CD vs. sprayer voltage at different ion lens voltages. The ion lens voltages used are from 0 to 3500 V.

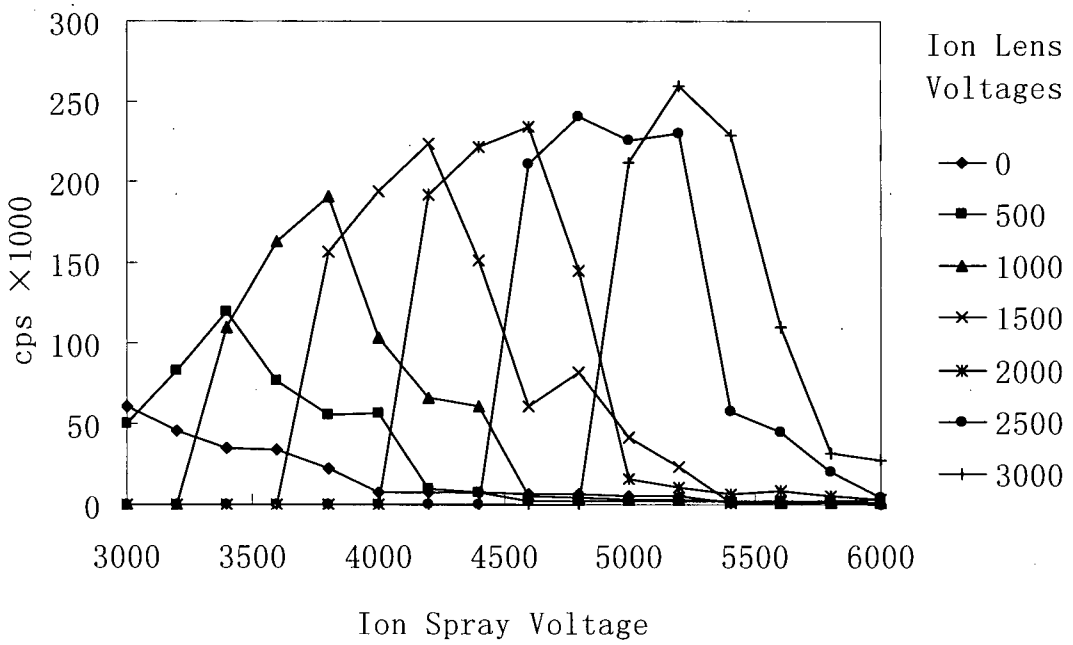

Figure 2-10 Signal intensity of bradykinin vs. sprayer voltage at different ion lens voltages. The ion lens voltages used are from 0 to 2500 V.

As described in Chapter 1, with positive voltage applied to the stainless steel tube, excess positive ions in the solution accumulate at the tip of the capillary, leading to the formation of a liquid cone. With the increase in electric field, a liquid filament enriched with positive ions is emitted from the cone tip, and fine charged droplets detach from the tip to form a steady jet[11-13]. The signal intensity increases with the voltage until a maximum is reached, as shown in each trace in Figure 2-7 to 2-10. This is in accordance with Smith and Wilm's suggestion that current and electric field follow a proportional relationship[10, 14]. Although it has also been shown that the electrospray emission is a constant current device once the minimum field threshold is satisfied[15], this does not conflict with our result, as the current cannot represent the ion signal, which depends not only on electrospray but also on the ionization process. Furthermore, at low potential, if the electrospray exists in a pulsing form instead of a stable and continuous spray, the signal will keep going up with the voltage due to the increasing emission pulsation frequency[11]. With a further increase in voltage, the length of the liquid filament decreases[13, 16], and the electrospray becomes unstable and generates multiple, gyrating jets of liquid filament[11, 17], collapsing the cone shape. Higher spray voltage may also cause a corona discharge, whereby some of the analyte ions from the solution can be neutralized and the analyte signal is reduced. It is also likely that the electric field around the sprayer will decrease when a discharge occurs[17, 18]. As a result, at voltages higher than the optimal range, a decrease in signal is observed, and the signal drops to a minimum when the cone jet collapses. Therefore, it is always necessary to set the spray voltage within a certain range to obtain stable and adequate signals. Even in this operational range, the signal still exhibits a certain range of variations.

Interestingly, with the application of the ion lens, adequate ion signal can be obtained far away from the optimal spray voltage range, as long as the potential difference between the sprayer and the ion lens is around a certain value. This observation implies that the electric field around the spray tip can be kept relatively constant only by choosing an appropriate voltage difference between the sprayer and lens, no matter what the absolute voltages are. This constant electric field assumption is further supported by calculations discussed in detail in Chapter 3.

An increased voltage difference between the sprayer and curtain plate would provide higher kinetic energy to the ions, which shortens the ion traveling time and limits the extent of ion dispersion. This acceleration effect, in addition to the focusing effect, results in a more than 10-fold increase in the ion signal when the ion lens is at 3000 V and the spray at 5500 V, compared to ion lens 0 V and spray 3600 V.

More quantitative results from the scan mode are listed in Table 2-1, where the intensities of the peaks were tabulated. Figure 2-11 shows the spectra of β-CD with 0 V and 3000 V applied on the ion lens. The electrospray and ion lens voltages, chosen from the results shown in Figure 2-9 (3600 V and 0 V in (a), and 5500 V and 3000 V in (b)), provide the optimal performance of the sprays in both traces. Table 2-1 also shows statistical results of the comparison of the 8 peaks with 3000 V and 0 V applied on the ion lens. Peaks from m/z 164 to 1136 are protonated fragments of β-CD consisting of 1 to 7 monosaccharides. The peak at m/z 1153 is molecular β-CD with an ammonium adduct. To compare the signal, two sets of data were collected. The average intensities of the peaks were obtained from 10 spectra, each of which is the sum of 10 scans, with a dwell time of 10 ms, and a scan step of 1 m/z.

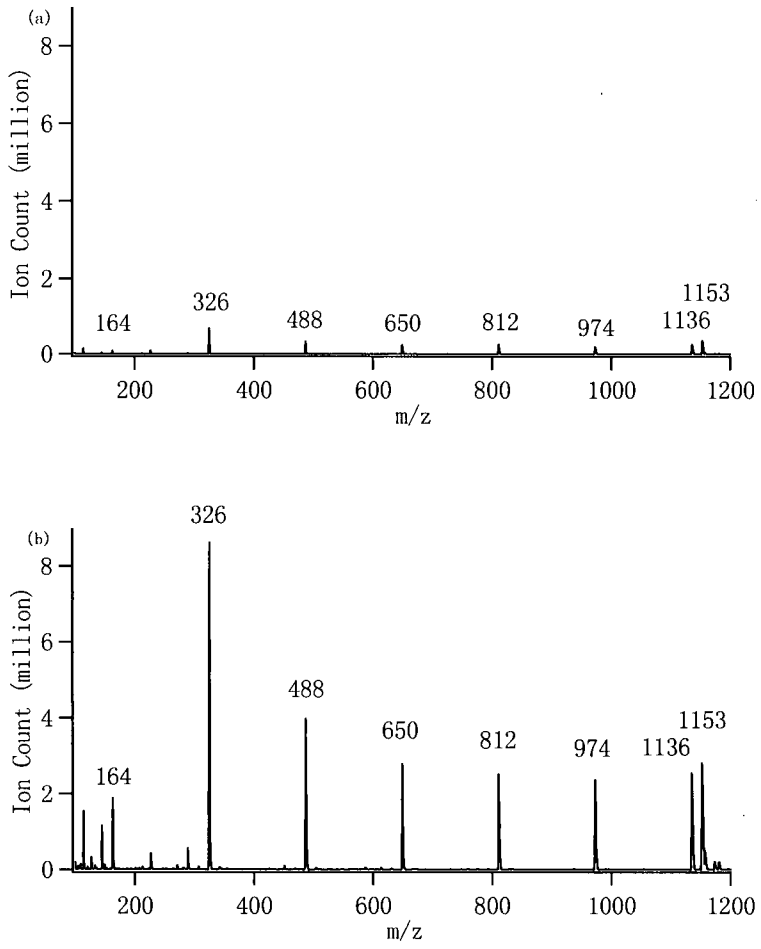

Figure 2-11 Mass spectra scanned from 100-1200 m/z when β-CD of 2×10^{-4}M was used as the analyte. (a) 3600V on the sprayer and 0 V on the ion lens (optimum condition without the ion lens). (b) 5500V on the sprayer and 3000V on the ion lens.

Table 2-1 Comparison of β-CD signals and the relative standard deviation of the signals with and without the ion lens. The subscript "I" denotes values obtained with the use of the ion lens.

m/z	164	326	488	650	812	974	1136	1153
S_I/S	23.2	12.3	11.9	12.2	11.1	11.3	10.2	7.9
RSD_I/RSD	0.87	0.22	0.16	0.22	0.22	0.24	0.1	0.38

As shown in Table 2-1, the average signal intensities are 10 to 23 times higher when 3000 V is applied on the ion lens than when 0 V is applied. The relative standard deviations on the

signals are much lower, which improves the precision for quantitative analyses. The signal increase varies for different fragments. The effect of the ion lens for the monosaccharide ions (m/z 164) is much higher, probably because the larger ion flux at a higher voltage usually results in a disproportionally high amount of saccharide monomer fragments. The peak at m/z 1153 is from β-CD molecules with an ammonium adduct, whose intensity is also limited by the adduct formation efficiency. Other than these two ions at m/z 164 and m/z 1153, it is interesting to see that the signals for fragments 2 to 6 increased almost to the same extent as the molecular ion, with smaller fragment populations slightly higher, as expected, indicating that no significant change in CID was observed due to different voltages.

One fact that cannot be ignored is that the effect of the ion lens set at 0 V is different from that with the ion lens floating or removed (the effects of these latter two conditions are very similar). When there is no ion lens, the space occupied before by the lens should be at a potential somewhere between the spray voltage and ground. Therefore, if the ion lens is forced to be 0 V, a larger potential drop is created between the spray tip and ion lens, and the electric field is changed in both magnitude and direction. Figure 2-12 compares the signal obtained with different ion lens voltages with that obtained with no lens applied. Unsurprisingly, the trace for no ion lens lies somewhere in the middle of the graph. However, the signal pattern implies the magnitudes of electric field at those five onset voltages are very close to each other, and so are the fields at the five voltages that give maximum signals in each trace.

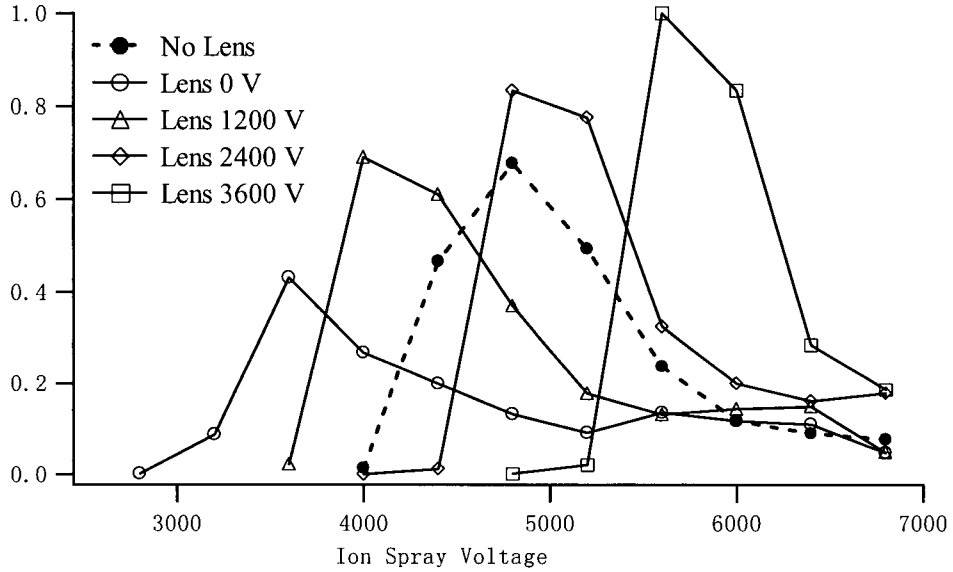

Figure 2-12 Signal intensity of β-CD vs. sprayer voltage at different ion lens voltages and with no lens applied. The dashed line indicates the signal when no lens is applied.

In conclusion, by adjusting the voltages applied on the ion lens and sprayer, the onset voltage and optimal operational voltage range can be significantly shifted, and the signal level enhanced in a systematic and ordered fashion.

2.3.2 Electric Current vs. Sprayer and Lens Voltages

The signal of ions cannot completely represent the electrospray process. Therefore, the current vs. voltages trend is to be studied next to provide a clearer perspective. The electric current measures the amount of charge separated from the sprayer, without considering the ionization and transmission processes for the analytes. The current flowing through the power supply to the ground is measured as shown in Figure 2-13. The electrospray setup is the same as that used in the ESI/MS, but the curtain plate in the MS is replaced by a grounded stainless steel plate. The current is measured from the output signal from the power supply using a multi-meter (Fluke Corp.).

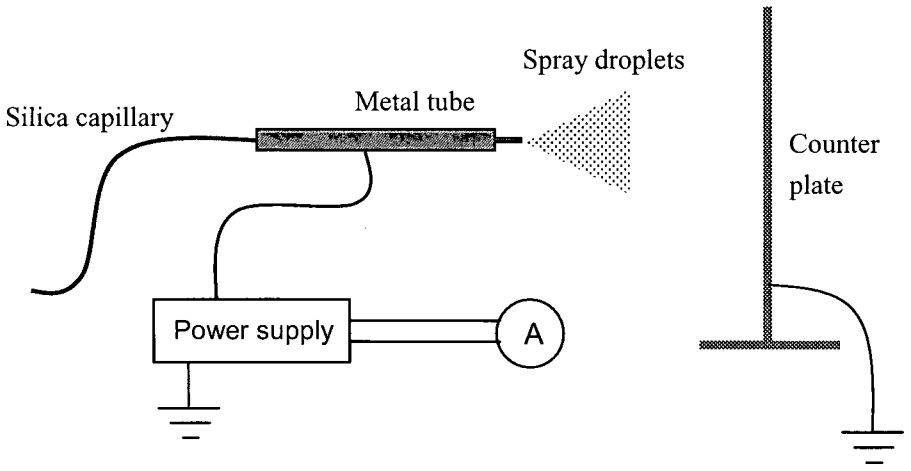

Figure 2-13 Current measurement set-up. A grounded stainless steel plate is set as the counter electrode. The current output signal from the power supply is measured by a multi-meter (A).

The current always kept increasing with the spray voltage, as shown in the current vs. voltage graph (Figure 2-14), although the ion signal starts to decrease after a certain point. If the current is larger than 100 nA, it is likely resulting from the corona discharge or other processes where ions such as solvent clusters, $H_3O^+(H_2O)_n$, appear at a much higher intensity[12, 18, 19]. An exponential form (Figure 2-15) is more preferable in that the discontinuous points in the plot indicate the initiation of discharge[18]. Before discharge occurs, the currents at all the lens voltages are almost the same, verifying the current generated by stable electrospray is constant. With the increase in the spray voltage, a discharge appears at a relatively low spray voltage for the ion lens at 0 V curve. However, as shown before, with the ion lens at 0 V, the onset spray voltage is also much lower than normal, which allows for lower operation voltages to avoid discharge. On the other hand, increasing the lens voltage accordingly could suppress the discharge, as shown in Figure 2-15, where discharge does not occur until the sprayer voltage reaches higher than 8000 V, when the ion lens is set at 6300 V.

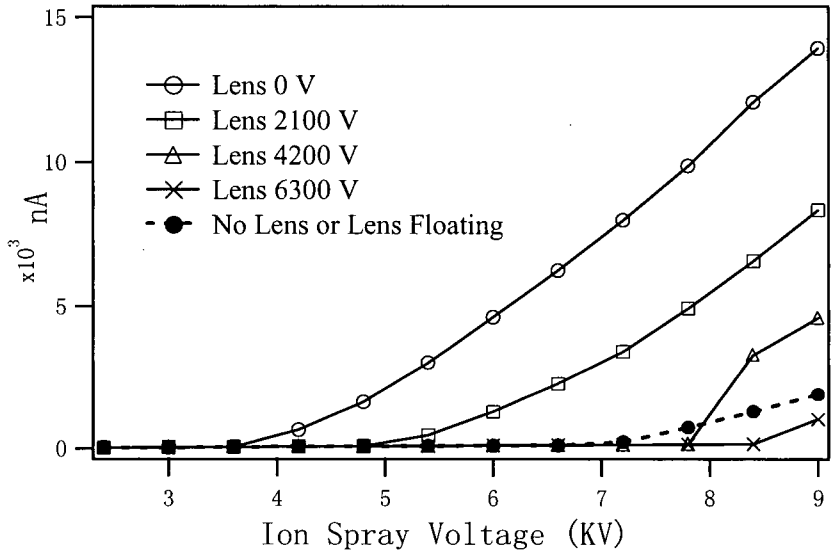

Figure 2-14 Current vs. spray voltage at different lens voltages and without the lens.

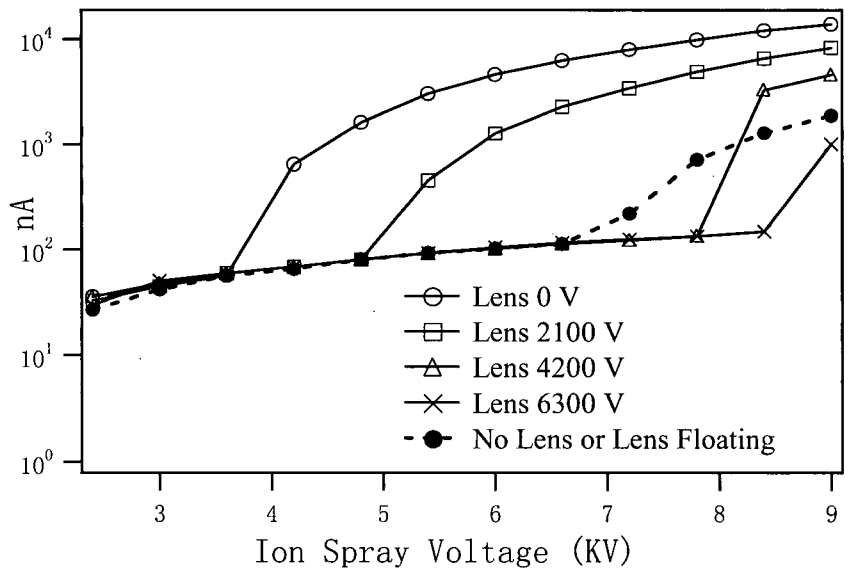

Figure 2-15 Exponential form of current vs. spray voltage with different lens voltage and no lens.

Another concern of the effect of the ion lens is whether the floating lens acts the same way as when the lens is removed. The current magnitude shown in Figure 2-16 suggests no distinct difference is present. Therefore, when the ion lens itself is floating in the space without connecting to any other conductor, the effect can be ignored.

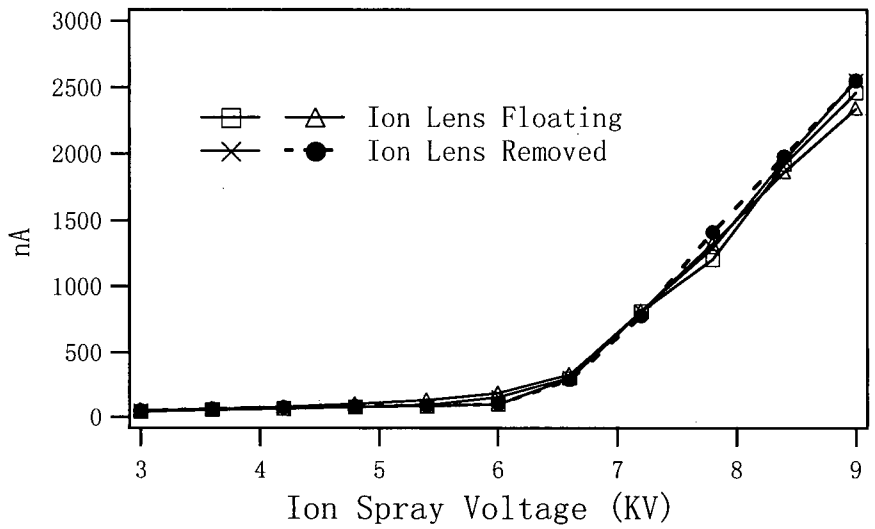

Figure 2-16 Current vs. Spray voltage with floating and removed ion lens. No systematic difference was observed.

2.4 Conclusions

The use of the ion lens can reshape the electric field. The electrospray ionization conditions are therefore made more flexible and adaptable through choosing different ion lens voltages.

Firstly, changing the ion lens voltage can significantly enlarge the applicable voltage range. Lower lens voltages allow for electrospray to be applied at lower voltages than normal with sufficient ion intensity, and higher lens voltages allow for much higher applied spray voltages without the corona discharge, which is otherwise inevitable at that voltage. The natural concern is what advantage it would present to widen the applied spray voltage range. The advantage of lowering the operational spray voltage is to soften the ionization condition. One advantage of a high spray voltage, verified by Wilm and Mann, is that higher spray voltages reduce the size of charged droplets emitted from the Taylor cone[14]. Smaller droplet size increases the surface area, which speeds up the solvent evaporation and the generation of gas

phase ions. Another benefit is that higher voltage differences between the sprayer and the curtain plate increase the kinetic energy of the generated ions and shorten the transmission time, which can restrict the coulombic repulsion induced dispersion.

Secondly, the ion lens changes the distribution of equipotential lines of the electric field and provides a focusing effect on the charged particles, leading to a larger portion of the total ions entering into the mass spectrometer. The signal intensity is enhanced with the application of the ion lens. By choosing an appropriate ion lens voltage, the enhancement can be as high as 10 to 20 times the signal obtained when the ion lens is set at 0 V.

In this chapter, the experimental results are shown to provide a straightforward view of the effect of the ion lens. To find the exact change in the electric field due to the use of the ion lens, more fundamental study is needed, as discussed in the next chapter.

2.5 References

1. Smith, R.D., Loo, J.A., Ogorzalek Loo, R.R., Busman, M. and Udseth, H.R., *Principles and practice of electrospray ionization-mass spectrometry for large polypeptides and proteins.* Mass Spectrometry Reviews, 1991. **10**: p. 359-451.

2. Zhou, L., Yue, B.F., Dearden, D.V., Lee, E.D., Rockwood, A.L. and Lee, M.L., *Incorporation of a venturi device in electrospray ionization.* Analytical Chemistry, 2003. **75**(21): p. 5978-5983.

3. Schneider, B.B. and Chen, D.D.Y., *Collision-induced dissociation of ions within the orifice-skimmer resion of an electrospray mass spectrometer.* Analytical Chemistry, 2000. **72**: p. 791-799.

4. Schneider, B.B., Douglas, D.J. and Chen, D.D.Y., *Collision-induced dissociation of bradykinin ions in the interface resion of an esi-ms.* Journal of the American Society for Mass Spectrometry, 2001. **12**: p. 772-779.

5. Schneider, B.B., Douglas, D.J. and Chen, D.D.Y., *Ion fragmentation in an electrospray ionization mass spectrometer interface with different gases.* Rapid Communications In Mass Spectrometry, 2001. **15**: p. 249-257.

6. Bruins, A.P., Covey, T.R. and Henion, J.D., *Ion spray interface for combined liquid chromatography/atmospheric pressure ionization mass-spectrometry.* Analytical Chemistry, 1987. **59**(22): p. 2642-2646.

7. Schneider, B.B., Douglas, D.J. and Chen, D.D.Y., *An atmospheric pressure ion lens that improves nebulizer assisted electrospray ion sourses.* Journal of the American Society for Mass Spectrometry, 2002. **13**: p. 906-913.

8. Jones, A.R. and Thong, K.C., *Production of charged monodisperse fuel droplets by electrical dispersion.* Journal of Physics D-Applied Physics, 1971. **4**(8): p. 1159-&.

9. Taylor, G., *Electrically driven jets.* Proceedings of the Royal Society of London Series a-Mathematical and Physical Sciences, 1969. **313**(1515): p. 453-475.

10. Smith, D.P.H., *The electrohydrodynamic atomization of liquids.* IEEE Transactions on Industry Applications, 1986. **22**(3): p. 527-535.

11. Juraschek, R. and Rollgen, F.W., *Pulsation phenomenon during electrospray ionization.* International Journal of Mass Spectrometry, 1998. **177**: p. 1-15.

12. Yamashita, M. and Fenn, J.B., *Electrospray ion-source - another variation on the free-jet theme.* Journal of Physical Chemistry, 1984. **88**(20): p. 4451-4459.

13. Kebarle, P. and Tang, L., *From ions in solution to ions in the gas phase: The mechanism of electrospray mass spectrometry.* Analytical Chemistry, 1993. **15**: p. 973A-986A.

14. Wilm, M.S. and Mann, M., *Electrospray and taylor-cone theory, doles beam of macromolecules at last.* International Journal of Mass Spectrometry and Ion Processes, 1994. **136**(2-3): p. 167-180.

15. Fernandez De La Mora, J. and I.G., L., *The current emitted by highly conducting taylor cones.* Journal of Fluid Mechanics, 1994. **260**: p. 155-184.

16. Ikonomou, M.G., Blades, A.T. and Kebarle, P., *Investigations of the electrospray interface for liquid chromatography/mass spectrometry.* Analytical Chemistry, 1990. **62**: p. 957-967.

17. Horning, D.W. and Hendricks, C.D., *Study of an electrically driven jet.* Journal of Applied Physics, 1979. **50**(4): p. 2614-2617.

18. Ikonomou, M.G., Blades, A.T. and Kebarle, P., *Electrospray mass-spectrometry of methanol and water solutions suppression of electric-discharge with sf6 gas.* Journal of the American Society for Mass Spectrometry, 1991. **2**(6): p. 497-505.

19. Wampler, F.M., III, Blades, A.T. and Kebarle, P., *Negative ion electrospray mass spectrometry of nucleotides: Ionization from water solution with sf6 discharge suppression.* Journal of the American Society for Mass Spectrometry, 1993. **4**: p. 289-295.

Chapter 3

Calculation of Electric Fields and Discussion of Experimental results

3 Calculation of Electric Fields and Discussion of Experimental results

3.1 Introduction

As described in previous chapters, the electric field is not only a necessity but also a controlling factor for electrospray ionization. In Chapter 2, it is demonstrated that at different lens voltages the signal of ions could differ dramatically even if the sprayer voltage was kept the same. In addition, with certain combinations of sprayer and lens voltages, a maximum in the signal intensity always appeared. Therefore, the study of the electric field in the space around the spray tip is important to understand the signal trend in Chapter 2.

The definition of the electric field is the negative of the gradient of the potential. If the distribution of the space potential can be obtained, the electric field can be solved by differentiating the space potential. Since the voltages applied on each of the electrodes and boundaries are known, theoretically it is possible to solve for the potential distribution. The physical basis is the Laplace equation, which requires any electrostatic region with no free charge to satisfy:

$$\nabla^2 V = \frac{\partial^2 V}{\partial x^2} + \frac{\partial^2 V}{\partial y^2} + \frac{\partial^2 V}{\partial z^2} = 0 \tag{3.1}$$

Direct solution of Laplace equation is an unrealistic task except for simple and ideal boundary conditions. In our case, the boundary condition is irregular with the spray capillary, the lens, counter plate and the grounded housing, and it is impractical to solve the Laplace equation directly. However, other approximation methods are available, including finite

difference method (FDM), finite element method (FEM) and boundary element method (BEM). Those methods, developed in applied mathematics but promoted greatly by engineering applications, especially aim at solving partial differential equations.

This chapter contains two parts. In the first part, we will explain the determination of the electric field by analytical and numerical methods, and in the second part we will show the estimated results for the electric field which are used to explain the experiment data in Chapter 2.

The following is a list of symbols that will be used in this chapter.

r_c = capillary radius
z_0 = distance from the capillary tip to the counter plate
θ = half cone angle
κ = curvature of the cone
R = radius of curvature
K = conductivity of solvent
V = electric potential on an electrode
  V_c = potential difference between capillary and counter plate. $V_c = V_0 - V_1$.
  V_0 = potential on the capillary
  V_1 = potential on the counter plate
$\boldsymbol{E}$ = electric field and E_z, E_r are the fields in the z and r directions.
  $E_0 = |\boldsymbol{E}|$ = norm electric field
γ = surface tension of the solvent
ε_0 = permittivity of vacuum
ε = permittivity of the solvent
σ = surface charge density
v = volume

3.2 Direct Solutions of the Laplace equation

3.2.1 General Solution of the Laplace Equation

The geometry of the electrodes in the system and the potentials on them are the only boundary conditions required to solve the Laplace equation. To simplify the model, an axis-symmetric geometry is assumed where the capillary lies on the z-axis and the lens has a round shape. In cylindrical coordinates, as shown in Figure 3-1(a), the capillary and ion lens are located as in Figure 3-1(b).

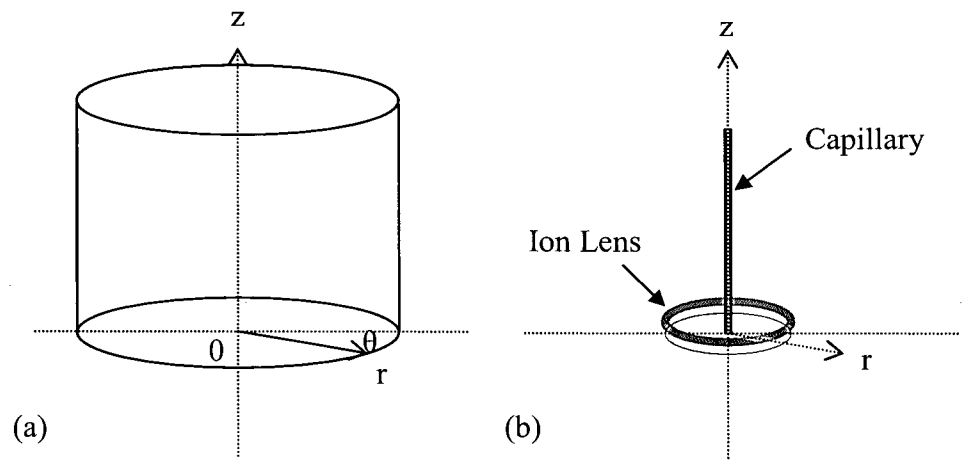

Figure 3-1 (a) Cylindrical Coordinates. (b) The location of capillary and ion lens in the coordinates.

The gradient operator in cylindrical coordinates is:

$$\nabla = \hat{r}\frac{\partial}{\partial r} + \hat{\theta}\frac{1}{r}\frac{\partial}{\partial \theta} + \hat{z}\frac{\partial}{\partial z} \tag{3.2}$$

The geometry of the setup is axis-symmetrical, and the potential is independent of the angle. Thus, the Laplace Equation in cylindrical coordinates is simplified to:

$$\nabla^2 V = \frac{\partial^2 V}{\partial r^2} + \frac{1}{r}\frac{\partial V}{\partial r} + \frac{\partial^2 V}{\partial z^2} = 0 \tag{3.3}$$

The normal method of solving the Laplace equation is to separate variables as $V(r,z) = R(r)Z(z)$. Thus, the Laplace equation becomes:

$$\frac{1}{R(r)}\left(\frac{d^2R}{dr^2}+\frac{1}{r}\frac{dR}{dr}\right)+\frac{1}{Z(z)}\frac{d^2R}{dz^2}=0$$

This transforms the partial differential equation into a system of ordinary differential equations:

$$\frac{d^2R}{dz^2}-k^2Z=0$$

$$\frac{d^2R}{dr^2}+\frac{1}{r}\frac{dR}{dr}=-k^2R$$

The solutions for these two equations are:

$$Z(z)=Ae^{kz}+Be^{-kz}$$

$$R(r)=C_1J_0(r)+C_2N_0(r)$$

A, B, C_1, and C_2 are to be determined by boundary conditions. J_0 and N_0 are zero order Bessel functions of the first and second kind. This gives the general starting step of solving the Laplace equation. However, we are not going to look further into the Bessel functions and their expansions, since numerical methods will be used to calculate the result.

3.2.2 Estimate the Electric Field at the Edge of the Capillary

Solving the electric field directly from the Laplace equation for the whole space is unrealistic. However, for special geometries, the electric field can be estimated in a certain region. For a semi-infinite conductive capillary (Figure 3-2(a)) with the radius r_c at a distance z_0

from an infinite plate, the electric field at the capillary tip is given by Equation (3.4) [1], where V_c is the potential difference between the capillary and the plate.

$$|E_r| \approx |E_z| \approx \frac{V_c}{r_c \ln(4z_0/r_c)} \tag{3.4}$$

The norm (magnitude) of the field is

$$E_0 = |E| = \frac{\sqrt{2}V_c}{r_c \ln(4z_0/r_c)} \tag{3.5}$$

Loeb *et al*[2] and Smith[3] used the same expression, except that instead of $\sqrt{2}$, Loeb used 2, and Smith used 1.5 as the coefficient. Smith treated the coefficient as an empirical constant and obtained it by fitting the experimental results to the equation. We believe that when considering the configuration of electrodes only, i.e. the capillary and the counter plate, without taking into account of the liquid cone or ion lens, this prediction is accurate and convincing.

When the liquid forms a cone shape with a half cone angle θ under this electric field, the critical point is that the electric pressure equals the surface tension:

$$P_\gamma = P_E \tag{3.6}$$

where P_γ is the surface tension pressure, and P_E is the electric pressure given by

$$P_\gamma = \gamma \frac{\cot\theta}{r_c} \tag{3.7}$$

$$P_E = \frac{1}{2}\varepsilon_0 E^2 \tag{3.8}$$

The derivation of these two equations is described in the Appendix. The electric field required to balance these two pressures is the threshold or "onset E" for electrospray. From (3.7) and (3.8), the onset electric field can be expressed as:

$$E_{on} = \left(\frac{2\gamma \cot\theta}{\varepsilon_0 r_c} \right)^{\frac{1}{2}} \tag{3.9}$$

When substituted into (3.5), the onset voltage, i.e. the potential to initiate the electrospray, is given by

$$V_{on} = \left(\frac{\gamma \cot\theta}{\varepsilon_0 r_c} \right)^{1/2} r_c \ln(4z_0/r_c) \tag{3.10}$$

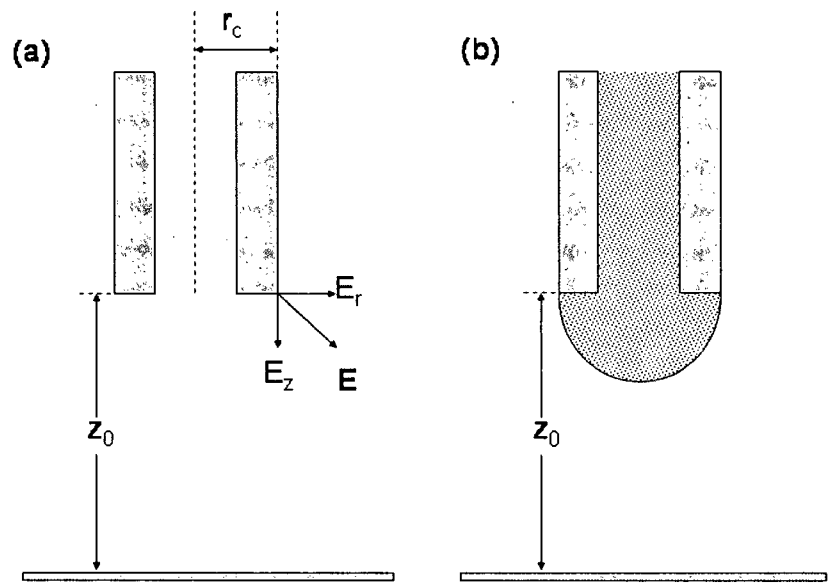

Figure 3-2 Configuration of the electrodes including a semi-infinite conductive capillary and an infinite counter plate. (a) shows electric field formed by electrodes only, and (b) shows the situation when there is liquid flowing in the capillary and forming a meniscus which changes the configuration of the electrodes in (a).

However, the expressions of onset electric field and voltage have an obvious flaw. Once the liquid fills the capillary and accumulates at the end of the capillary to form a meniscus,

if the solvent is considered to be highly conductive which is true in most cases, the whole capillary and liquid meniscus combination is an equipotential entity (Figure 3-2b). Thus, the configuration of the electrodes is altered from an angled shape to a continuous shape, and the electric field at a continuous shaped electrode is much smaller than that at a sharp point. Therefore the prediction made by (3.5) will be largely biased, and the real onset voltage will have to be much higher than predicted by (3.10).

3.2.3 Calculate the Electric Field Based on Solving Laplace's Equation

Without considering the geometry change due to liquid accumulating at the capillary tip, the electric field calculated is inaccurate. Although this bias might be minute and negligible when the whole space potential distribution is to be studied, this error could be serious in the region closest to the spray tip. When the solvent fills the capillary and forms a meniscus, equation (3.5) is no longer appropriate to give an estimate of the electric field. A better method is to take the liquid cone as part of the electrode [4]. This assumes that for an electrostatic situation, a liquid cone is formed at the end of capillary and has the same potential as the capillary. Considering the cone angle as an additional unknown variable, it is more convenient to set the Laplace equation in spherical coordinates with the tip of the cone as the origin (Figure 3-3). Define R to be the distance (radius) from a point to the origin, θ the polar angle from the z-axis (half cone angle), and φ the azimuthal angle in the xy-plane, which can be omitted because of the symmetric property. Note the origin in these coordinates is set at a different position from that in cylindrical coordinates. The Laplace equation in spherical coordinates with only two variables, R and θ, is:

$$\nabla^2\phi = R^2\left(\left[R^2\frac{\partial^2}{\partial R^2}+2R\frac{\partial}{\partial R}\right]+\left[\frac{\partial^2}{\partial\theta^2}+\frac{\cos\theta}{\sin\theta}\frac{\partial}{\partial\theta}\right]\right)V=0$$

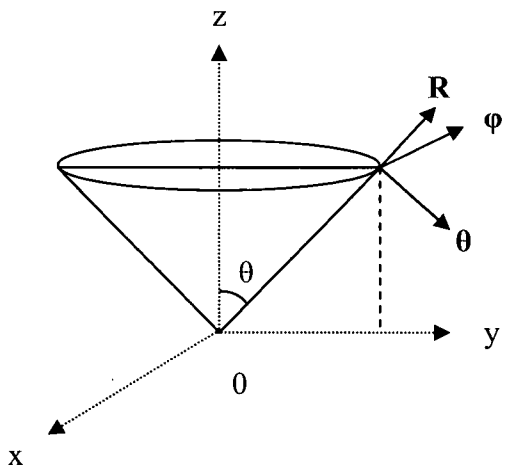

Figure 3-3 Spherical coordinates for the cone.

See Appendix for the steps of solving the spherical Laplace equation. The potential is solved to be

$$V(R,\theta)=f(R)g(\theta)=\left(A_nR^n+B_nR^{-(n+1)}\right)P_n(\cos\theta)=0$$

where A_n and B_n are coefficients to be determined by the boundary conditions, and $P_n(\cos\theta)$ is the Legendre function. This is a general solution for all points on the cone surface except the singular point at the cone apex. For interior problems where the points to be studied are inside the sphere, $B_n=0$. The general solution becomes:

$$V(R,\theta)=A_nR^nP_n(\cos\theta)=0$$

The static electric field is defined by

$$\vec{E}=-\vec{\nabla}V$$

where $\vec{\nabla}$ is the gradient operator in spherical coordinates given by:

$$\vec{\nabla} = \frac{\partial}{\partial R}\vec{e}_R + \frac{1}{R\sin\theta}\frac{\partial}{\partial \varphi}\vec{e}_\varphi + \frac{1}{R}\frac{\partial}{\partial \theta}\vec{e}_\theta$$

Since the electric field ***E*** is always orthogonal to the cone surface, $\vec{E}_r$ and $\vec{E}_\varphi$, which are parallel to the cone surface, should be zero. The only term left is $\vec{E}_\theta$, which is expressed as:

$$\vec{E}_\theta = -\phi_0 R^{n-1}\frac{\partial}{\partial r}P_n(\cos\theta)|_P\ \vec{e}_\theta$$

The electric pressure is therefore expressed as

$$P_E = \frac{1}{2}\varepsilon_0{\phi_0}^2 R^{2(n-1)}\left[\frac{\partial}{\partial r}P_n(\cos\theta)\right]^2$$

The surface pressure is given by:

$$P_\gamma = \gamma\frac{\cos\theta}{(1-\cos^2\theta)}\frac{1}{R}$$

If the electric pressure equals the surface pressure, they must have the same order dependence on R, which gives n to be 0.5.

The prerequisite of $\vec{E}_r$ and $\vec{E}_\varphi$ being zero requires $P_n(\cos\theta)|_o = 0$. Taylor showed that by solving $P_{0.5}(\cos\theta)|_o = 0$, the only solution for θ lying in the range $0 < \theta < \pi$ is 130.7°, and the cone half angle is thus 180°-130.7° = 49.3°[5]. This static cone with half cone angle 49.3° is the so-called Taylor cone.

In the ideal static equilibrium condition, the Taylor cone angle 49.3° should remain unchanged and independent of all the other parameters, because it is only based on the assumptions of pressure balance and an equipotential cone surface. With θ=49.3°, n=0.5 as well as some approximations for an elliptic shaped cone tip in a dynamic situation, Wilm and Mann were able to show the onset voltage[4]:

$$V_{on} = 0.863\left(\frac{\gamma z_0}{\varepsilon_0}\right)^{0.5} \tag{3.11}$$

This equation is quite different from (3.10), in that it does not depend on the capillary radius r_c, which is a crucial parameter in (3.10). As well, the half cone angle is presumed to be 49.3° while in (3.10) it has not been considered. The calculated results of onset voltages by these two equations are very different as well. By substituting the vacuum permittivity $\varepsilon_0 = 8.8 \times 10^{-12}$ $J^{-1}C^2m^{-1}$, surface tension of H_2O ($\gamma = 0.073$ N/m), and θ=49.3°, the onset voltages versus r and z are shown in Figure 3-4. Here, r is the capillary radius, and z is the distance from the capillary end to the counter electrode. Figure 3-4(a) demonstrates the onset voltage obtained by (3-11), which is derived from solving Laplace equation for a liquid cone, with the cone considered as an equipotential entity with pressure balance on the surface. Since the cone angle is fixed at 49.3° and is independent from r, the onset voltage only depends on z, and increases rapidly with it. Figure 3-4(b) displays the onset voltage calculated by (3-10), which is based on an approximated expression of electric field created by the electrodes shown in Figure 3-2(a). The onset voltage calculated this way changes rapidly with r and slowly with z.

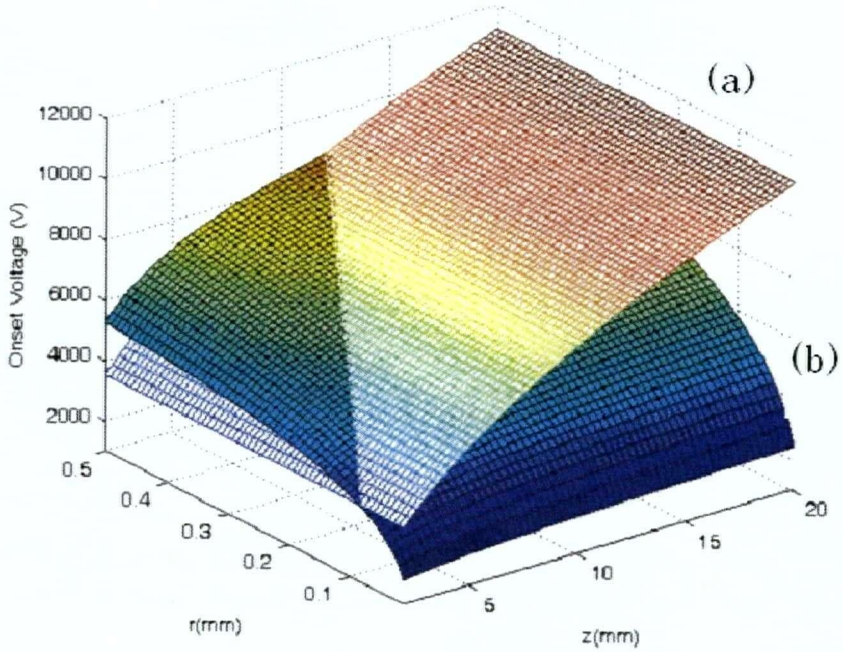

Figure 3-4 Comparison of onset voltages calculated by Equation (3.10) and (3.11) Surface (a) is the onset voltage calculated by Equation (3.11), which only depends on z (the distance from capillary to the counter plate), and surface (b) is from Equation (3.10), which changes rapidly with the capillary radius r and slowly with z.

3.3 Numerical Methods of Solving Laplace's Equation

The above approximation and calculation give important information concerning the tip of the capillary and the liquid cone. However, a complete solution of the potential distribution or electric field for the region is still out of reach. Also, the assumptions used differ greatly from the real situation in that the approximation is based on a completely static liquid cone shape with an ideally shaped counter electrode. Furthermore, with an additional ion lens, these approximations will deviate considerably from the real situation.

In most practical problems including this one, the domain to be solved is geometrically irregular and complicated, and the exact mathematical solution (a closed-form algebraic

expression of the potential) is difficult, often impossible, to obtain. Therefore, practical and effective methods based on numerical techniques and digital computation are preferred[6]. We will briefly describe two of these techniques: the finite difference method and the finite element method.

3.4 Finite Difference Method (FDM)

3.4.1 Relaxation

One of the simpler numerical methods of calculating the potential distribution in a bounded region is the finite difference method. The space is treated as a regular lattice of discrete points. The points representing electrodes are assigned fixed potentials as specified for those electrodes. All the free space points are initially set to a potential of 0 V. A rectangular two-dimensional lattice is shown in Figure 3-5. Each point, except those on the boundaries (electrodes that have a fixed potential), is surrounded by four neighbouring points.

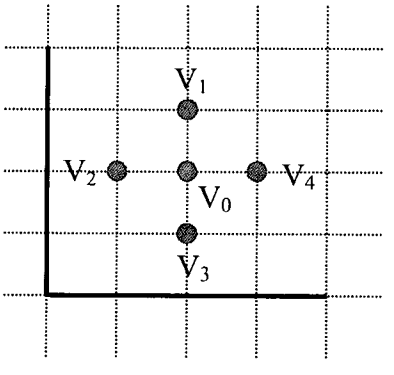

Figure 3-5 The lattice of a 2-D space. The potential of points on the lattice are to be calculated.

The potential of each of the four neighbouring points can be expressed by Taylor expansion of the potential of the center point and its derivatives[7].

$$V(x-h,y)=V(x,y)-h\frac{\partial V}{\partial x}+\frac{1}{2}h^2\frac{\partial^2 V}{\partial x^2}-\frac{1}{6}h^3\frac{\partial^3 V}{\partial x^3}+\frac{1}{24}h^4\frac{\partial^4 V}{\partial x^4}-\cdots$$
$$V(x+h,y)=V(x,y)+h\frac{\partial V}{\partial x}+\frac{1}{2}h^2\frac{\partial^2 V}{\partial x^2}+\frac{1}{6}h^3\frac{\partial^3 V}{\partial x^3}+\frac{1}{24}h^4\frac{\partial^4 V}{\partial x^4}+\cdots \quad (3.12)$$

Similarly, we can get the expression for $V(x,y+h)$ and $V(x,y-h)$, and by adding them together, we find

$$V(x-h,y)+V(x+h,y)+V(x,y-h)+V(x,y+h)-4V(x,y)=h^2\left(\frac{\partial^2 V}{\partial x^2}+\frac{\partial^2 V}{\partial y^2}\right) \quad (3.13)$$

According to the Laplace equation (3.1), the right hand side of (3.13) equals zero. Therefore, the potential of each point in the lattice is the average of the potentials of four adjacent points. Using the denotation in Figure 3-5, this relationship can be written as:

$$V_0=\frac{1}{4}(V_1+V_2+V_3+V_4) \quad (3.14)$$

The estimation is started from a boundary point which has a fixed voltage and moved on to all the points in the lattice row by row, with the potential changes propagating along the lattice. After the potential of every point within the lattice is estimated, a single iteration is finished. As the iteration is repeated time and again, the potential converges to the true value. The process is finished when the potential change between successive iterations is smaller than a preset tolerance.

This repeated iteration method is called relaxation. A larger number of iterations increases the accuracy and precision, but it requires a longer computation time. Therefore, a modified method called successive over-relaxation is more commonly used.

3.4.2 Over-Relaxation

The method known as "successive over-relaxation" reduces the iteration number by adding an extra factor to the estimated potential. When the potential is calculated from the average of its neighbours, by recognizing the fact that it will still change towards the same direction in the next iteration, we move it closer to its final value by adding an additional change immediately.

$$V_0^* = (1-g)V_0 + \frac{g}{4}(V_1 + V_2 + V_3 + V_4) \tag{3.15}$$

Where V_0 is the value of potential from the preceding iteration, and g is called the acceleration factor. This factor ranges from 1 (same as relaxation) to 2 (unstable over-relaxation). A larger g gives a smaller number of iterations needed to reach within the tolerance around the true value. However, increasing the acceleration factor has the same effect as reducing the damping effect, so that excessive correction might result in instability or oscillatory conditions. The system becomes unstable and oscillating when g is greater than 2.

Over-relaxation is the method used in commercial software such as the SIMION program (Scientific Instrument Services Inc., Ringoes, NJ). There is a unique acceleration factor for each electrode that gives the fastest solution convergence. SIMION makes use of a dynamically self-adjusting factor to seek the ideal acceleration factor.

The precision and accuracy of the finite difference method depend on the size of the points on the lattice and the number of iterations. Increasing the density of the lattice increases the time for each iteration, and a larger number of iterations is needed, since the change takes

longer to propagate through the entire lattice. Another obvious problem is that the accuracy at the edges and the corners is very poor because the potential changes there are large.

3.5 Finite Element Method (FEM)

3.5.1 Principle of FEM

By directly solving differential equations, we consider the whole domain as a continuous region. However, in the finite element method (FEM), the domain is divided into finite elements so that the elements are not in a differential form (infinite), but instead have a finite size[8, 9]. In each element, FEM calculates the potential on both the boundary and its interior region.

In a given axis-symmetrical domain with boundary conditions, the Laplace equation for electric potential without free space charge in cylindrical coordinates is

$$\nabla^2 V = \frac{\partial^2 V}{\partial r^2} + \frac{1}{r}\frac{\partial V}{\partial r} + \frac{\partial^2 V}{\partial z^2} = 0 \tag{3.16}$$

For most potential problems, the principle of minimum potential energy can be applied, which requires the potential V to distribute itself in such a way as to minimize the potential energy $W[V]$ in the whole domain[10]. The general form of potential energy in a given domain G is given by:

$$W[V] = c \iint_G \left[\left(\frac{\partial V}{\partial r} \right)^2 + \left(\frac{\partial V}{\partial z} \right)^2 \right] dr dz \tag{3.17}$$

The minimum energy principle is mathematically equivalent to the Laplace equation in that solving the Laplace equation in a domain G is equivalent to finding a function that

minimizes a functional and satisfies the boundary conditions. This is one of the "variational methods"[11]. In the study of an electrostatic field, the function to be found is the potential V in the space, and the functional to be minimized is the energy stored in the electric field which is defined by:

$$W = \frac{\varepsilon_0}{2} \int E^2 dv \tag{3.18}$$

where v is the volume of the space.

The derivation of (3.18) is shown in Appendix.

In these 2D coordinates (r, z), the square of the electric field can be written as:

$$E^2 = E_r^{\,2} + E_z^{\,2} = \left(\frac{\partial V}{\partial r}\right)^2 + \left(\frac{\partial V}{\partial z}\right)^2 \tag{3.19}$$

Thus, the electric field stored energy appears in the general form of a potential energy functional as (3.17):

$$W[V(r,z)] = \frac{\varepsilon_0}{2} \iint \left[\left(\frac{\partial V}{\partial r}\right)^2 + \left(\frac{\partial V}{\partial z}\right)^2\right] dr dz \tag{3.20}$$

The minimum of the potential energy is found by setting the derivative of the energy on unknown potential to be zero. Thus, the basic principle for solving potential problem by the finite element method is

$$\frac{\partial W}{\partial V} = 0 \tag{3.21}$$

3.5.2 Main Procedure of FEM

To summarize the procedure of how the finite element method works, six main steps are listed:

1. Discretizing the continuum.

The first step of FEM is to divide a solution region into finite elements. For a 2-D region, the finite element can be a triangle or quadrilateral, and for a 3-D region, it can be a tetrahedron or hexahedron. The finite element mesh is typically generated by a pre-processor program. The vertices of the triangle are called nodal points (or nodes) at which the values of the unknown function (electric potential V in this study) are to be explicitly calculated.

2. Selecting interpolation functions.

Within a given element, interpolation functions are used to interpolate the nodal values of the unknown function over the element. Often, polynomials are selected as interpolation functions because of the simplicity of their differential and integral calculation. The degree of the polynomial depends on the number of nodes assigned to each element.

3. Finding the element properties.

A matrix equation for the finite element should be established which relates the values of the unknown function to the coordinates of the nodal points. Two approaches are commonly used for this task. The above mentioned "variational method" is one of them, and another is the weighted residue method.

4. Assembling the element equations.

To solve for the whole domain, we must assemble all of the element matrix equations to set up the global equation system. Conjunct nodal points that connect adjacent elements are used for the assembly process. Before solving the global equation system for the potential of

the whole domain, boundary conditions (nodal points on the electrodes with known potential) should be imposed.

5. Solving the global equation system.

The finite element global equation system is typically sparse, symmetric and positive definite. Direct and iterative methods can be used for solution. The nodal values of the sought function are produced as the result.

6. Computing additional results.

In many cases, additional parameters are of interest, such as electric field in this study, which is obtained from the gradient of the potential.

3.5.3 Mathematical Calculation of Potential Distributions by FEM

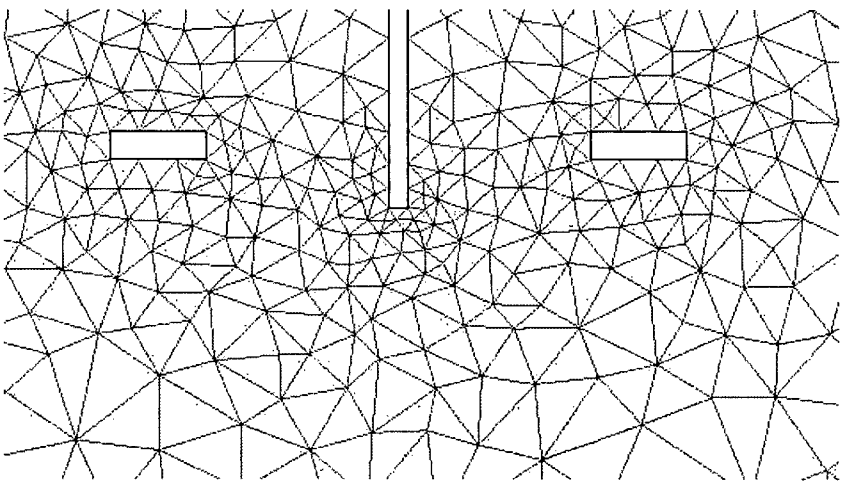

Figure 3-6 Part of the initial mesh in our lens model.

In the finite element method, the region is most commonly divided into finite triangular elements because of their simplicity and least degree of freedom for 2D system (Figure 3-6). The vertices of the triangles are the nodal points. So the continuous domain is discretized.

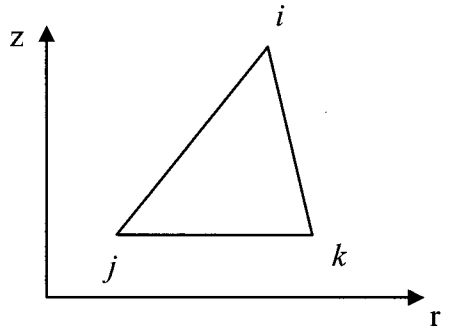

Figure 3-7 Triangle i-j-k as a finite element.

To study the triangle with vertex points i, j, and k (Figure 3-7), the coordinates for the three nodal points i, j, k are (r_i, z_i), (r_j, z_j) and (r_k, z_k). A superscript (e) describes variables in a single element. The space potential $V^{(e)}$ in an element is approximated by a linear function of r and z:

$$V^{(e)}(r,z) = \alpha_1 + \alpha_2 r + \alpha_3 z \tag{3.22}$$

For the element of Figure 3-7, let the potentials at the nodal points be:

$$\begin{aligned} V_i &= \alpha_1 + \alpha_2 r_i + \alpha_3 z_i \\ V_j &= \alpha_1 + \alpha_2 r_j + \alpha_3 z_j \\ V_k &= \alpha_1 + \alpha_2 r_k + \alpha_3 z_k \end{aligned} \tag{3.23}$$

We can then express α_1, α_2, and α_3 in terms of V_i, V_j, V_k and the nodal point coordinates (r_i, z_i), (r_j, z_j) and (r_k, z_k).

$$\begin{aligned} \alpha_1 &= \frac{a_i V_i + a_j V_j + a_k V_k}{2\Delta^{(e)}} \\ \alpha_2 &= \frac{b_i V_i + b_j V_j + b_k V_k}{2\Delta^{(e)}} \\ \alpha_3 &= \frac{c_i V_i + c_j V_j + c_k V_k}{2\Delta^{(e)}} \end{aligned} \tag{3.24}$$

where a_n, b_n and c_n are used to simplify the expression, determined only by the coordinates of the nodal points:

$$
\begin{aligned}
a_i &= z_j r_k - z_k r_j, \quad a_j = z_k r_i - z_i r_k, \quad a_k = z_i r_j - z_j r_i. \\
b_i &= z_k - z_j, \quad b_j = z_i - z_k, \quad b_k = z_j - z_i, \\
c_i &= r_j - r_k, \quad c_j = r_k - r_i, \quad c_k = r_i - r_j,
\end{aligned} \tag{3.25}
$$

and $\Delta^{(e)}$ is the area of the triangle element expressed by

$$
2\Delta^{(e)} = \begin{vmatrix} 1 & r_i & z_i \\ 1 & r_j & z_j \\ 1 & r_k & z_k \end{vmatrix} \tag{3.26}
$$

Now we define interpolation functions N_i, N_j, and N_k of an element which are functions of coordinates.

$$
\begin{aligned}
N_i(r,z) &= \frac{1}{2\Delta^{(e)}}(a_i + b_i r + c_i z) \\
N_j(r,z) &= \frac{1}{2\Delta^{(e)}}(a_j + b_j r + c_j z) \\
N_k(r,z) &= \frac{1}{2\Delta^{(e)}}(a_k + b_k r + c_k z)
\end{aligned} \tag{3.27}
$$

Interpolation functions interpolate the nodal values of the potential over the element:

$$
V^{(e)}(r,z) = N_i(r,z)V_i + N_j(r,z)V_j + N_k(r,z)V_k \tag{3.28}
$$

Therefore, the potential $V^{(e)}$ in the whole element can be expressed by the nodal point potentials and coordinates of the element. To transform the potential into the matrix form, we define:

$$
[N] = \begin{bmatrix} N_i(r,z) & N_j(r,z) & N_k(r,z) \end{bmatrix} \tag{3.29}
$$

$$
\{V\}^{(e)} = \begin{bmatrix} V_i \\ V_j \\ V_k \end{bmatrix} \tag{3.30}
$$

Thus, the matrix equation of the potential in an element is given by:

$$
V^{(e)}(r,z) = [N]\{V\}^{(e)} \tag{3.31}
$$

The energy functional in a 2D element is:

$$W[V^{(e)}(r,z)] = \frac{\varepsilon_0}{2}\iint\left[\left(\frac{\partial V^{(e)}}{\partial r}\right)^2 + \left(\frac{\partial V^{(e)}}{\partial z}\right)^2\right]drdz \tag{3.32}$$

According to Equation (3.31) and (3.27) we have

$$\frac{\partial V^{(e)}}{\partial r} = \frac{\partial}{\partial r}\left([N]\{V\}^{(e)}\right) = \frac{b_i V_i + b_j V_j + b_k V_k}{2\Delta^{(e)}} \tag{3.33}$$

$$\frac{\partial V^{(e)}}{\partial z} = \frac{c_i V_i + c_j V_j + c_k V_k}{2\Delta^{(e)}}$$

Therefore,

$$\left(\frac{\partial V^{(e)}}{\partial r}\right)^2 + \left(\frac{\partial V^{(e)}}{\partial z}\right)^2$$

$$= \frac{1}{4\Delta^{(e)2}}\begin{bmatrix} V_i & V_j & V_k \end{bmatrix}\begin{bmatrix} b_i^2 + c_i^2 & b_i b_j + c_i c_j & b_i b_k + c_i c_k \\ b_j b_i + c_j c_i & b_j^2 + c_j^2 & b_j b_k + c_j c_k \\ b_k b_i + c_k c_i & b_k b_j + c_k c_j & b_k^2 + c_k^2 \end{bmatrix}\begin{bmatrix} V_i \\ V_j \\ V_k \end{bmatrix} \tag{3.34}$$

With $\iint drdz = \Delta^{(e)}$, we can get the energy functional of an element:

$$W^{(e)} = \frac{\varepsilon_0}{8\Delta^{(e)}}\begin{bmatrix} V_i & V_j & V_k \end{bmatrix}\begin{bmatrix} b_i^2 + c_i^2 & b_i b_j + c_i c_j & b_i b_k + c_i c_k \\ b_j b_i + c_j c_i & b_j^2 + c_j^2 & b_j b_k + c_j c_k \\ b_k b_i + c_k c_i & b_k b_j + c_k c_j & b_k^2 + c_k^2 \end{bmatrix}\begin{bmatrix} V_i \\ V_j \\ V_k \end{bmatrix} \tag{3.35}$$

It is helpful to define an element matrix $[K]^{(e)}$ which is only determined by the element nodal points coordinates.

$$[K]^{(e)} = \frac{\varepsilon_0}{8\Delta^{(e)}}\begin{bmatrix} b_i^2 + c_i^2 & b_i b_j + c_i c_j & b_i b_k + c_i c_k \\ b_j b_i + c_j c_i & b_j^2 + c_j^2 & b_j b_k + c_j c_k \\ b_k b_i + c_k c_i & b_k b_j + c_k c_j & b_k^2 + c_k^2 \end{bmatrix} \tag{3.36}$$

Thus

$$W^{(e)} = \{V\}^{(e)T}[K]^{(e)}\{V\}^{(e)} \tag{3.37}$$

When the entire domain is considered, the total energy is the sum of that of all of the elements:

$$W = \sum_e W^{(e)} = \sum_e \{V\}^{(e)T}[K]^{(e)}\{V\}^{(e)} \tag{3.38}$$

$\{V\}^{(e)}$ denotes the potential of nodal points in a single element, which is the unknown variable to be solved. However, it cannot be solved within a single element; the whole domain and all the nodal points have to be involved to minimize the energy and solve for the potential. If there are N_p nodal points in the domain, the potential vector becomes:

$$\{V\} = \begin{bmatrix} V_1 \\ V_2 \\ \vdots \\ V_{N_p} \end{bmatrix} \tag{3.39}$$

When the potential on all the nodal points is considered as a whole vector, the element matrix $[K]^{(e)}$ should be extended to be $[\tilde{K}]^{(e)}$:

$$[\tilde{K}]^{(e)} = \begin{bmatrix} & \vdots & & \vdots & & \vdots & \\ \cdots & K_{ii}^{(e)} & \cdots & K_{ij}^{(e)} & \cdots & K_{ik}^{(e)} & \cdots \\ & \vdots & & \vdots & & \vdots & \\ \cdots & K_{ji}^{(e)} & \cdots & K_{jj}^{(e)} & \cdots & K_{jk}^{(e)} & \cdots \\ & \vdots & & \vdots & & \vdots & \\ \cdots & K_{ki}^{(e)} & \cdots & K_{kj}^{(e)} & \cdots & K_{kk}^{(e)} & \cdots \\ & \vdots & & \vdots & & \vdots & \end{bmatrix} \tag{3.40}$$

If i, j, and k are nodal points of a triangular element, all the other components in the stiffness matrix except the nine shown in the matrix are zero.

The total energy of all the nodal points in the domain expressed by the whole potential vector $\{V\}$ is equivalent to (3.38), and is given by:

$$W = \sum_e \{V\}^T [\tilde{K}]^{(e)} \{V\} = \{V\}^T \sum_e [\tilde{K}]^{(e)} \{V\} \tag{3.41}$$

With the denotation

$$[K] = \sum_e [\tilde{K}]^{(e)} \tag{3.42},$$

the total energy is:

$$W = \{V\}^T [K]\{V\} \tag{3.43}$$

Now that we have obtained the expression of the total energy W in terms of potential V, minimizing the total energy W of the domain requires finding the vector $\{V\}$ that satisfies $\frac{\partial W}{\partial V_n} = 0$ (n=1,2...N_p). Thus, we get

$$\frac{\partial W}{\partial V_n} = \frac{\partial}{\partial V_n}\left(\{V\}^T [K]\{V\}\right) = 0 \tag{3.44}$$

By solving equation (3.44), we get a matrix equation:

$$[K]\{V\} = 0 \tag{3.45}$$

The vector $\{V\}$, containing the potential of all the nodal points in the domain, is to be solved, except those points on the boundaries. So before solving Equation (3.45), the boundary conditions should be imposed for the corresponding nodal points. Since $[K]$ is only determined by the nodal points coordinates, theoretically $\{V\}$ can be solved completely. The calculation is usually an enormous process, the complexity of which depends on the number of nodal points. When vector $\{V\}$ is calculated, the potentials on all of the nodal points are determined. Then, with the interpolation function N_i, the whole domain including the interior of elements can be calculated.

3.5.4 Comparison of the Finite Difference and Finite Element Methods

The solution of potential in the entire domain accentuates the major difference between FEM and the finite difference method: in the latter, only the points in the lattice are resolved to obtain specific potentials. A remarkable result of this contrast is that the gradient of potential (which is the definition of electric field) can be approached in FEM (to a certain level), but not

in the finite difference method. To implement our aim of calculating the electric field with acceptable accuracy, FEM is preferable due to its ability to give continuous potential for the entire domain. Furthermore, in FEM, every element is connected at its nodal points to its adjacent elements, ensuring continuity of the potential across element boundaries as well.

The limitation of FEM is that the linear function assumption within an element might cause error. And even though the potential is continuous in the whole domain, the continuity of the gradient of the potential across inter-elements does not generally exist, bringing up a discrepancy with the Laplace equation which is a second order differential equation of the potential. However, since the potential on the nodal point is accurate, by increasing the number of nodal points, it is possible to get whatever accuracy is needed.

3.6 Calculation Results and Explanation of Experimental data

3.6.1 Introduction to FEMLAB

FEMLAB ® (COMSOL, Burlington, MA), is an interactive program for modeling and solving scientific and engineering problems based on partial differential equations. When solving the partial differential equations, FEMLAB runs the finite element analysis together with meshing and error control using a variety of numerical solvers.

The procedure of FEMLAB modeling and analysis includes creating models, setting model properties, generating and refining mesh, and processing the analysis.

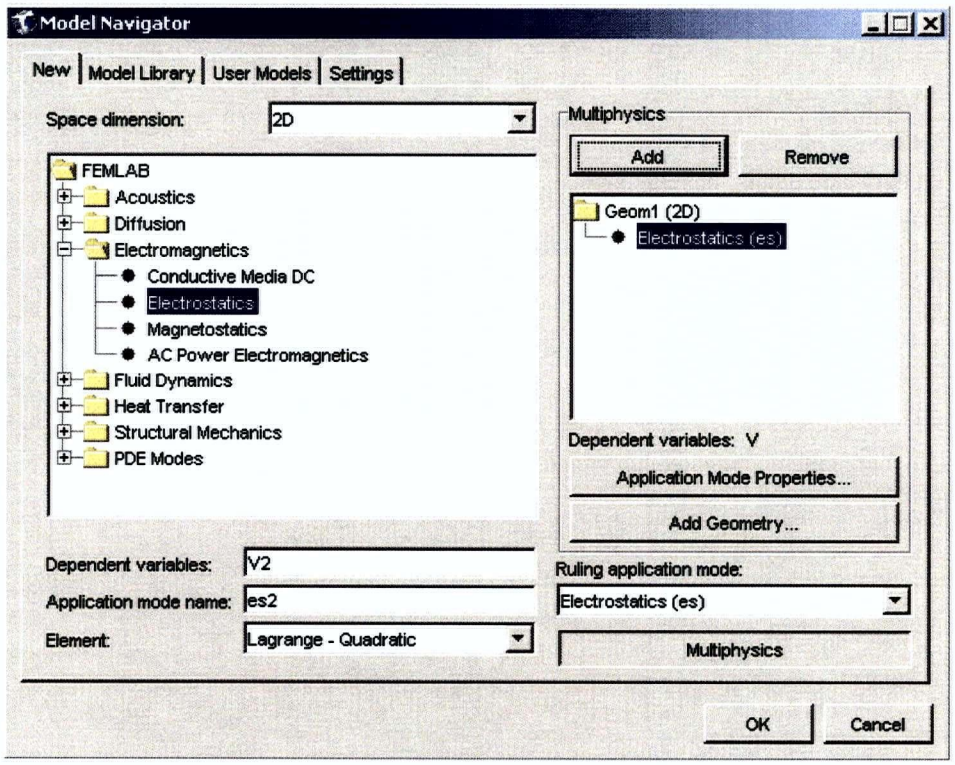

Figure 3-8 Creating a new 2D electrostatic model with the dependent variable V.

The model navigator is loaded when FEMLAB is started. Figure 3-8 shows the window that establishes a new 2D electrostatic model. Then the application window comes up to provide a graphic user interface (GUI) that handles all aspects of the modeling process: pre-processing and CAD; specification of the physics through equations, material data, boundary conditions, coupling and other properties; meshing, assembly, and solution of the finite element model; post-processing and visualization of the solution and other quantities.

By using the mode navigation buttons, various selections and display models can be used to access the model from different aspects. Figure 3-9 shows the model navigation buttons. FEMLAB provides six different modes to modify and display the model. In *Boundary Mode*, for example, the condition of each boundary can be designated (Figure 3-10).

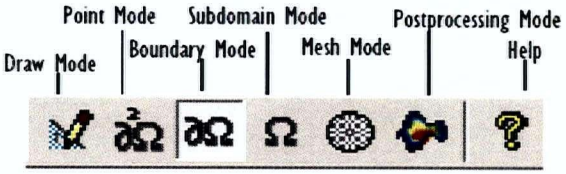

Figure 3-9 Selection and display modes.

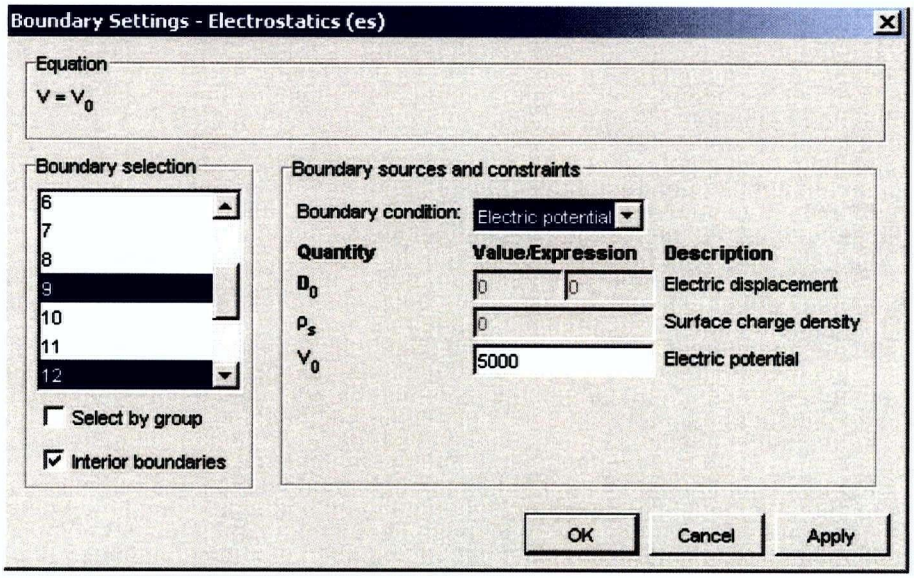

Figure 3-10 Setting boundary mode.

3.6.2 Model Description

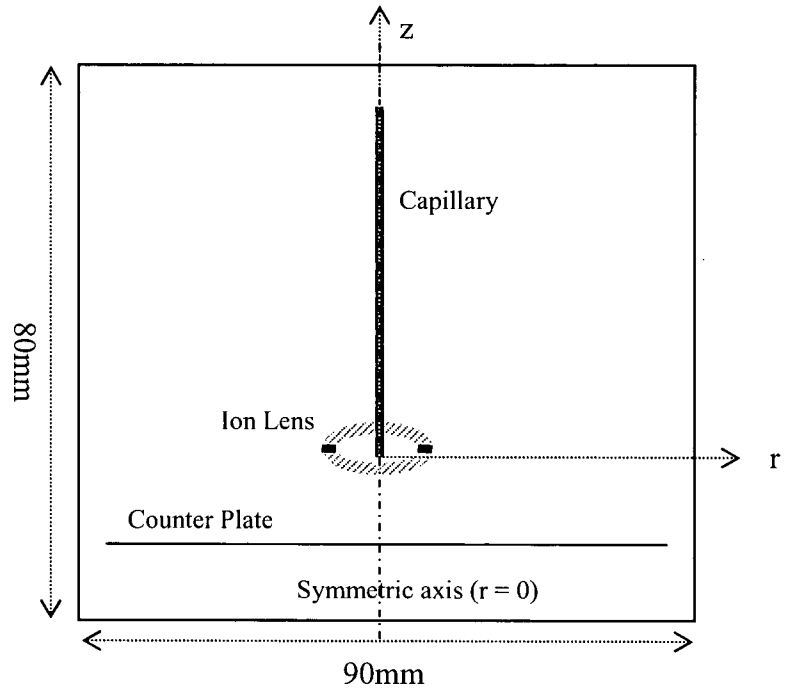

Figure 3-11 Model of the electrospray ion source. The whole model is set in a 90 mm × 80 mm rectangle.

A 2-D model was built in FEMLAB. The whole model is in a 90 mm × 80 mm rectangular region symmetric about z axis ($r = 0$). The capillary and the ion lens are set in cylindrical coordinates. Although in the experiment we used an oblong-shaped lens, in the calculating model, we replaced it with a round ring-shaped lens with inner and outer radii of 4 mm and 6 mm, respectively, and 1mm thick. The capillary is approximated to be a 0.4 mm o.d. wire, the end of which is 10 mm away from a counter plate. Figure 3-11 describes the geometry of the lens, capillary and the counter plate.

After the model is built, FEMLAB is able to generate an initial mesh, as shown in Figure 3-6. Then the mesh can be selectively refined to generate more nodal points in the region (Figure 3-12). Then the potential distribution is solved by FEMLAB for the entire modeling

domain following steps 2 to 5 in section 3.5.2. The electric field is calculated from the gradient of the potential.

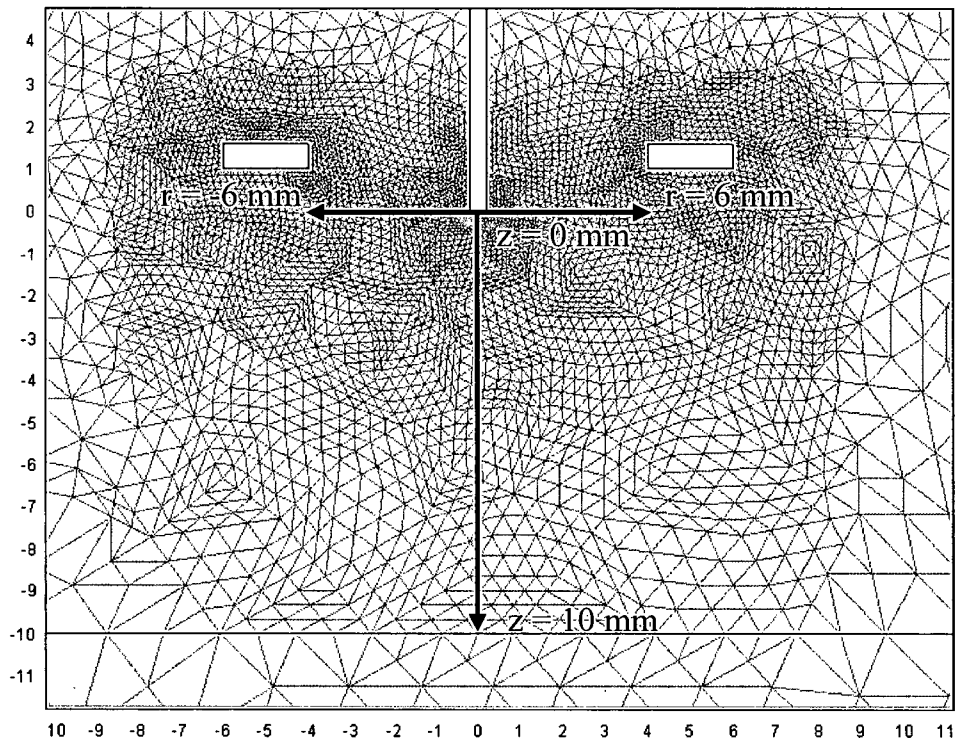

Figure 3-12 Refined mesh of part of the modeling region. The vertical line indicates the area with 0 mm < z < 10 mm, and -0.1 mm < r < 0.1 mm. The horizontal line indicates the area with -6 mm < r < 6 mm, -0.1 mm < z < 0.1 mm.

3.6.3 Comparing the Potential and Field under Different Lens Voltages

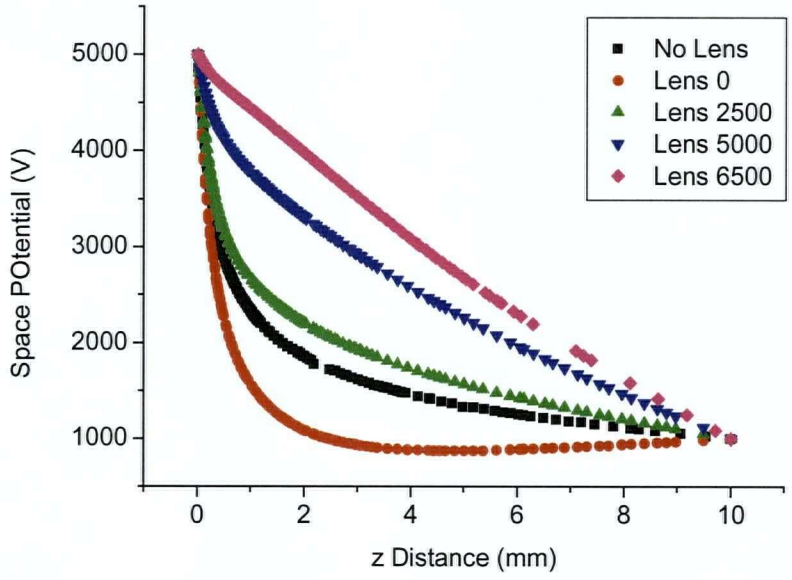

Figure 3-13 Potential distribution on the z axis from z=0 to z=10. The ion spray potential is 5000 V.

As observed in our experiment (Figures 2-7 to 2-10), at the same ion spray voltage but different lens voltages, the ion signal differs dramatically. The electric potential at the *z* axis from the capillary tip to the counter plate is the first to be studied. So in the FEMLAB model, the capillary is set at 5000 V, the counter plate 1000 V, and housing 0 V according to the experimental conditions. The space potential is solved for no lens, lens 0 V, 2500 V, 5000 V and 6500 V. The area within -0.1 mm $< r <0.1$ mm is chosen to approximate the *z* axis ($r=0$). The *z* range of interest is from the tip of the capillary ($z=0$ mm) to the counter plate ($z=10$ mm). Note in the model in Figure 3-11 and Figure 3-12, the counter plate is at $z=-10$ mm, but for convenience we use the absolute value for z), which is denoted by the vertical line in Figure 3-12. Thus the potentials on points within the range $-0.1<r<0.1$ and $0<z<10$ are plotted as the axial potential distribution (Figure 3-13). The potentials on the sprayer and the counter plate are

fixed, and thus each curve has the same starting and ending point. However, the rates of decrease for the four curves are different due to the presence of lens and different lens potentials. From the potential distribution in Figure 3-13, it can be predicted that the electric field at the spray tip, which is the starting point, varies significantly for the four situations. Since the ion lens 0 V curve has the greatest dropping rate, it would not need any calculation to verify that when the ion lens is at 0 V, the electric field at the spray tip will be the largest among the four.

To be more quantitative, the electric field is calculated as the gradient of the potential. Being a vector, the electric field has a norm value. Because of axial symmetry, the axial electric field should be always parallel to the *z* axis and perpendicular to the counter plate. As an expected result, the field in the *z* direction (Figure 3-15) is very close to the norm of the field (Figure 3-14). In the following plots we only show the norm of E.

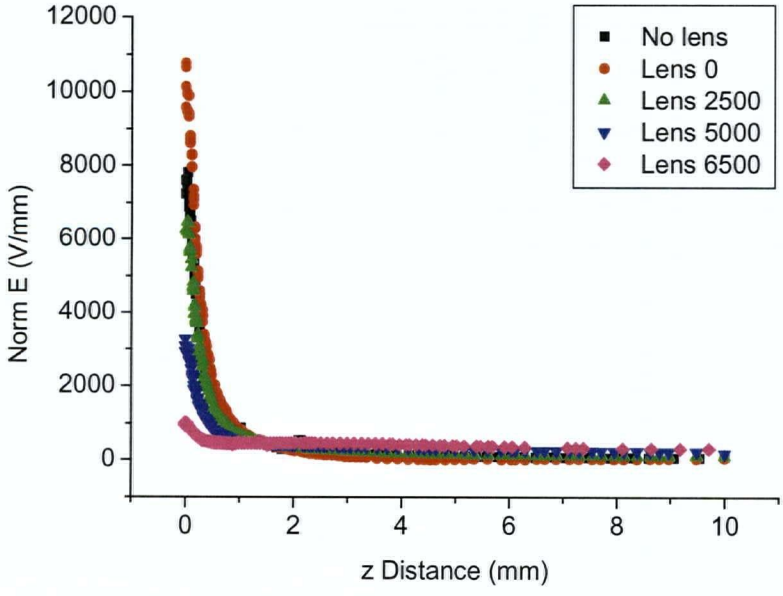

Figure 3-14 Axial norm electric field. The ion spray potential is 5000 V

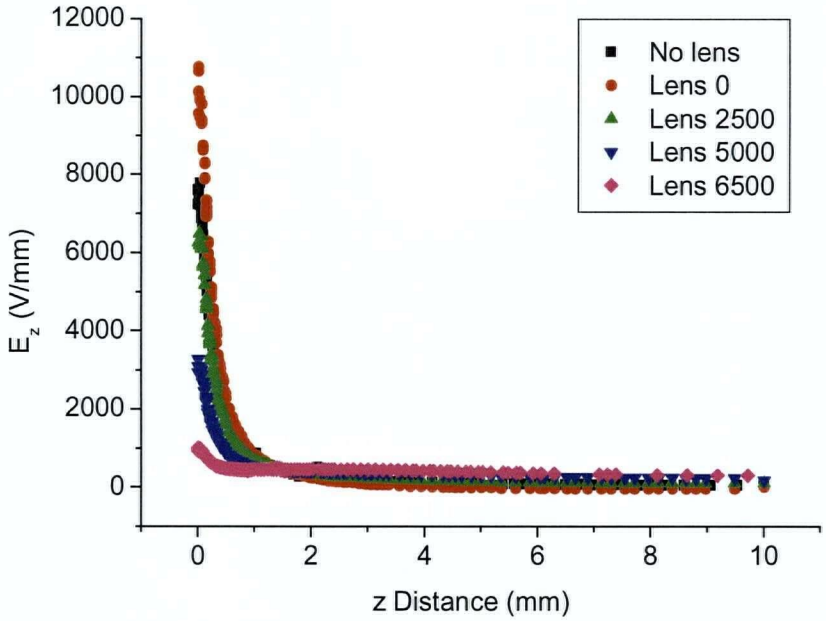

Figure 3-15 Axial electric field in the z direction. The ion spray potential is 5000 V.

Figure 3-16 is the same as Figure 3-14 except for the smaller axis range. With the lens at 0 V, the potential decreases fastest with *z* distance (Figure 3-13), resulting in the largest electric field in the *z* direction (red curve in Figure 3-16). The lens at 6500 V gives the smallest electric field (purple curve in Figure 3-16), which might suppress the electrospray completely. The curve for no lens (black curve in Figure 3-16), lying in between red and green curves, implies that the "no lens" setting will have the same effect as when the ion lens is set between 0 and 2500 V. The differences of magnitudes of the electric fields at the spray tip are so significant that it varies from 1000 V/mm to 11000 V/mm, which we believe will affect the performance of electrospray ionization dramatically.

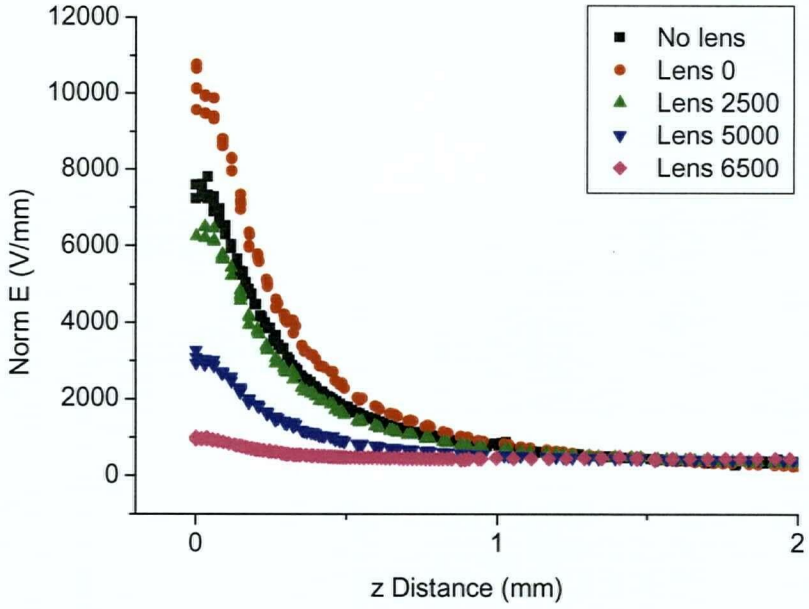

Figure 3-16 Axial norm of electric field in a smaller z range. The ion spray potential is 5000 V.

Another representative region is the *r* axis (*z=0*), which is the plane perpendicular to the capillary while touching the tip. We chose this region by sorting out points with *-0.1* mm < *z* < *0.1* mm and *-6* mm < *r* < *6* mm, which is denoted by the horizontal line in Figure 3-12. The potential distribution is plotted in Figure 3-17. In this figure, the lens with 6500 V curve has the lowest potential at the middle, so it is the least possible for ions to go off-axis when the ion lens is at 6500 V. The ability to restrain ions from going off the axial direction is what we called the focusing effect. Figure 3-17 therefore shows lens 6500 V produces the best focusing effect, while lens 0 V the worst.

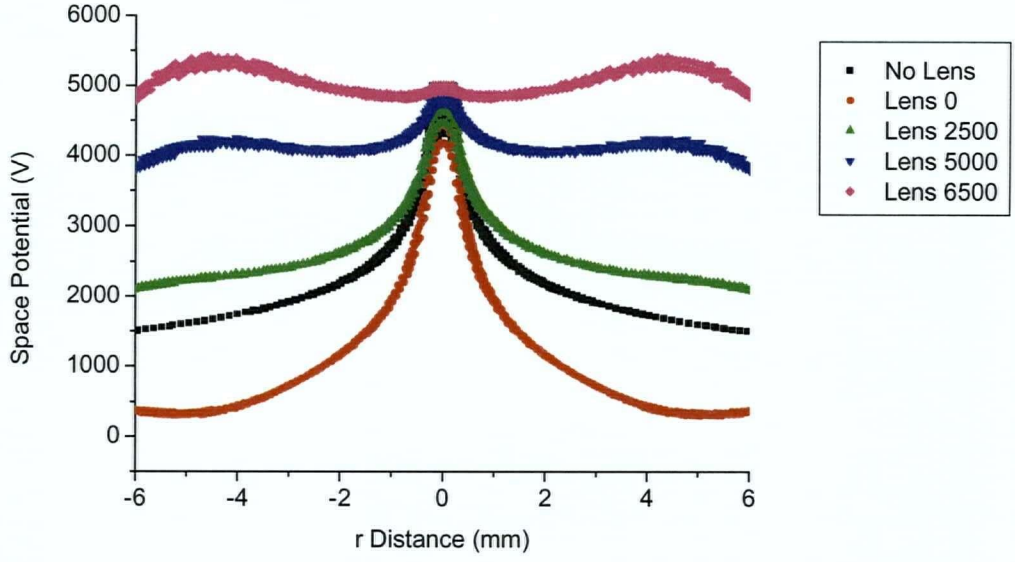

Figure 3-17 Space potential distribution at z=0 direction. The spray potential is 5000 V.

A more explicit description of the focusing effect is the distribution of equipotential lines, and the magnitude of the electric field is represented by the density of equipotential lines (Figure 3-18, Figure 3-19, Figure 3-20, Figure 3-21 and Figure 3-22). Figure 3-18 shows the equipotential lines for spray 5000 V and lens 0 V, where the equipotential lines are greatly condensed at the tip of the capillary, forming the largest electric field at the tip. However, the curvature of lines at the *z* axis is also the largest and weakens the focusing effect. Figure 3-21 shows equipotential lines for spray 5000 V and lens 6500 V. The equipotential lines are very sparsely distributed along the *z* axis, resulting in the smallest electric field at the tip. In contrast, the equipotential lines are nicely flattened and even form a concave shape, providing the best focusing effect. Thus, a balancing issue has to be taken into consideration. The lens at 0 V generates the largest axial electric field and the least focusing effect, while the lens at 6500 V

gives the best focusing effect and the smallest field. The trade-off of the two effects is the key to get highest efficiency in the electrospray ionization procedure.

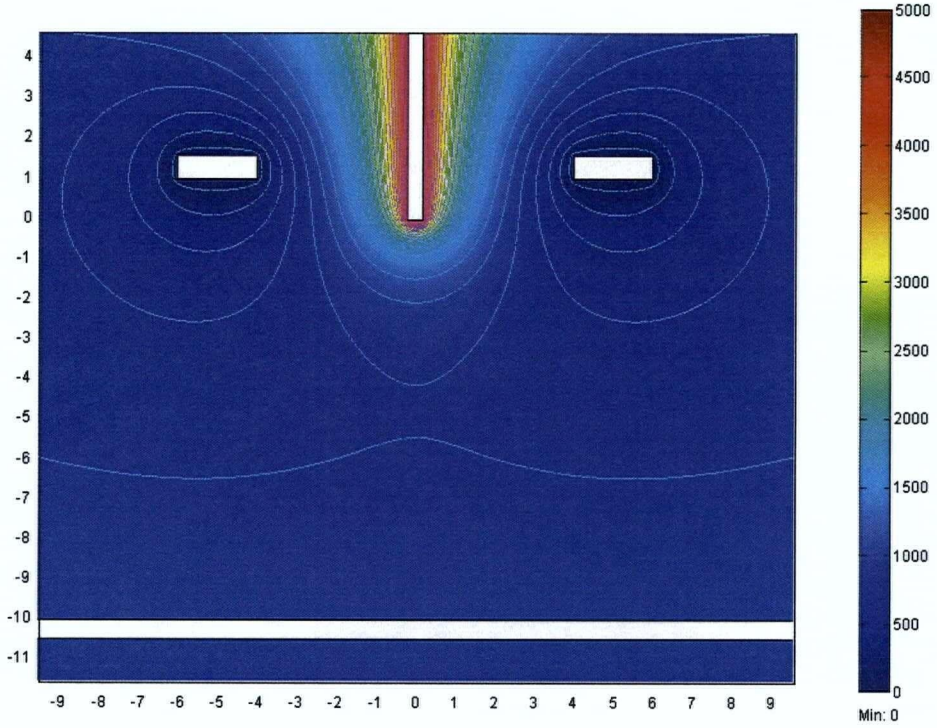

Figure 3-18 Equipotential lines with ion spray 5000 V, lens 0 V.

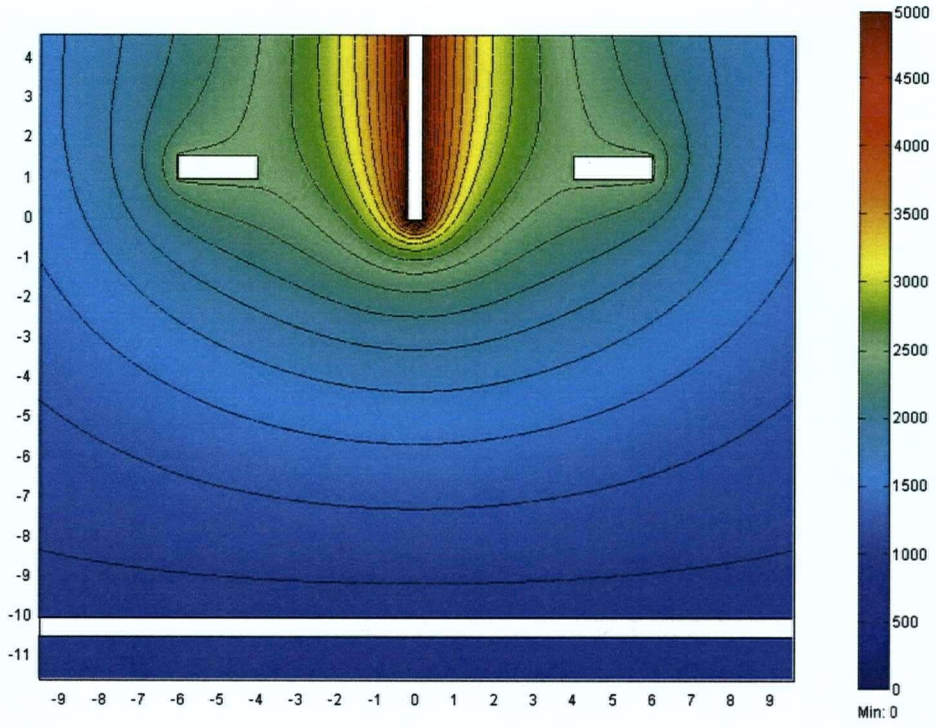

Figure 3-19 Equipotential lines with ion spray 5000 V, lens 2500 V.

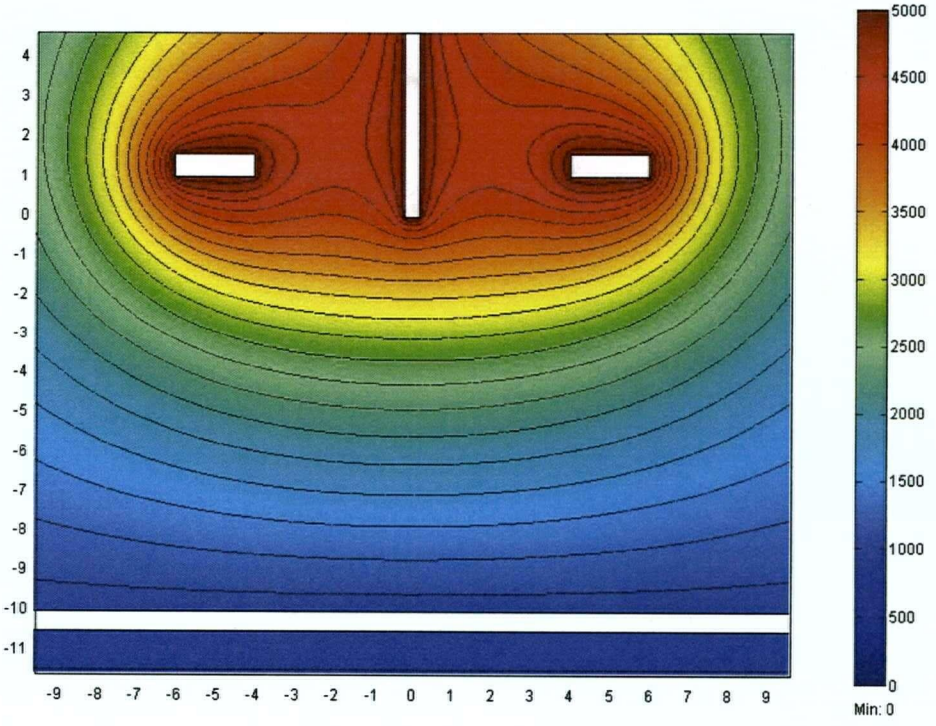

Figure 3-20 Equipotential lines with ion spray 5000 V, lens 5000 V.

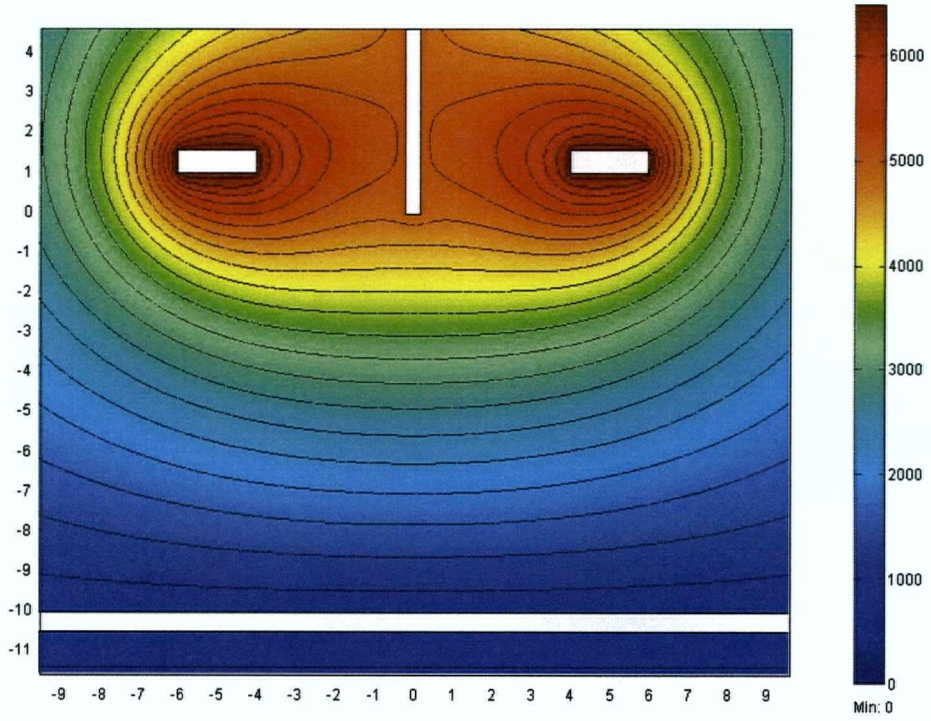

Figure 3-21 Equipotential lines with ion spray 5000 V, lens 6500 V.

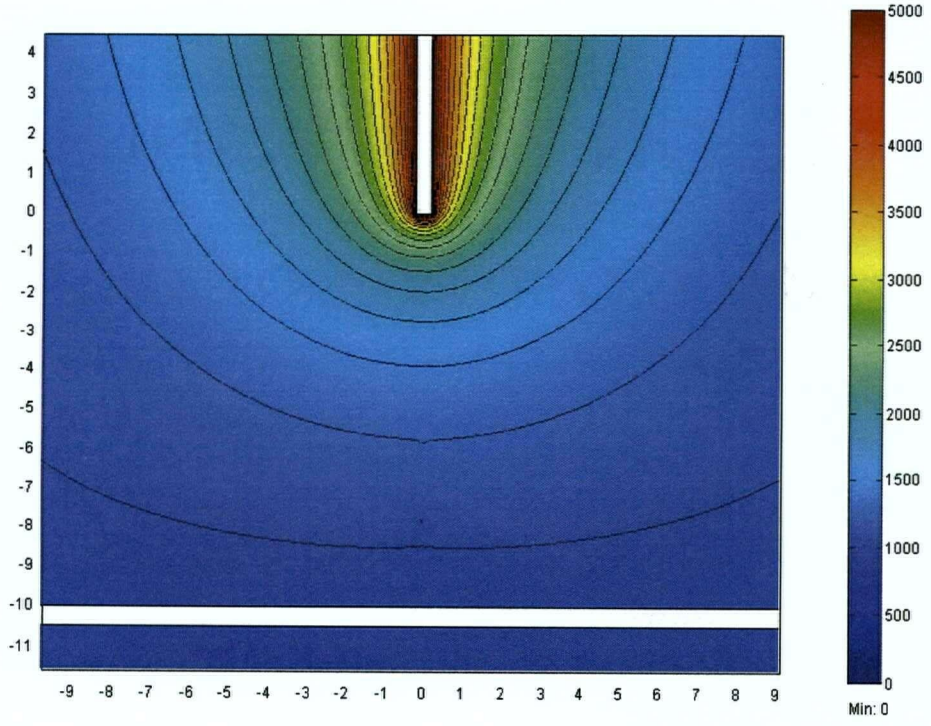

Figure 3-22 Equipotential lines with ion spray 5000 V, no ion lens.

The equipotential lines with no ion lens are shown in Figure 3-22. The no lens model gives an intermediate ability in both focusing effect and electric field strength, in between lens 0 V (Figure 3-18) and lens 5000 V (Figure 3-20). However, there is no flexibility of choosing between focusing and high field. Therefore, when the ion lens is in position, more freedom of adjusting the performance of ESI is allowed, which is one of the significant advantages of using the ion lens.

3.6.4 Explanation of Experimental Data

In Chapter 2, we showed several experimental results concerning the ion signal at different spray and lens voltages. With certain combinations of the spray and lens voltages, fair signal can always be obtained, even if the spray voltage is much lower than normally required. We hypothesized that the optimum electric field around the spray tip must be relatively constant when the appropriate potential difference between the sprayer and the lens is chosen, no matter what the absolute voltages are.

Part of the α-CD data can be used as an example. In Figure 3-23, at four different lens voltages, there are four maxima in the signal, and the four maxima are at different spray potentials. The four combinations for spray and lens voltages are: (3500, 0), (4000, 1000), (4750, 2000), and (5500, 3000), as indicated by the arrows. We first set the model at the potential conditions in accordance with the four apexes to plot an axial potential distribution. Figure 3-24 shows the potential distribution at the r axis from $z=0$ to $z=10$ mm. When the potential at the capillary tip was changed from 3500 to 5500, the potential distribution for the four conditions also was also changed significantly.

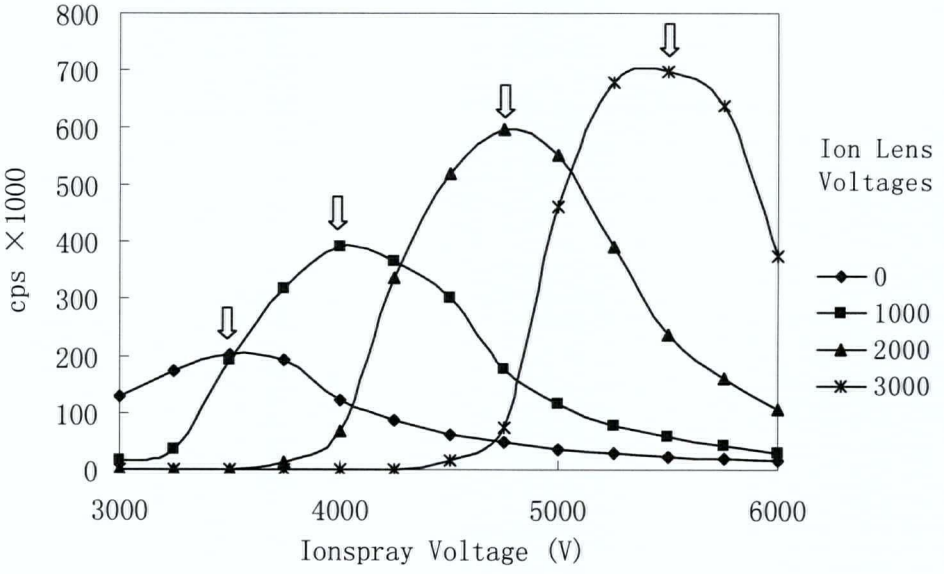

Figure 3-23 Signal intensity of α-CD vs. sprayer voltage at different ion lens voltages. The ion lens voltages used are from 0 to 3000 V. Arrows point at the four maxima of signal at each lens voltage where the voltages for the sprayer and lens are (3500, 0), (4000, 1000), (4750, 2000), and (5500, 3000)

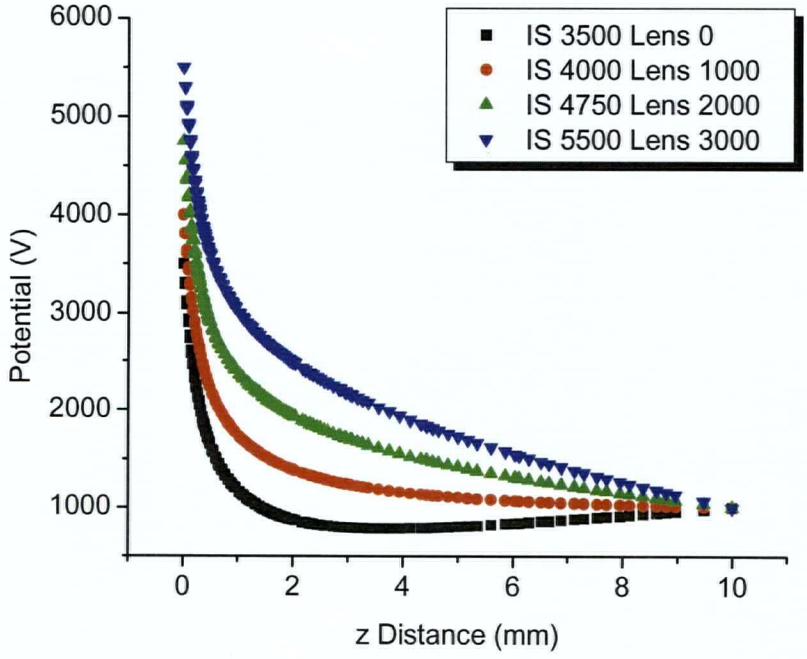

Figure 3-24 Axial potential distribution for four MAXIMUM signal conditions.

However, when we plot the norm of electric field, the field distribution in the four conditions are very close to each other (Figure 3-25), which verified the constant field hypothesis, especially at positions near the capillary tip (*z=0*).

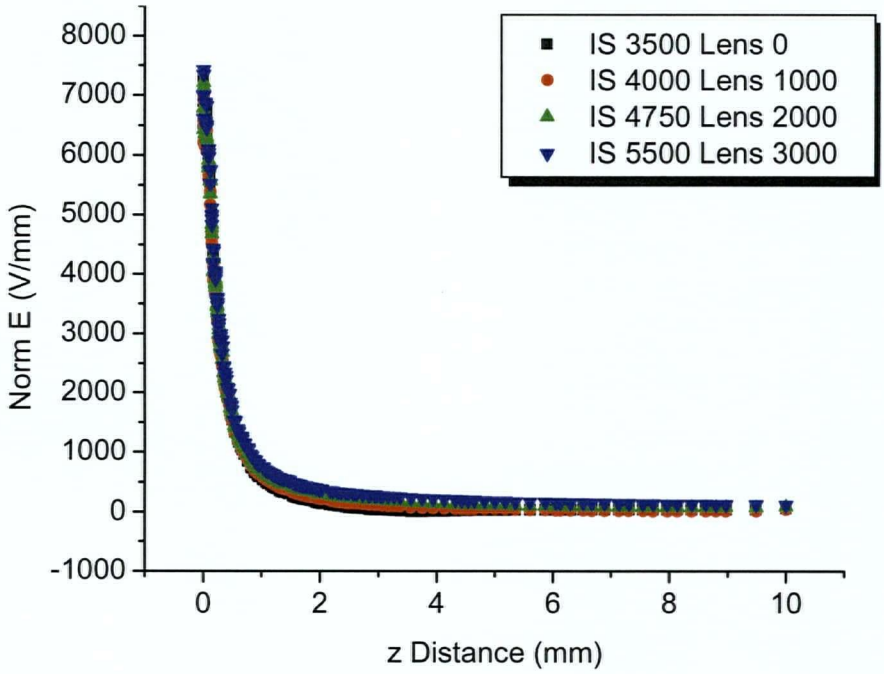

Figure 3-25 Axial norm electric field versus z distance for four MAXIMUM signal conditions.

Then we shall look at the signal onset points. We omitted the zero lens voltage case because the signal onset point is out of range in the experimental data. The combination of spray and lens voltages for the three remaining conditions are: (3000, 1000), (3750, 2000) and (4500, 4000). Arrows in Figure 3-26 indicate the three points we simulated.

When the potential distribution and the norm of electric field are plotted, the result once again meets our expectation. As shown in Figure 3-27 and Figure 3-28, the potentials have different distribution curves for the three onset cases, while the electric field curves are very similar. Our hypothesis thus proves correct again.

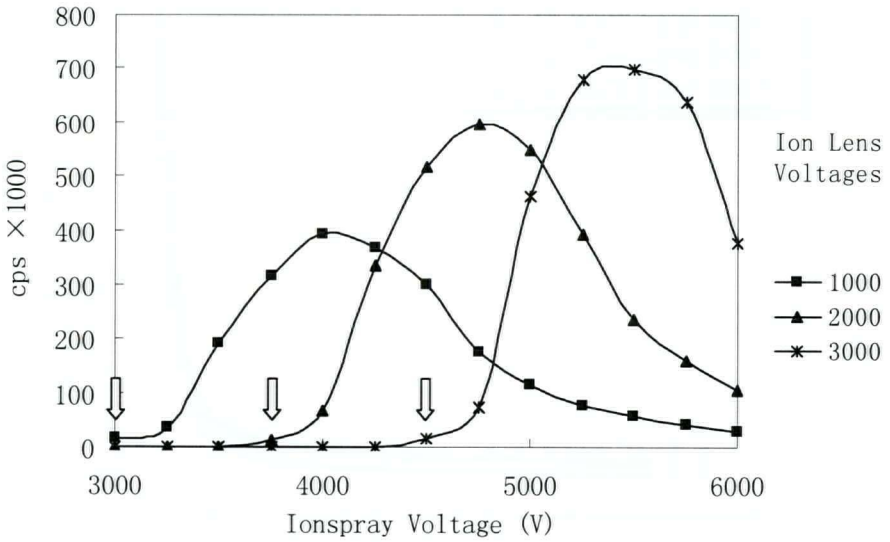

Figure 3-26 Signal intensity of α-CD vs. sprayer voltage at different ion lens voltages. The ion lens voltages used are from 1000 to 3000 V. Arrows point at the three ONSET voltages of signal at each lens voltage where the voltages for sprayer and lens are (3000, 1000), (3750, 2000) and (4500, 4000)

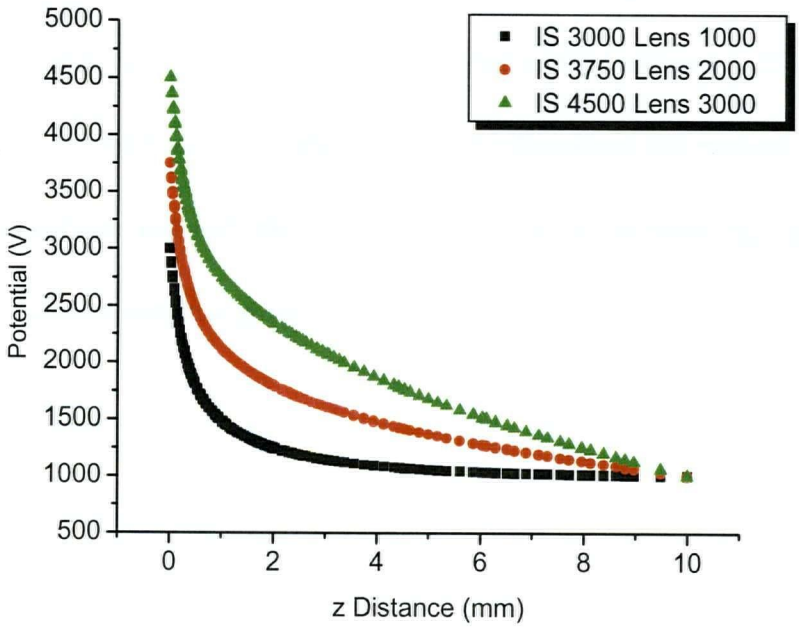

Figure 3-27 Axial potential distribution versus z distance for three ONSET signal conditions.

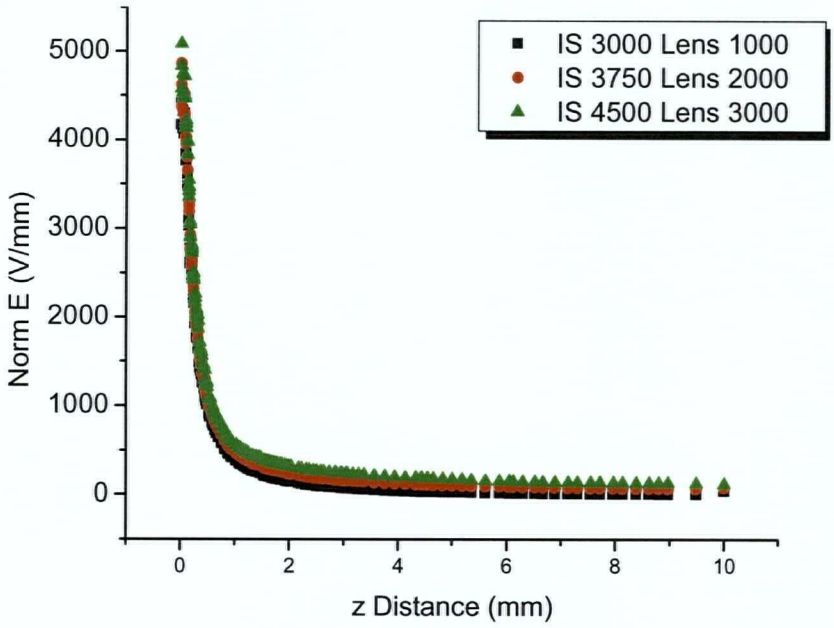

Figure 3-28 Axial norm electric field versus z distance for three ONSET signal conditions.

The comparison of Figure 3-25 and Figure 3-28 is shown in Figure 3-29, in which the two groups of curves are plotted. The curves in the top group represent E generated from the potential combinations to produce maximum signal (refer to Figure 3-23), and the bottom curve group represent E generated from the potential combinations that initiate signal (refer to Figure 3-26). The difference between the two groups is shown to be more significant than the difference of curves within a group.

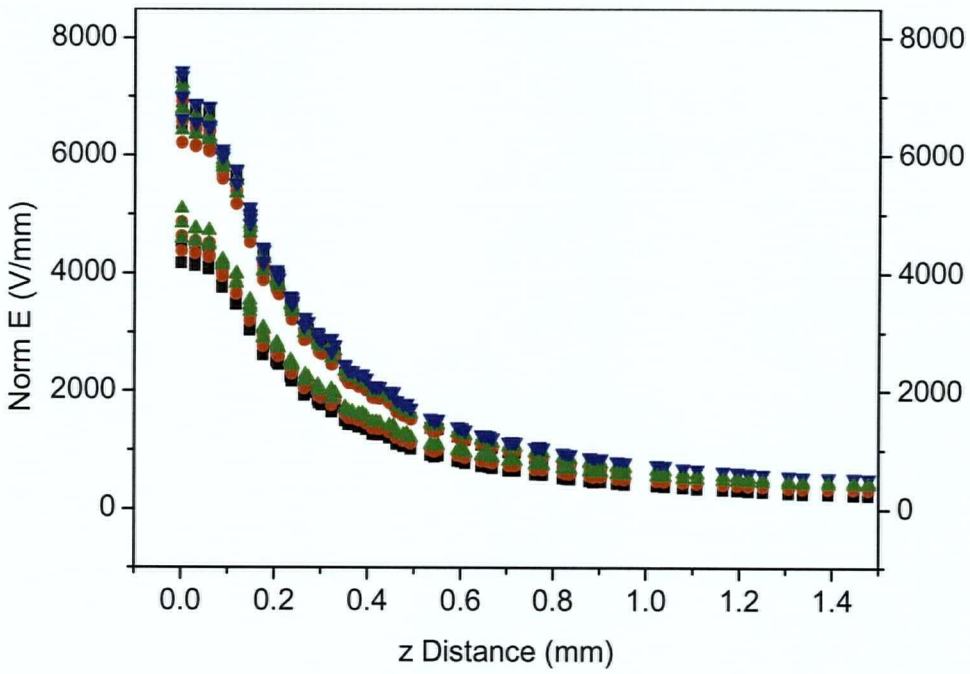

Figure 3-29 Comparison of axial norm electric field versus z distance for maximum and onset signal conditions. The group of curves on top is field giving MAXIMUM signal, and group of curves at bottom is field that gives ONSET signal.

Despite the closeness of E, the maximum signal magnitudes for each of the voltage combinations are still different (Figure 3-23). One reason is that different magnitudes still exist in E within a group. Another reason is the difference in focusing effects. Figure 3-30 shows four equipotential line distributions with the same settings as to generate maximum signals indicated by arrows in Figure 3-23. The combinations for spray and lens voltages are (3500, 0) (4000, 1000) (4750, 2000) and (5500, 3000). When the whole domain is studied, the distributions of equipotential lines exhibit much difference in spite of the similarity in axial potential distributions. As apparently shown in Figure 3-30, the focusing effect is at its best when the spray is at 5500 V and the lens 3000 V.

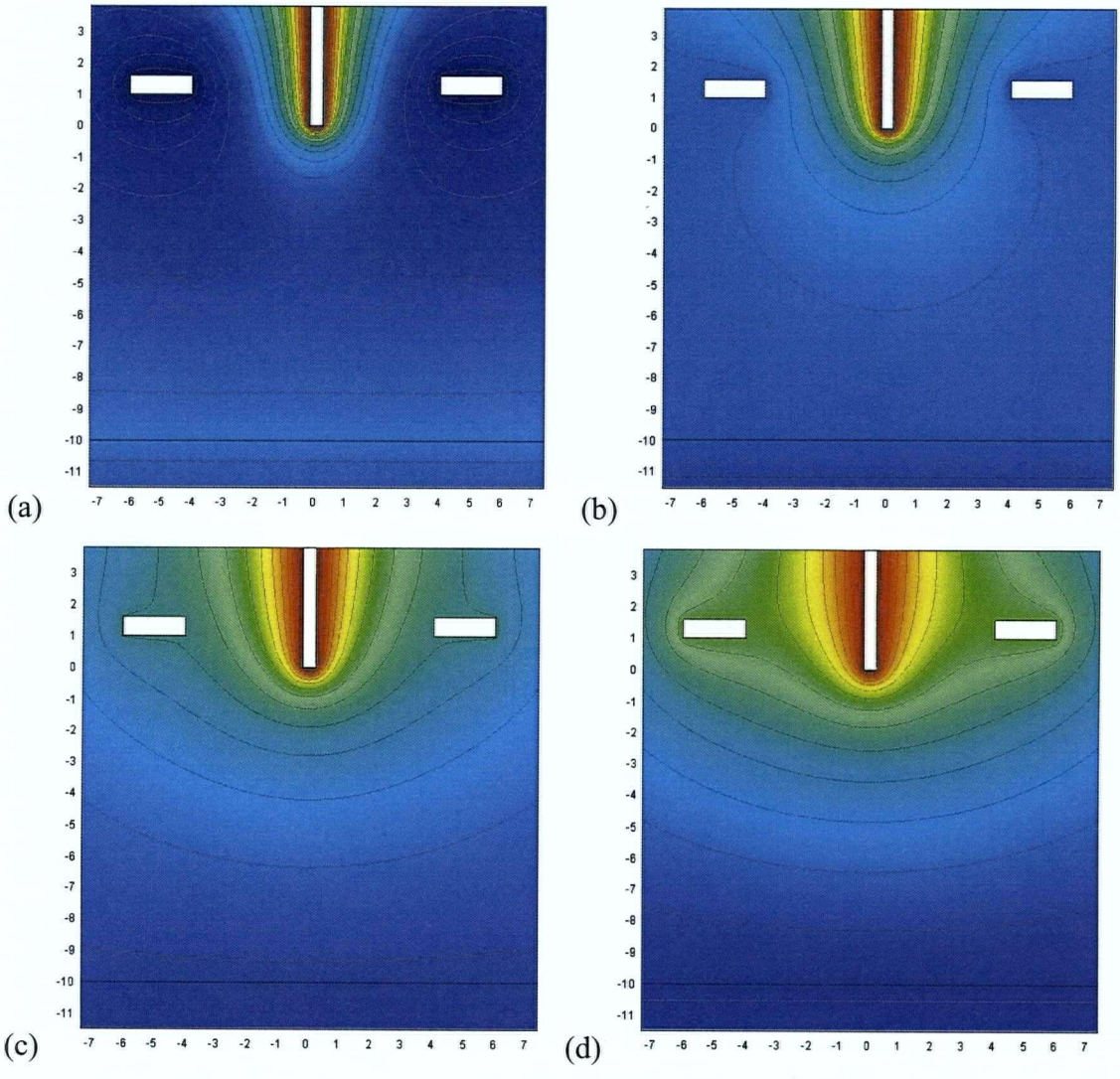

Figure 3-30 The equipotential line distribution for the four maximum signal conditions. The voltages on spray and lens for (a) (b) (c) and (d) are (3500, 0) (4000, 1000) (4750, 2000) and (5500, 3000)

3.7 Conclusions

To calculate the electric field is to solve the Laplace equation in an electrostatic space with no free charge. An attempt to solve the electric field leads to an informative result. The basis of the direct solution is the balance of electric pressure and the surface tension pressure. Given that these two pressures are equal at the surface of a static Taylor cone, the Taylor cone angle was derived. The onset voltage of electrospray was calculated by the Laplace equation.

However, quantitative solution of the entire electric field is still out of reach because of the complexity of boundary conditions.

Numerical methods can be utilized to estimate the electric field. The finite difference method and the finite element method are two widely used numerical methods that were described briefly in this chapter. Even though the basic principles of these methods are simple, the amount of calculation is tremendous. The calculation in this chapter was done by virtue of commercial software, FEMLAB. A model to simulate the geometry of the ion source and ion lens was built to generate the mesh for calculation.

Quantitative results showed that the ion lens voltage can be adjusted to either enforce the focusing effect or increase the magnitude of the electric field, without needing to change spray voltage. A low lens potential produces higher field, while a high lens potential enables a better focusing effect. These two effects, however, are not necessarily additive, leaving the choice of preference to the operator.

The results in Chapter 2 showed that, at different lens voltages, the onset spray voltages could vary by several kilovolts. By processing the model at those different combinations of spray and lens voltages, it was found that electric fields at the spray tip were actually similar, in spite of the large difference of spray voltages. In the same way, the electric field generated from different voltage combinations to give maximum signal are close to each other as well. This proves our constant electric field hypothesis, and verifies that a higher electric field can optimize the performance of electrospray ionization. While maintaining that optimal electric

field, the spray and lens voltages can be increased and adjusted to improve the focusing effect, and hence the ion signal.

3.8 References

1. Jones, A.R. and Thong, K.C., *Production of charged monodisperse fuel droplets by electrical dispersion.* Journal of Physics D-Applied Physics, 1971. **4**(8): p. 1159-&.

2. Loeb, L.B., Kip, A.F. and Hudson, G.G., *Pulses in negative point-to-plane corona.* Physical Review, 1941. **60**: p. 714-722.

3. Smith, D.P.H., *The electrohydrodynamic atomization of liquids.* IEEE Transactions on Industry Applications, 1986. **22**(3): p. 527-535.

4. Wilm, M.S. and Mann, M., *Electrospray and taylor-cone theory, doles beam of macromolecules at last.* International Journal of Mass Spectrometry and Ion Processes, 1994. **136**(2-3): p. 167-180.

5. Taylor, G., *Disintegration of water drops in an electric field.* Proceedings of the Royal Society of London Series a-Mathematical and Physical Sciences, 1964. **280**: p. 383-397.

6. Larsson, S. and Thomee, V., *Partial differential equations with numerical methods*, ed. J.E. Marsden, S.S. Antman and L. Sirovich. 2000, New York: Springer.

7. Heddle, D.W.O., *Electrostatic lens systems*. 2000, London: Institute of Physics Publishing.

8. Ern, A. and Guermond, J.-L., *Theory and practice of finite element*. 2000, New York: Springer.

9. Gupta, O.P., *Finite and boundary element methods in engineering*. 1999, Rotterdam: A.A. Balkema Publisher.

10. Silvester, P.P. and Ferrari, R.L., *Finite elements for electrical engineers*. 1996, Cambridge: Cambridge University Press.

11. Mura, T. and Koya, T., *Variational methods in mechanics*. 1992, New York: Oxford University Press.

Chapter 4

Continued Study of an ESI Sources and Future Prospects

4 Continued Study of an ESI Sources and Future Prospects

4.1 Variables affecting Ionspray Ionization

In Chapters 2 and 3, where the ion lens and the change of electric field are studied, other variables are not taken into consideration simply because they are irrelevant to the electric field. However, some other variables, such as solution composition, nebulizing condition, and the location of the sprayer, are also critical to optimizing the performance of ESI. In this section, we will study some of those variables.

4.1.1 Solutions with Different Water Contents

Most of the experiments in Chapter 2 were carried out with pure water solution with 10 mM ammonium acetate in order to be consistent. However, the content of the solution is a critical factor for ESI performance. Water is the most commonly used solvent since large peptides, proteins and polysaccharides usually dissolve in water, but some proportion of methanol is often added to the solution to assist in solvent evaporation by decreasing the forces on the surface solvent molecules.

10^{-4} M β-CD was prepared in water/methanol mixtures with 10 mM ammonium acetate. The ratio of water percentage varies from 25%, 50%, 75% to 100%. Figure 4-1 shows the spectra of these four solutions that were obtained with all the parameters (including the sprayer position) optimized. The spectra contain peaks of molecular ion *m/z* 1136, a series of fragments, and an ammonium adduct at *m/z* 1153. The intensity of the peaks decreases with the increase of

water content. On the other hand, there is no noticeable fragmentation difference in the four spectra. Figure 4-2 shows the intensities of *m/z* 1136 and 1153. With a pure water solution, the ion signal is much lower than when using the mixtures of methanol and water. This can be explained by the decrease of surface force among the solvent molecules, which is related to surface tension (surface tension γ is 0.0226 N/m for methanol and 0.073 N/m for water)[1, 2]. Smaller force among molecules expedites solvent evaporation, resulting in faster production of gas phase ions. It should be noted that surface force is not the only parameter that determines the process. Solvent polarity will decrease with the proportion of methanol, resulting in less excess charges in the droplets and lower efficiency in ionization[3]. Therefore, except the obvious lower signal for a pure water solution, the relationship between the methanol proportion and ion intensity are obscured by the combined effects of solvent surface force, and polarity. The factors considered above are only from the solvent; however, the efficiency of electrospray is also dependent on the surface activity of the solute to be analysed. It was suggested that for non-polar ions in polar solution, the ions would have high affinity for the droplet surface (surface active analyte), and tend to detach from the droplets easier[4].

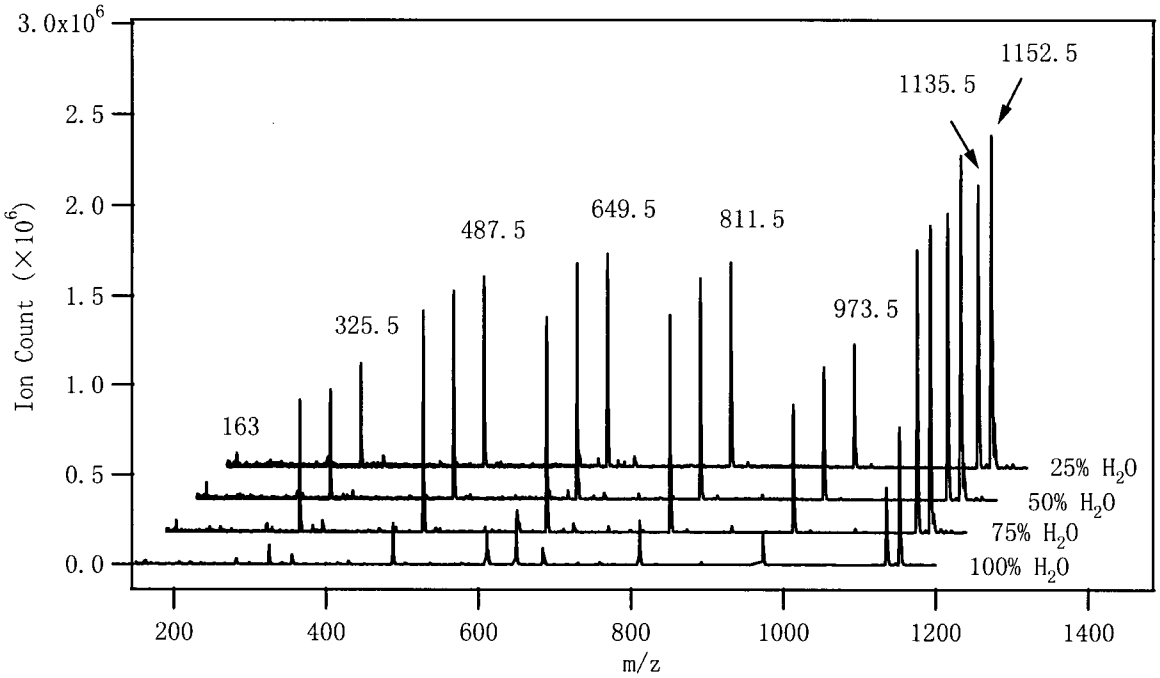

Figure 4-1 Spectra from 10^{-4} M β-CD solution with 10mM ammonium acetate dissolved water/methanol mixtures with 25%, 50%, 75%, and 100% water. Signal is optimized for each solution.

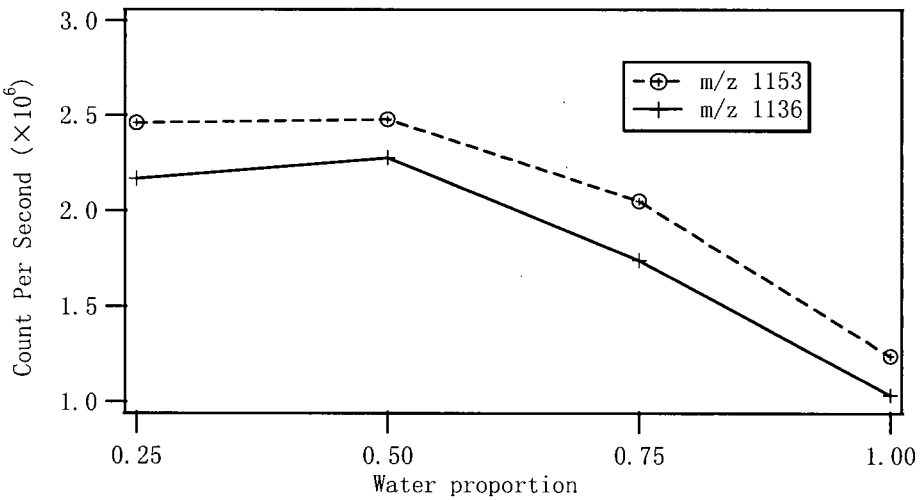

Figure 4-2 Intensities for two ions m/z 1153 and 1136 in four solutions with 0.25, 0.5, 0.75 and 1 water proportions.

In chapter 3, we showed the expression for onset voltage of ESI (Equation 3.10)[5], which increases with the square root of surface tension. That is because the formation of the Taylor cone is based on the balance of surface tension and electric force on the surface, and

higher surface tension requires higher voltage to produce adequate electric force to balance it. This resulted in the highest onset voltage for a pure water solution (data not shown). However, the optimal voltage for a pure water solution is observed to be the lowest among the four (Table 4-1). The onset voltage only depends on the formation of the Taylor cone, but getting the best signal mainly depends on desorption of ions from the charged droplets. Due to the high polarity of the water solution leading more excess charges to the droplet surface and thus faster generation of gas phase ions, a high spray voltage may not be required to produce excess charges as needed by the water/methanol mixtures. Therefore, the optimal voltage required by water solution is the lowest.

Table 4-1 Optimal voltages for solvents with different water contents.

Water Proportion	0.25	0.5	0.75	1
Optimal Voltage (V)	5500	5600	5400	4300

For different solution content in ESI, we only provided a qualitative trend. Future work is still needed to understand the combination of all of the effects resulting from the change of solution content.

4.1.2 Nebulizer

The nebulizing gas is flushed out between the two concentric metal tubes that support the silica capillary. It is expected that the relative position of the inner metal tube and the silica capillary influences the electrospray substantially due to the dramatic change in electric field around the metal tube. It is not so self-evident that the change of the relative position of the two

metal tubes (Figure 4-3) can lead to even greater variation in signal. The nebulizer flow rate is optimized to be about 1 L/min. Figure 4-4 shows the signal variation due to the change in distance between the two metal tubes, where each data point is obtained from the average of 200 scans. Within 0 to 3 mm, further distance unexpectedly generates higher signal. Full understanding of this phenomenon requires the study of the dynamics of the nebulizer. We speculate that the advantage of the nebulizer lies in assisting solvent evaporation and ion focusing. If the nebulizer is too close to the spray tip, it might destabilize the Taylor cone and degrade the electrospray.

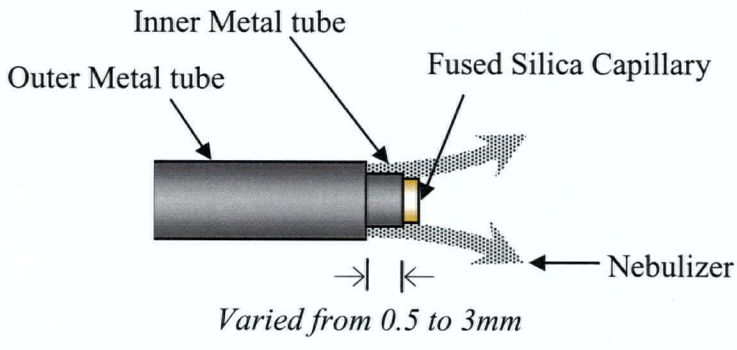

Figure 4-3 The distance between the inner and outer metal tubes varies from 0.5 to 3 mm, with the relative position of the silica capillary and the inner metal tube fixed.

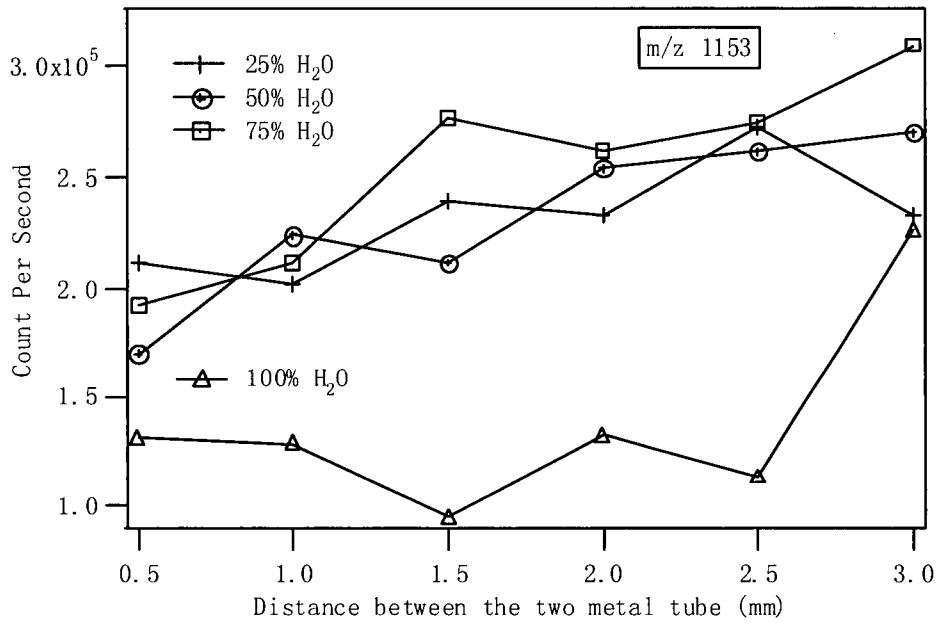

Figure 4-4 The influence of the distance between the two metal tubes on signal intensity.

The 100% water solution produces the lowest signal, consistent with the previous result, with the other three solutions showing similar intensity levels.

4.1.3 Fragmentation Study

Collision induced dissociation (CID) with peripheral air molecules is the main origin of the fragmentation of ions produced by ESI. In the single quadrupole MS used in our study, fragmentation happens mainly in the orifice-skimmer region. The majority of the curtain gas flow is flushed out from the curtain plate in an opposite direction to the coming sprayed mixture, to assist in desolvation of the droplets and to protect the orifice and ion path from bulk solvent and contaminants. There is also a small part of curtain gas flow downstream with the ion mixture into the orifice region to form a free jet expansion, in which the enthalpy of the gas molecules is converted to kinetic energy. By colliding with the high kinetic energy gas

molecules, gas phase ions acquire internal energy which, when high enough, results in dissociation of the ions.

This has been previously described in a model to determine the collision induced dissociation happening in the orifice-skimmer region[6-8]. The potential difference between the orifice and the skimmer relates to the kinetic energy that ions obtain through electric field acceleration, and also to the number of collisions that occur in the region, which determines the amount of energy converted into internal energy. The skimmer is normally grounded and the orifice potential can be adjusted from 0 to 250 V. Supposedly, all the ions have similar kinetic energy at the orifice. That is because the potential drop between the curtain plate and the orifice is relatively large, therefore, small variations in the orifice potential will not result in significant energy difference. In the orifice-skimmer region, however, ions receive completely different amounts of kinetic energy due to the relatively larger difference in potential drop and higher vacuum in this region. Figure 4-5 shows the fragmentation states of 10^{-4} M β-CD under different orifice voltages, varying from 30 to 250 V. When the orifice is increased to 50 V and higher, fragments of β-CD start to appear and gradually become dominant, while the total ion flux decreases.

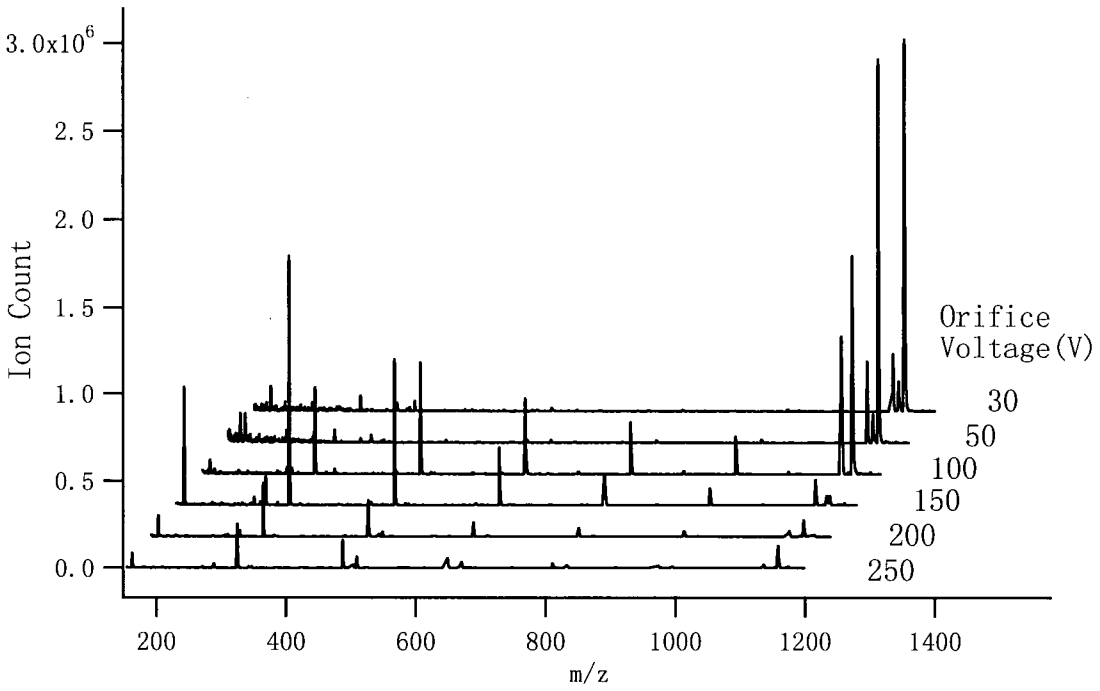

Figure 4-5 Spectra of 10^{-4} M β-CD in H_2O/Methanol (3:1) solution with different orifice potentials. The orifice potential is increased from 30 V to 250 V.

As calculated in the model[7], an increase in the electric field results in a linear increase in the amount of internal energy acquired by the ions. Theoretically, more extensive fragmentation would occur with increasing orifice potential. However, this is not always the case as shown in Figure 4-5, in which orifice potentials higher than 150 V surprisingly result in a decrease in all peaks. There is a possibility that should not be neglected, that under higher electric field, even the monosaccharide rings could dissociate to generate fragments smaller than m/z 200. However, if all the peaks decreased without smaller fragments appearing, there should be other explanations. One possible reason would be the breaking down of gas between the orifice and the skimmer under high electric field, resulting in a noisy baseline with undesired peaks in the spectrum, as in the spectrum with orifice at 250 V. Another possible reason could be that the focusing effect decreases with the orifice voltage.

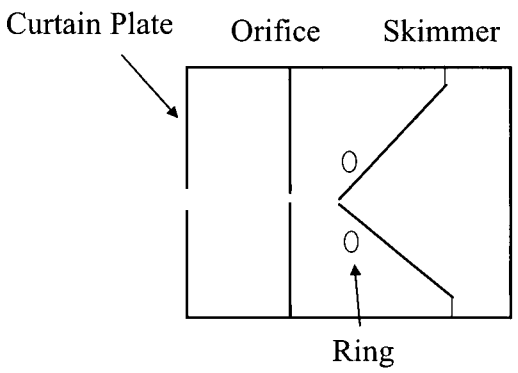

Figure 4-6 Geometry of the orifice-skimmer. The distance from curtain plate to orifice is 4 mm, and from orifice to skimmer is 1.7 mm. The aperture diameters are 3 mm, 0.25mm, 0.75mm for the curtain plate, orifice, and skimmer, respectively. A ring with diameter about 3 mm is located at the back of the skimmer.

Figure 4-6 gives a view of the geometry of the curtain plate, orifice, and the skimmer with a ring around it. The ring acts as a focusing lens and is set at 200 V. According to the experimental results, adjusting the ring potential has only a slight effect on the signal. Therefore, the equipotential line distribution is plotted in Figure 4-8 for different orifice potentials. It is clearly shown that the equipotential lines at lower orifice potential are more concave along the ion path, which implies a better focusing effect. Potential and electric field distribution along the center line of the ion path are plotted in Figure 4-8 and Figure 4-9.

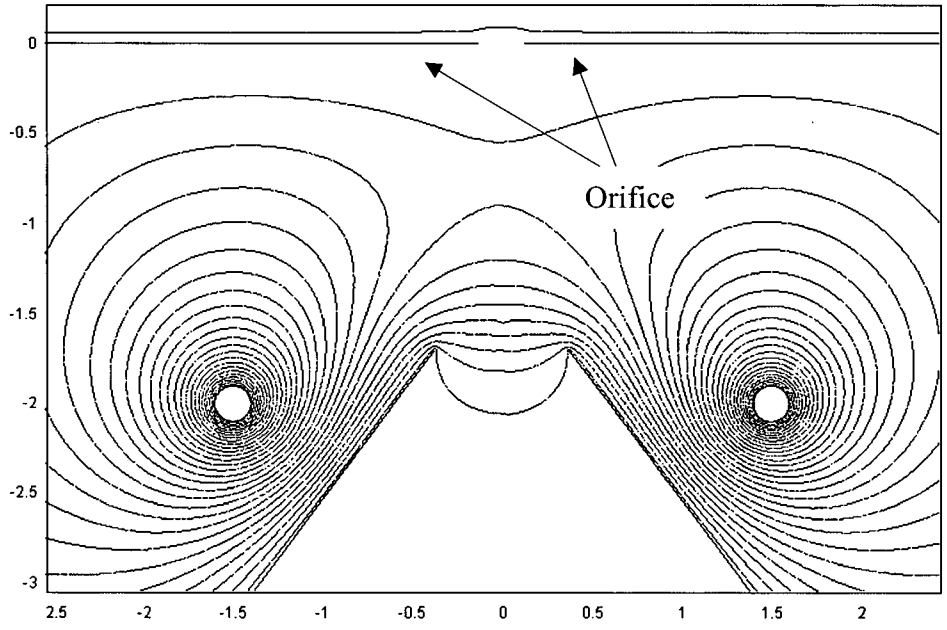
Orifice
0
-0.5
-1
-1.5
-2
-2.5
-3
2.5
-2
-1.5
-1
-0.5
0
0.5
1
1.5
2

(a)

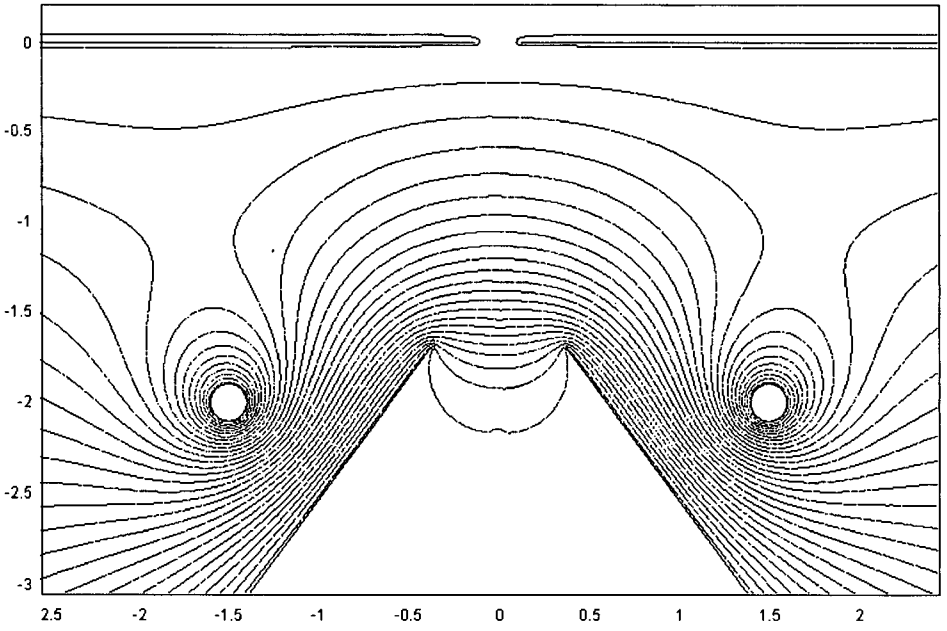
0
-0.5
-1
-1.5
-2
-2.5
-3
2.5
-2
-1.5
-1
-0.5
0
0.5
1
1.5
2

(b)

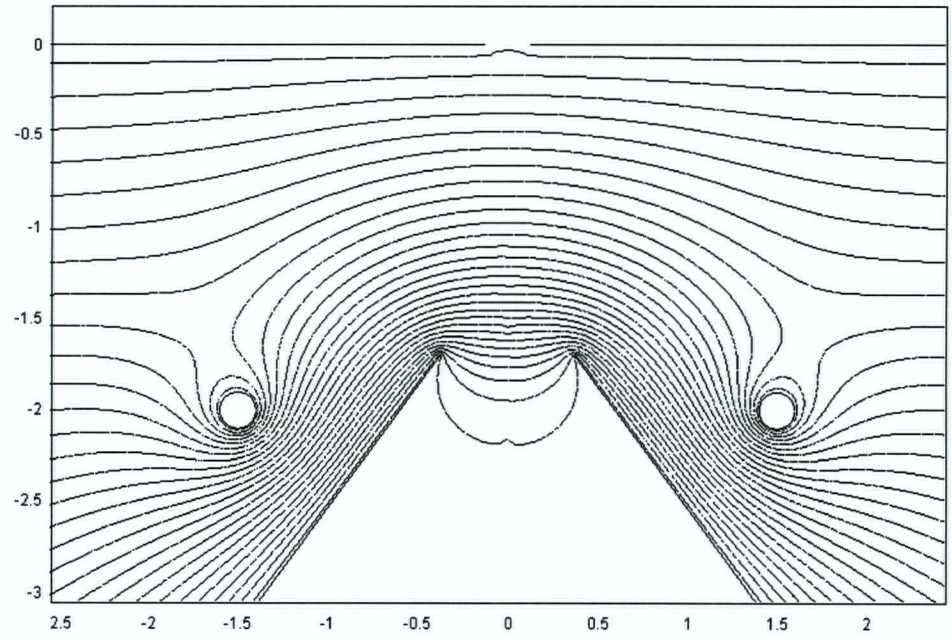

(c)

Figure 4-7 Equipotential line distribution for orifice potential at (a) 50 V, (b) 150 V, (c) 250 V. The ring and skimmer are fixed at 200 V and 0 V, respectively.

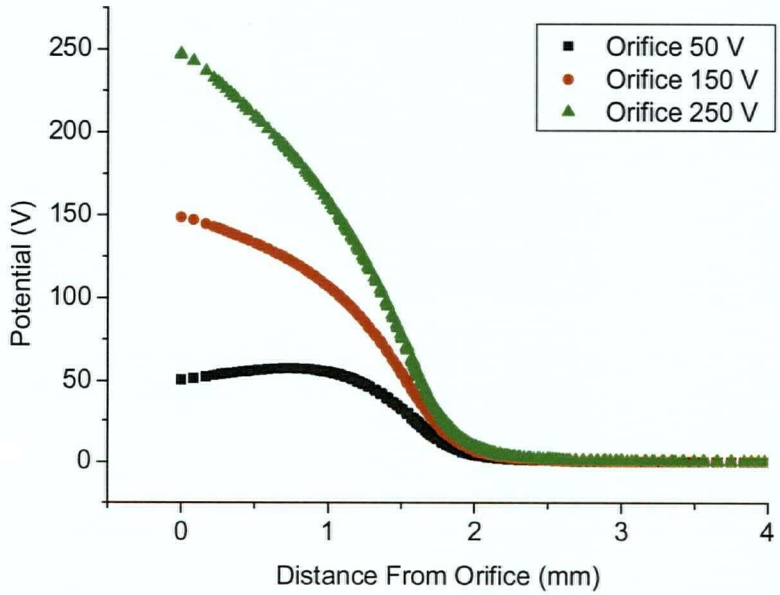

Figure 4-8 Potential distribution along the center line of ion path, starting from the orifice towards skimmer. Orifice potentials are 50, 150, 250 V in the three curves.

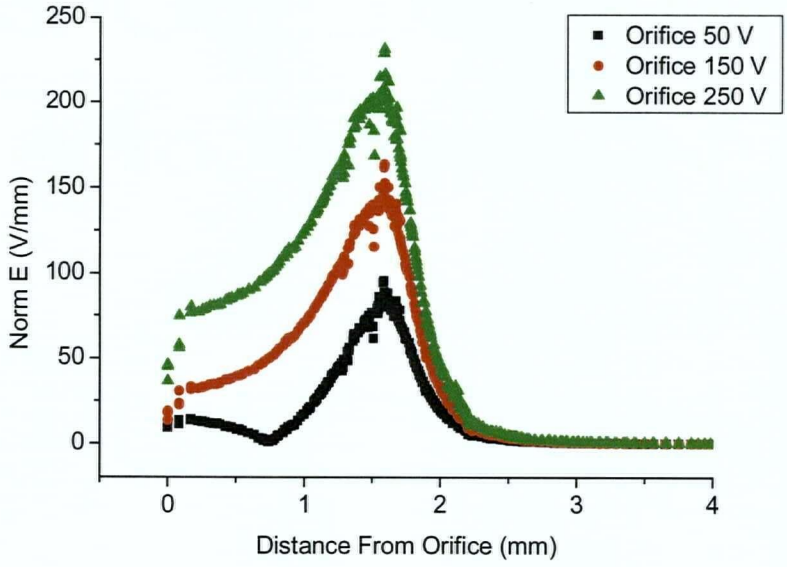

Figure 4-9 Electric field distribution along the center line of the ion path, starting from the orifice towards skimmer. Orifice potentials are 50, 150, 250 V in the three curves.

Higher electric field in the orifice-skimmer region, on one hand, provides higher kinetic energy to ions, resulting in more effective collisions, while on the other hand, it attenuates the efficiency of ion focusing. Also, ions with higher kinetic energy require even stronger focusing forces to change their moving trajectories, and this is unfortunately the deficiency of using a high orifice potential, leading to lower ion transmission and decreased ion signals. More study is needed to clarify the ion motion quantitatively. However, for application purposes, simply optimizing the orifice potential and curtain gas flow rate is enough to give the desired fragmentation and signal intensity.

4.2 Microion Spray and Its Application

Another part of this study is on a new ion source called the "microion" spray source (Figure 4-10). The microion spray unit provided by Sciex (Concord, Canada) was used to

connect a tapered fused silica sprayer tip (360 μm o.d. tapered to 15 μm i.d.) from New Objective (Woburn, MA) to a transfer tubing. A low dead volume connection tee (Valco Instruments Co., Houston, TX) was fastened into the microion spray assembly. A home-made bracket with the ion lens assembled at one end was used to hold the microion spray unit. The electrospray potential was applied directly to the stainless steel microion spray assembly to generate a liquid junction within the conductive connection tee. The tapered sprayer tip protruded approximately 7 mm from the microion spray head[9]. The flow rate can vary from 0.1 to 1 μL/min. The spray tip has a 15 μm i.d., smaller compared to a microspray tip (50 μm i.d.) but considerably larger than a nanospray tip (about 1 μm i.d.). It uses nebulizing gas to break up charged droplets, as do most of the other microspray sources, but different from other microspray ion sources, its spray tip points to the aperture perpendicularly. The operation of the microion source shows properties of both microspray and nanospray. The rest of the MS is the same as described in Chapter 2. Figure 4-10 shows the pictures of the microion spray source (top) and the source with an ion lens on the bracket connected to the housing (bottom).

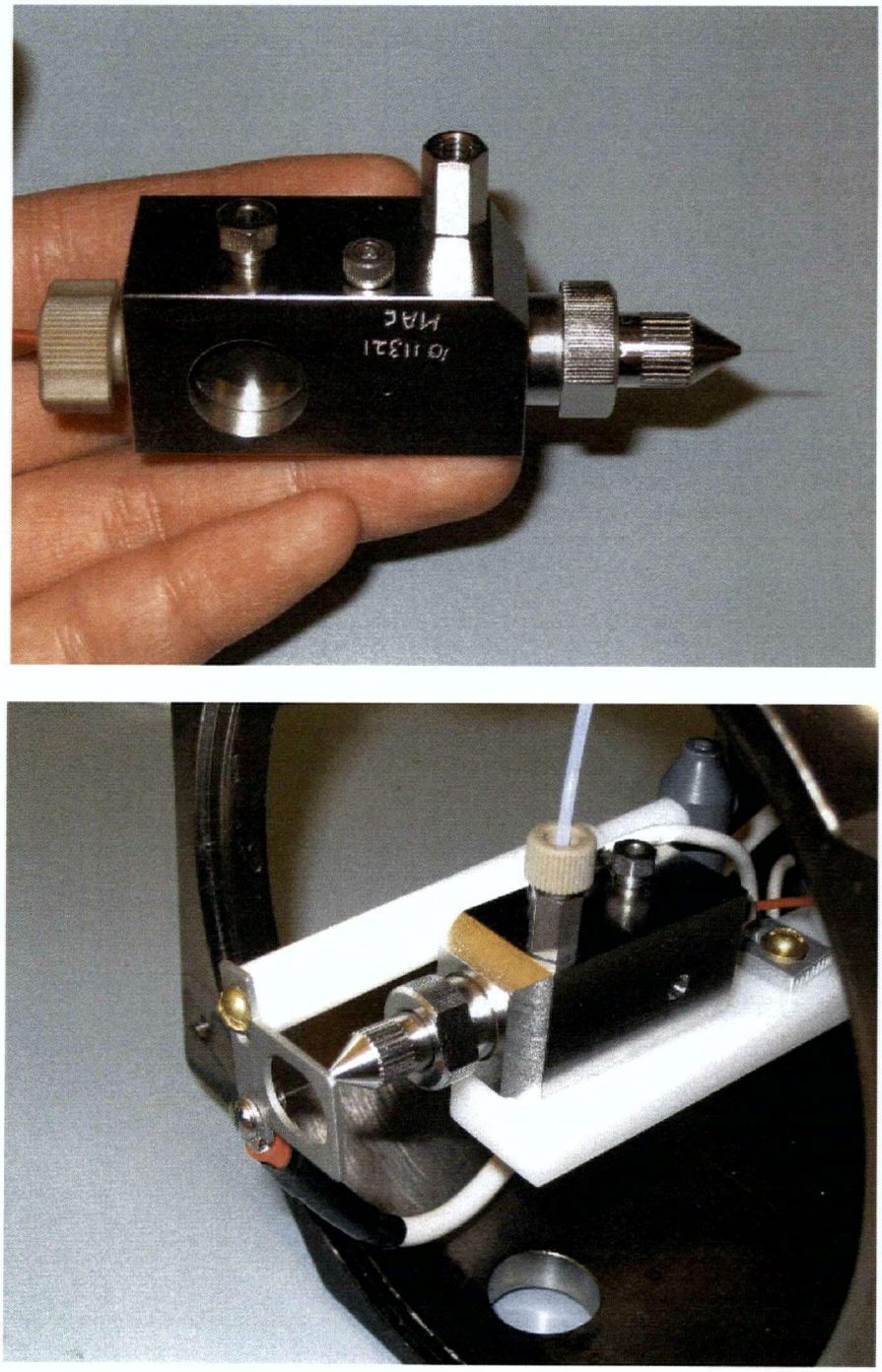

Figure 4-10 Top: Microion spray source provided by Sciex. Bottom: Micronion spray source located on a home-made bracket, with ion lens set in front of the source but about 2 mm backward from the capillary tip.

4.2.1 Sprayer Position

Signal attenuation with the distance from the sprayer tip to the curtain plate is studied. Due to Coulombic repulsion and collisions with air molecules, ions are dispersed and ion transmission efficiency decreases rapidly with increasing distance. This attenuation in signal can be partly relieved by the use of the ion lens (Figure 4-11), since the ion lens provides a focusing effect to the ions. Signal was optimized for both no lens and with lens conditions. The sample used here is 10^{-4} M β-CD in water/methanol (3/1) solution with 10 mM ammonium acetate. Very close to the curtain plate (3mm or less), ion transmission is already very high, and focusing of ions might restrict droplet desolvation. Furthermore, the ion lens is likely to cause a discharge if it is too close to the curtain plate; this would deform the electrospray. The result is the lower signal at the left side of Figure 4-11. When the spray is located at normal operational distance (5mm or more), the focusing effect starts to be important, and the ion signal is improved by the lens.

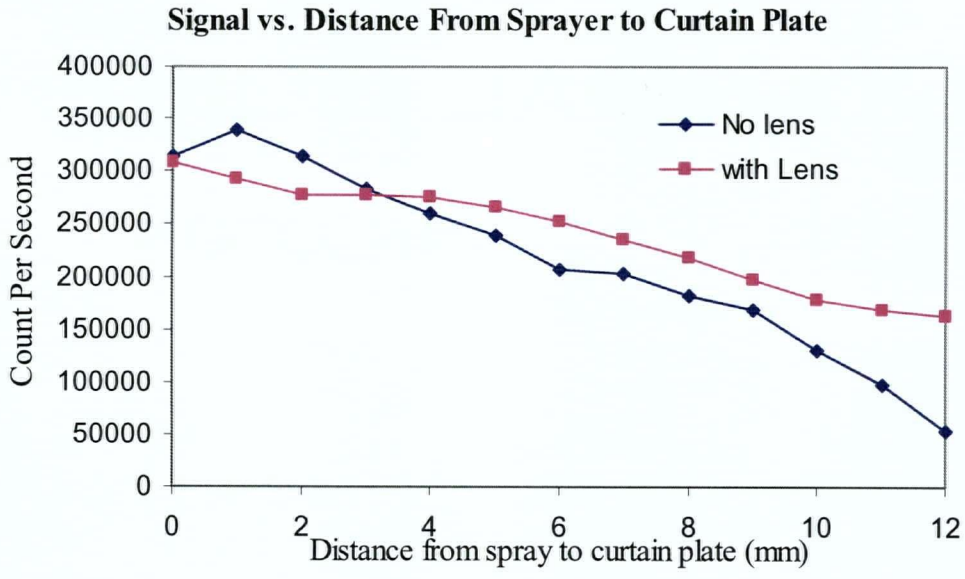

Figure 4-11 Ion signal (m/z 1153) vs. the distance from the sprayer to curtain plate. The distance varies from 0 mm (with the sprayer tip at exact the aperture of the curtain plate) to 12 mm. Each point is obtained from the average of 100 scans.

4.2.2 Lens Position

In the microion spray source, a silica sprayer tip extrudes out 7 mm from the conductive tube, which is conical at the end. Data in Figure 4-12 shows that a small change in the lens position relative to the spray tip has very small, if any, effect on the local potential distribution. At each lens potential, the lens is located from 2 mm in front of the tip (d = -2 mm), to 4 mm back of the tip (d = 4 mm). There appears to be only small differences when the lens is within -2 mm and 2 mm. When the lens is further back of the tip (d = 4 mm), its affect becomes obscure, and the signal tends to be close to that obtained for the no lens situation (the horizontal line across Figure 4-12). The ion lens starts to improve the signal only when its potential is higher than 2000 V, which is the same trend as seen with the home-made ionspray source in Chapter 2.

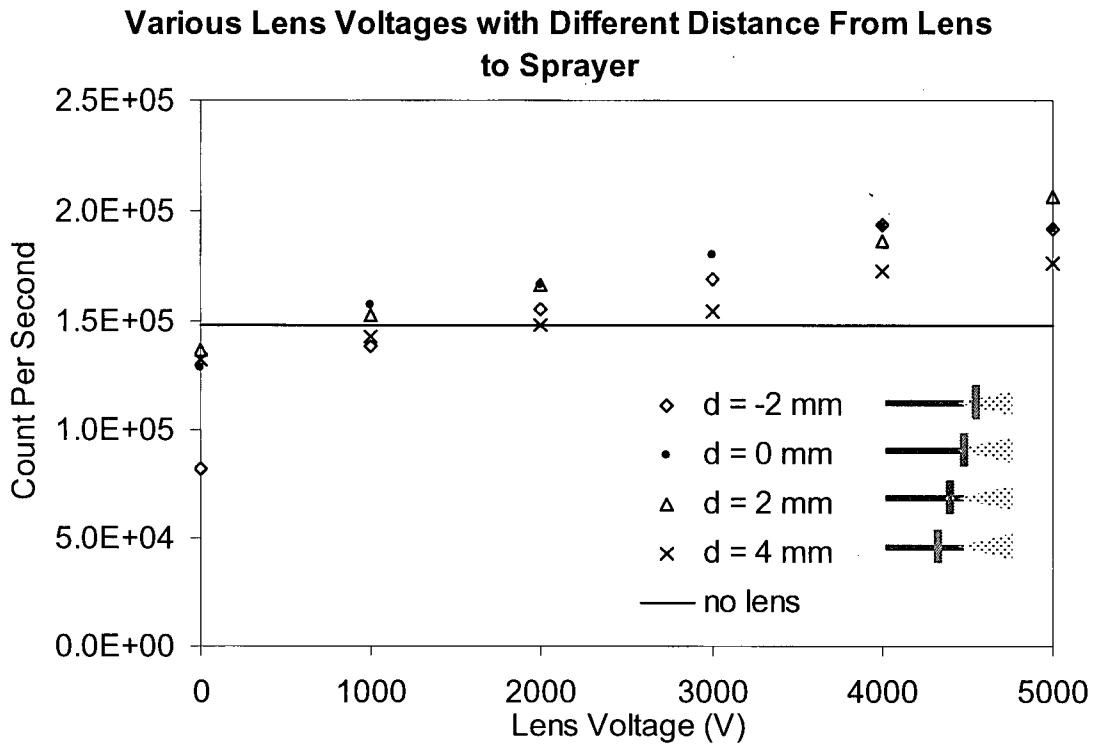

Figure 4-12 Different lens position on the effect of ion count. At each lens potential, the spray voltage is optimized to get best signal. The notation in the figure indicates the way that the lens is located from 2 mm in front of the spray tip (d = -2 mm) to 4 mm at the back of the spray tip (d = -4 mm). The line in the middle indicates the ion counts without lens.

The calculation by FEMLAB also verified that the difference in electric field, although slightly different with the different lens location, is not large enough to result in different spray process or focusing effect (data not shown).

4.2.3 Fragmentation Study

We studied fragmentation with different orifice potentials in 4.1.3, but the distance between the spray and the curtain plate also plays an important role in the extent of fragmentation. Figure 4-13 shows spectra with different distances under both with lens and no lens conditions. When the sprayed droplets have a long distance to travel before reaching the

curtain plate, desolvation of the droplets occurs more completely due to the constant collisions in atmospheric pressure. Thus, collisions happening in the orifice-skimmer region supply energy for dissociation of the ions rather than desolvation of the droplets. Therefore, with further distance, more fragments appear in the spectra. The two columns in Figure 4-13 represent the spectra with and without ion lens. The spray potential 3500 V was optimized for the non-lens condition, and the lens potential 3000 V was also optimized for the with-lens condition. A comparison of the two columns shows that the ion lens improves the signal by 2- to 3-fold, especially for high mass ions.

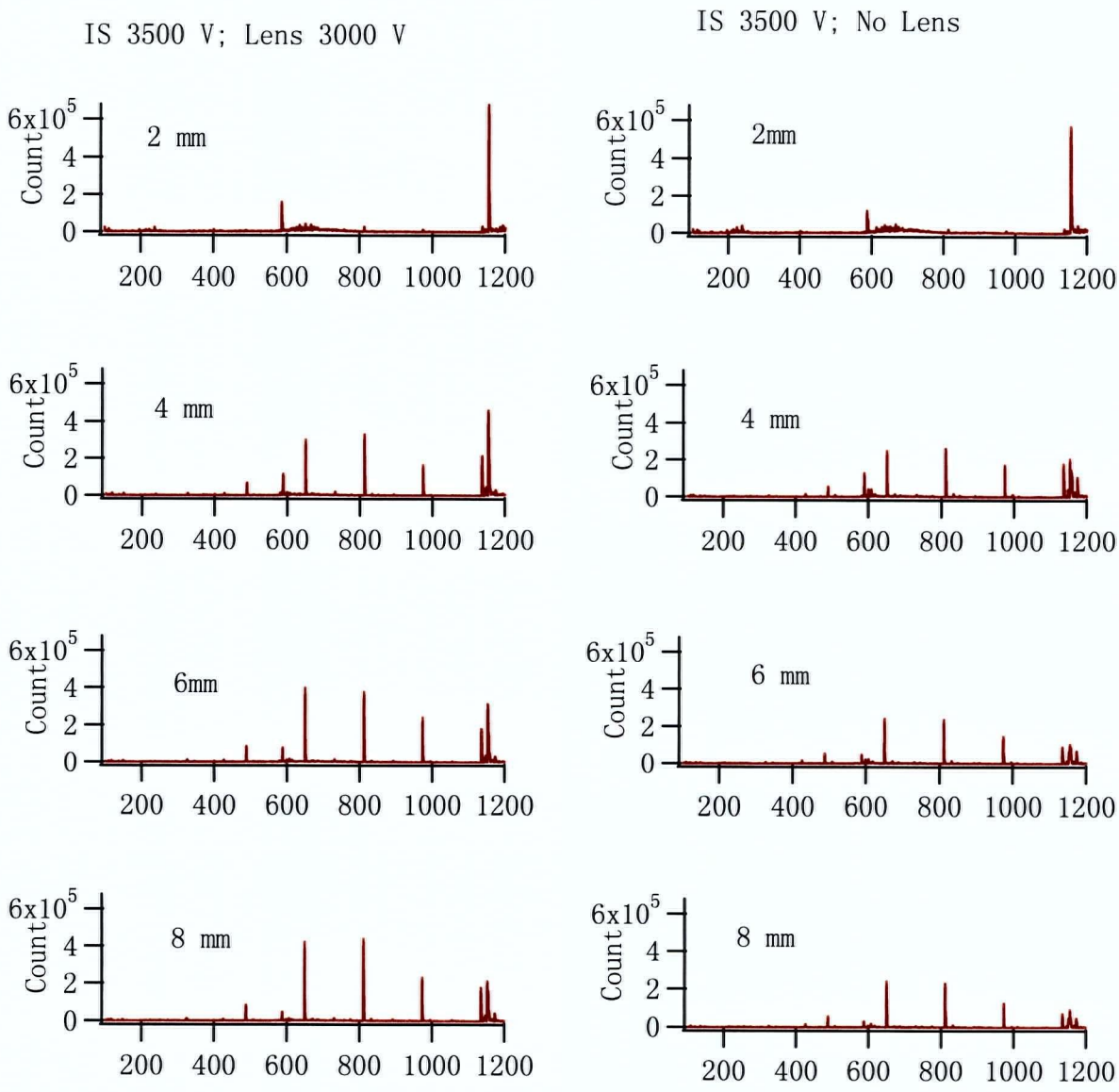

Figure 4-13 Spectra of β-CD spray tip located 2 mm, 4 mm, 6 mm, 8 mm away from the curtain plate. The left column is results with spray 3500 V, and lens 3000 V; the right column is with spray 3500 V and no lens is used.

4.3 Multiple-spray Source

The combination of the two ion sources is one of the future interests (Figure 4-14). The microion source is set parallel to the axis and directed towards the aperture in the curtain plate. On the modified bracket, another home-made spray source (same as described in Chapter 2) is

located beside the microion source, providing another sample flow. This additional liquid flow can be a calibration solution with higher concentration than the sample flow so that the sensitivity of the second spray source does not need to be as high as the microion source. When the exact molecular weight of analyte is required, simultaneous mass calibration with compounds of known molecular weights is the best way to achieve enough accuracy for ion mass.

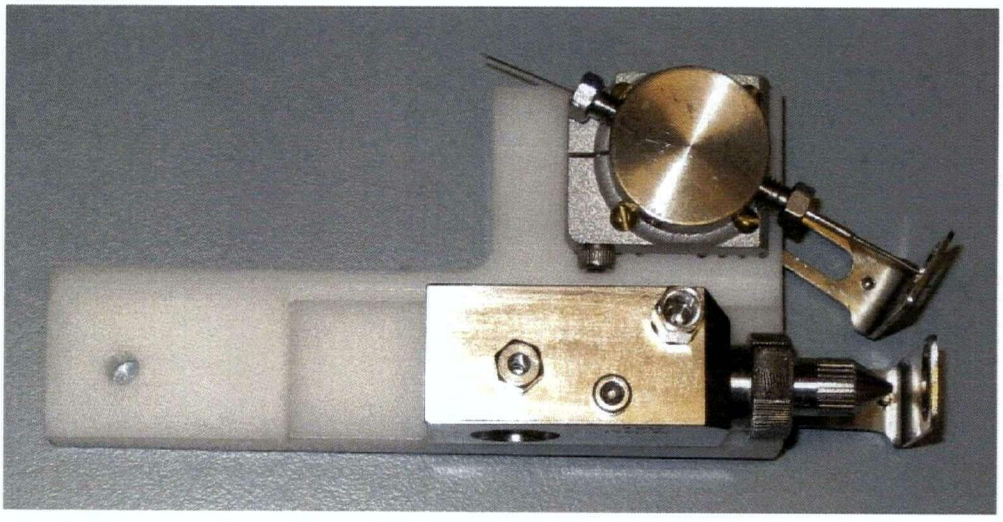

Figure 4-14 Two ion sources for sample and calibration solution. The microion source (bottom) is set at normal operational position, while another spray source (top) is located at the side to provide calibration reagent.

4.4 Conclusions

In the first part of this chapter some properties of ESI were investigated. Although complete understanding of the experimental results requires further study, some conclusions are cautiously made, as follows:

1. A sample solution with a small amount of methanol content would produce better signal, while increasing the methanol proportion does not have a clear trend of improvement in signal, due to the change in surface tension, conductivity, and polarity of the solvent.
2. The nebulizer is normally optimized with its flow rate, but its position was found to be important as well. If it is too close to the spray tip, the nebulizer is likely to deform the Taylor cone and degrade the electrospray; if it is too far from the tip, the nebulizer will lose its effect on desolvation and focusing.
3. A higher orifice potential provides higher kinetic energy to ions, and thus more energy can be converted into internal energy, resulting in more fragments in the spectra. However too high an orifice potential decreases the transmission of ions into the skimmer, because of the weakened focusing effect.

In the second part of this chapter, a new ion source called a "microion" sprayer is used and some of its characteristics are studied. The ion lens is shown to improve the signal when the spray tip is more than 3 mm away from the curtain plate. The ion lens was located from 4 mm back of the tip to 2 mm in front of the tip, and the result shows that it is not critical to accurately locate the lens at the back of the tip. The improvement seen with the use of the ion lens is more significant for heavier ions than for lighter ones.

The fragmentation of ions is also found to be dependent on the distance of the spray tip to the curtain plate, since the collision of ions with air molecules acts as a source of enthalpy so that desolvation of ions is more complete.

A two-source setup is built for the purpose of online calibration. The auxiliary source provides a flow of calibration solution, without weakening the sensitivity of the primary source. Our future work will be focusing on the study of the sensitivity difference of these two sources, and the application of the ion lens when both sources are used simultaneously.

4.5 References

1. Cech, N.B. and Enke, C.G., *Practical implications of some recent studies in electrospray ionization fundamentals.* Mass Spectrometry Reviews, 2001. **20**: p. 362-387.

2. Cech, N.B. and Enke, C.G., *Effect of affinity for droplet surfaces on the fraction of analyte molecules charged during electrospray droplet fission.* Analytical Chemistry, 2001. **73**: p. 4632-4639.

3. Cole, R.B., *Some tenets pertaining to electrospray ionization mass spectrometry.* Journal of Mass Spectrometry, 2000. **35**: p. 763-772.

4. Iribarne, J.V., Dziedzic, P.J. and Thomson, B.A., *Atmospheric-pressure ion evaporation mass-spectrometry.* International Journal of Mass Spectrometry and Ion Processes, 1983. **50**(3): p. 331-347.

5. Smith, D.P.H., *The electrohydrodynamic atomization of liquids.* IEEE Transactions on Industry Applications, 1986. **22**(3): p. 527-535.

6. Schneider, B.B., Douglas, D.J. and Chen, D.D.Y., *Ion fragmentation in an electrospray ionization mass spectrometer interface with different gases.* Rapid Communications In Mass Spectrometry, 2001. **15**: p. 249-257.

7. Schneider, B.B., Douglas, D.J. and Chen, D.D.Y., *Collision-induced dissociation of bradykinin ions in the interface resion of an esi-ms.* Journal of the American Society for Mass Spectrometry, 2001. **12**: p. 772-779.

8. Schneider, B.B. and Chen, D.D.Y., *Collision-induced dissociation of ions within the orifice-skimmer resion of an electrospray mass spectrometer.* Analytical Chemistry, 2000. **72**: p. 791-799.

9. Schneider, B.B., Baranov, V.I., Javaheri, H. and Covey, T.R., *Particle discriminator interface for nanoflow esi-ms.* Journal of the American Society for Mass Spectrometry, 2003. **14**(11): p. 1236-1246.

Chapter 5

Conclusions and Future Prospects

The initial intent of this work was to study the focusing effect of the atmospheric pressure ion lens so as to improve the ion transmission efficiency, which is the bottleneck of ESI-MS sensitivity. For this purpose, we investigated the ion lens effects systematically and found that the use of the ion lens not only increased transmission efficiency, but also improved electrospray by reshaping the electric field distribution.

It was shown both experimentally and mathematically that certain combinations of the ion lens and spray voltages were able to produce an optimal electric field for best electrospray throughput. By calculating the electric field, the ion lens was found to have two compensating effects. At low lens voltages, the ion lens produced condensed but concave equipotential lines at the spray tip, resulting in a high electric field and defocusing effect. In contrast, at high lens voltage, the ion lens reshaped the equipotential lines to a flattened but sparse distribution, which results in a focusing effect but low electric field strength. This leads to the concern that to focus ions, the electric field strength has to be sacrificed. However, raising both voltages on the spray and lens could make it possible to have both benefits of the ion lens. We therefore conclude that choosing a certain combination of spray and lens voltage is critical to obtain the desired electric field strength and focusing effect. The calculation of electric field is able to provide insight into the optimization of voltages.

It has to be noted that, due to constant fission of charged droplets and the formation of gas phase ions, ion conditions were not likely to remain the same, which restricted the calculation of space charge. Therefore, in our model, the space charge was neglected, which may lead to errors in estimating the real field strength. Furthermore, it is unrealistic to simulate

the ion trajectories because of the uncertainty of the ion condition, as well as ion collisions with air molecules in the atmospheric pressure.

However, out study verified the effectiveness of the ion lens and provided guidance for optimizing the ion lens effect. Our future work on the multiple-spray ion source will benefit from current knowledge of the ion lens. This multiple-spray ion source can enhance the accuracy of mass spectrometers by applying simultaneous mass calibration. The ion lens also has the potential to compensate for the sensitivity loss when multiple sprayers are used. Future work also includes the combination of the new source with a particle discriminator interface[1]. The particle discriminator, in addition to the ion lens, is intended to further increase the transmission efficiency. We believe this technique will make a valuable contribution to present ion source and interface design, with significant improvement in ESI-MS throughput.

Reference

1. Schneider, B.B., Baranov, V.I., Javaheri, H. and Covey, T.R., *Particle discriminator interface for nanoflow esi-ms.* Journal of the American Society for Mass Spectrometry, 2003. **14**(11): p. 1236-1246.

Appendix

I The Electrostatic Pressure on the Cone

The pressure caused by the electrostatic force at the charged surface is:

$$P_E = \frac{1}{2}\varepsilon_0 E^2$$

We can verify this equation by Gauss' Law, which states that the integration of the electric field over a closed surface is equal to the total charge in the space divided by the vacuum permittivity.

$$\oint_S E \cdot dS = \frac{1}{\varepsilon_0}\int_V \rho \cdot dV$$

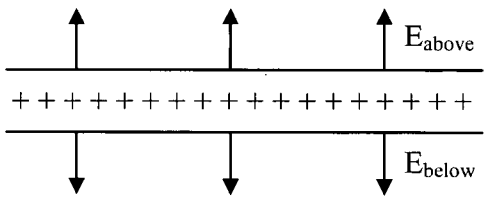

Figure A-1 An infinite sheet with surface charge density σ.

For a symmetric sheet with surface charge density σ (Figure A-1), Gauss' law yields a symmetric electric field:

$$E_{above} = +\frac{\sigma}{2\varepsilon_0}$$

$$E_{below} = -\frac{\sigma}{2\varepsilon_0}$$

However, the electric field generated by a conductor is asymmetric, and is zero inside the surface, so we have to add in an external field to compensate for the inside field.

$$E_{ext} = \frac{\sigma}{2\varepsilon_0}$$

Thus, we obtain

$$E_{above} = +\frac{\sigma}{\varepsilon_0}$$

$$E_{below} = 0$$

The pressure, or force per unit area, acting on the surface of the conductor can only be exerted by the external field because the field generated locally by the sheet cannot exert a force on itself.

$$P_E = \sigma E_{ext} = \frac{1}{2\varepsilon_0}\sigma^2 = \frac{1}{2}\varepsilon_0 E^2$$

II The Surface Pressure on the Cone

The surface pressure is defined by

$$P_\gamma = \gamma\kappa$$

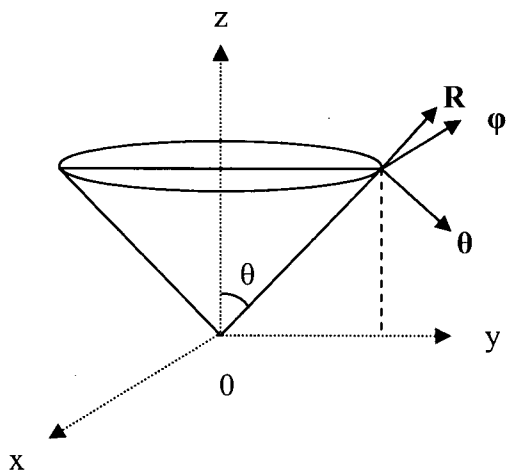

Figure A-2 Cone in spherical coordinates.

where γ is the surface tension and κ is the curvature of the cone surface. In spherical coordinates (Figure A-1), the curvature is given by

$$\kappa = \frac{\cot\theta}{(x^2+y^2)} = \frac{\cos\theta}{(1-\cos^2\theta)}\frac{1}{R}$$

$$P_\gamma = \gamma\frac{\cos\theta}{(1-\cos^2\theta)}\frac{1}{R}$$

III Solving the Laplace Equation in Spherical Coordinates

In a charge free region, we have the Laplace equation:

$$\nabla^2\phi = 0$$

With the potential independent from φ, the Laplace equation for spherical coordinates becomes

$$\nabla^2 V = \frac{1}{r^2}\left(\left[r^2\frac{\partial^2}{\partial r^2} + 2r\frac{\partial}{\partial r}\right] + \left[\frac{\partial^2}{\partial\theta^2} + \frac{\cos\theta}{\sin\theta}\frac{\partial}{\partial\theta}\right]\right)V = 0$$

In this case, the variables R, θ can be separated $V(R, \theta)=f(R)g(\theta)$

Therefore:

$$\left(\left[R^2\frac{\partial^2}{\partial R^2} + 2R\frac{\partial}{\partial R}\right]f(R)\right)\frac{1}{f(R)} + \left(\left[\frac{\partial^2}{\partial\theta^2} + \frac{\cos\theta}{\sin\theta}\frac{\partial}{\partial\theta}\right]g(\theta)\right)\frac{1}{g(\theta)} = 0$$

This can be written as:

$$\left(\left[R^2\frac{\partial^2}{\partial R^2} + 2R\frac{\partial}{\partial R}\right]f(R)\right)\frac{1}{f(R)} = c$$

$$\left(\left[\frac{\partial^2}{\partial\theta^2} + \frac{\cos\theta}{\sin\theta}\frac{\partial}{\partial\theta}\right]g(\theta)\right)\frac{1}{g(\theta)} = -c$$

The separation constant is chosen as $c=n(n+1)$.

The general solution for the first equation gives $f(R)=A_nR^n+B_nR^{-(n+1)}$. The coefficients A and B are to be determined by the boundary conditions.

To fit the form of the Legendre Equation $(1-t^2)y'' - 2ty' + \rho(\rho+1)y = 0$, the second differential equation can be transformed into

$$\left(1-\cos^2\theta\right)\frac{\partial^2}{\partial\cos\theta^2}g(\theta)-2\cos\theta\frac{\partial}{\partial\cos\theta}g(\theta)+n(n+1)g(\theta)=0$$

The Legendre differential equation has two linearly independent solutions. One solution is called the Legendre function of the first kind, $P_n(\cos\theta)$, which is regular at finite points, while the other solution, called the Legendre function of the second kind, $Q_n(\cos\theta)$, is singular at ± 1. For all points on the cone surface except the apex, which is a singularity, $P_n(\cos\theta)$ is the general solution for the Legendre differential equation. If n is an integer, $P_n(\cos\theta)$ can be reduced to a polynomial known as the Legendre polynomial. If not, $P_n(\cos\theta)$ can still be calculated[Gary 1953].

So it follows

$$V(R,\theta)=f(R)g(\theta)=\left(A_nR^n+B_nR^{-(n+1)}\right)P_n(\cos\theta)=0$$

IV Electric Field Stored Energy

To relate energy W to the electric field, we first consider the potential energy of a charge Q in a certain space volume v. The work to bring charge Q from a place of zero potential to a place of final potential V is given by the expression

$$W=\frac{1}{2}QV$$

where Q is the final net charge of the system involved. The energy can be expressed as the potential energy of the charges. In a very real sense, when some charges are collected together, work must be done against the force of mutual repulsion. Therefore, the energy is stored in the system as potential energy. An equivalent way of looking at the stored energy is to emphasize the reality of the electric field by asserting that, in the act of creating an electric field, for instance between a needle and a plate, the same amount work has to be done to accumulate

enough charges on the two opposing electrodes. From this point of view, the energy has been stored in space by virtue of the presence of an electric field.

To develop a quantitative statement of the energy per unit volume in a given field, we can assume that the energy is proportional to E^2, since **E** is a vector and energy is a scalar. So the energy stored in an electric field is assumed to be

$$W' = k\int E^2 dv$$

where k is the constant to be determine and v is the volume. The energy stored in the electric field is denoted by W', as distinguished from the potential energy W, but they are actually the same energy expressed in two different ways.

To simplify the derivation, we consider a metal sphere carrying charge Q with radius R. The potential at this metal sphere is

$$V = \int_{\infty}^{R} \mathbf{E} d\mathbf{r} = \frac{1}{4\pi\varepsilon_0}\frac{Q}{R}$$

Then in an isolated system with final net charge Q and final potential V, the stored potential energy of the sphere is therefore

$$W = \frac{1}{2}QV = \frac{1}{2}\frac{Q^2}{4\pi\varepsilon_0 R}$$

The electric field at distance r from a point or center of a sphere with charge Q is

$$E = \frac{Q}{4\pi\varepsilon_0}\frac{1}{r^2}$$

According to the assumed expression between the stored energy and the electric field, we have

$$W' = k\int_{\infty}^{R} E^2 dv = k\int_{\infty}^{R} \frac{Q^2}{(4\pi\varepsilon_0)^2 r^4} 4\pi r^2 dr$$

$$= k\frac{Q^2}{4\pi\varepsilon_0{}^2 R}$$

To get $W = W'$, we find $k = \frac{\varepsilon_0}{2}$. Thus, the electrostatic field energy can be expressed as

$$W = \frac{\varepsilon_0}{2}\int E^2 dv$$